## General Disclaimer

## One or more of the Following Statements may affect this Document

- This document has been reproduced from the best copy furnished by the organizational source. It is being released in the interest of making available as much information as possible.

- This document may contain data, which exceeds the sheet parameters. It was furnished in this condition by the organizational source and is the best copy available.

- This document may contain tone-on-tone or color graphs, charts and/or pictures, which have been reproduced in black and white.

- This document is paginated as submitted by the original source.

- Portions of this document are not fully legible due to the historical nature of some of the material. However, it is the best reproduction available from the original submission.

# DIGITAL COMPENSATION OF THE THRUST VECTOR CONTROL SYSTEM

PREPARED BY
SAMPLED-DATA CONTROL SYSTEMS GROUP
AUBURN UNIVERSITY
C. L. PHILLIPS, TECHNICAL DIRECTOR

THIRD TECHNICAL REPORT
28 MAY, 1965 TO 28 SEPTEMBER, 1965

CONTRACT - NAS8-11274
GEORGE C. MARSHALL SPACE FLIGHT CENTER
NATIONAL AERONAUTICS & SPACE ADMINSTRATION
HUNTSVILLE, ALABAMA 35812



SEPTEMBER 28, 1965



AUBURN RESEARCH FOUNDATION
AUBURN UNIVERSITY
AUBURN, ALABAMA

ELECTRICAL ENGINEERING

# DIGITAL COMPENSATION OF THE THRUST VECTOR CONTROL SYSTEM

PREPARED BY

SAMPLED-DATA CONTROL SYSTEMS GROUP
AUBURN UNIVERSITY

C. L. PHILLIPS, TECHNICAL DIRECTOR

THIRD TECHNICAL REPORT

28 MAY, 1965 TO 28 SEPTEMBER, 1965

CONTRACT NAS8-11274

GEORGE C. MARSHALL SPACE FLIGHT CENTER

NATIONAL AERONAUTICS AND SPACE ADMINISTRATION

HUNTSVILLE, ALABAMA 35812

SEPTEMBER 28, 1965

APPROVED BY

M. A. Honnell
Acting Head
Electrical Engineering

SUBMITTED BY

H. M. Summer
Project Leader

TABLE OF CONTENTS


LIST OF FIGURES..... iii

LIST OF TABLES..... vi

LIST OF SYMBOLS..... vii

FOREWORD..... viii

SUMMARY..... iv

PERSONNEL..... x

I. INTRODUCTION..... 1

II. ANALYSIS OF THE SYSTEM..... 4

III. METHODS OF APPROACH.. ..... 7

IV. DERIVATION OF TRANSFER FUNCTION USING A FICTITIOUS SAMPLER AND FICTITIOUS HOLD..... 15

V. APPLICATION OF FICTITIOUS SAMPLER AND FICTITIOUS IDEAL HOLD METHOD..... 27

Analysis of a Low-Pass System..... 2[illegible]

Analysis of High-Pass System..... 34

Limitations of the New Method of Analysis..... 41

VI. INVESTIGATION OF NUMERICAL ACCURACY OF ANALYIS IN W-PLANE..... 47

VII. APPROXIMATE TRANSFER FUNCTION USING THE DESCRIBING FUNCTION..... 56

VIII. AN INVESTIGATION OF THE EFFECTS OF VARYING THE SAMPLING RATE IN THE $\phi$ CHANNEL..... 70

IX. CONCLUSIONS..... 91

REFERENCES..... 93

APPENDIX A..... 94

APPENDIX B..... 96

APPENDIX C..... 98

APPENDIX D..... 101

LIST OF FIGURES


1. Sampled-data control system..... 2

2. Composite signal flow graph for system shown in Figure 1..... 8

3. System broken in $\beta_c$ channel with fictitious multirate sampler and hold at input terminal..... 9

4. Equivalent signal flow graph of multirate sampler..... 10

5. Composite signal flow graph of Figure 3 (N = 2)..... 12

6. Input-output spectrum of ideal sampler (a) input amplitued frequency spectrum (b) output frequency spectrum..... 17

7. Gain characteristics of ideal filter..... 18

8. Sampler followed by ideal hold..... 18

9. Open-loop sampled system..... 22

10. Sampled system with an unsampled input..... 22

11. System shown in Figure 10 with ficititious sampler and ideal hold inserted at the input terminal..... 25

12. System shown in Figure 1 redrawn..... 29

13. Nyquist diagrams of Figure 3 (with N = 1)..... 31

14. Nyquist diagram of system broken in $\phi$ channel with marginal gain as determined by system broken in $\beta_c$ channel..... 32

15. Nyquist of system given by (33) broken in $\beta_c$ channel..... 35

16. Frequency responses of holds (a) gain characteristics of zero-order hold, polygonal hold, averaging parabolic hold, and ideal hold. (b) phase characteristics of zero-order hold..... 37

17. System broken at $\beta_e$ with fictitious sampler and polygonal hold in $\phi$ channel..... 39

18. Nyquist diagrams of system shown in Figure 1 broken in $\beta_c$ channel and described by (41) and (42)..... 43

19. Nyquist of system described by (41) and (42), broken at $\phi$..... 45

20. System in Figure 1 with an input at $\beta_e$..... 46

21. Sampled-data control system..... 48

22. Nyquist diagram of system of Figure 21, broken at $\phi$..... 50

23. Sampled-data control system with compensation..... 57

24. Nyquist diagram broken in $\phi$ channel of the system shown in Figure 23 with $a_o = a_1 = 1$..... 60

25. Nyquist diagram broken in $\dot{\phi}$ channel of system shown in Figure 23 with $a_o = a_1 = 1$..... 61

26. Nyquist diagram broken in $\beta_c$ channel of the system shown in Figure 23 with $a_o = a_1 = 1$..... 62

27. Nyquist diagram broken in $\phi$ channel of the system shown in Figure 23 with $a_o = a_1 = 0.5$..... 65

28. Nyquist diagram broken in $\dot{\phi}$ channel of system shown in Figure 23 with $a_o = a_1 = 0.6$..... 66

29. Nyquist diagram broken in $\beta_c$ channel of the system shown in Figure 23 with $a_o = a_1 = 0.5$..... 67

30. Nyquist diagram broken in $\phi$ channel of system shown in Figure 23, T = 0.01..... 73

31. Nyquist diagram broken in $\dot{\phi}$ channel of system shown in Figure 23, T = 0.01..... 74

32. Nyquist diagram broken in $\beta_c$ channel of system shown in Figure 23, T = 0.01..... 75

33. Nyquist diagram broken in $\phi$ channel of system shown in Figure 23, T = 0.04..... 76

34. Nyquist diagram broken in $\dot{\phi}$ channel of system shown in Figure 23, T = 0.04..... 77

35. Nyquist diagram broken in $\beta_c$ channel of system shown in Figure 23, T = 0.04..... 78

36. Nyquist diagram broken in $\phi$ channel of system shown in Figure 23, T = 0.08..... 79

37. Nyquist diagram broken in $\dot{\phi}$ channel of system shown in Figure 23, T = 0.08..... 80

38. Nyquist diagram broken in $\beta_c$ channel of system shown in Figure 23, T = 0.08..... 81

39. Nyquist diagram broken in $\phi$ channel of system shown in Figure 23, T = 0.1..... 82

40. Nyquist diagram broken in $\dot{\phi}$ channel of system shown in Figure 23, T = 0.1..... 83

41. Nyquist diagram broken in $\beta_c$ channel of system shown in Figure 23, T = 0.1..... 84

42. Nyquist diagram broken in $\phi$ channel of system shown in Figure 23, T = 0.4..... 85

43. Nyquist diagram broken in $\dot{\phi}$ channel of system shown in Figure 23, T = 0.4..... 86

44. Nyquist diagram broken in $\beta_c$ channel of system shown in Figure 23, T = 0.4..... 87

45. Nyquist diagram broken in $\phi$ channel of system shown in Figure 23, T = 0.8..... 88

46. Nyquist diagram broken in $\dot{\phi}$ channel of system shown in Figure 23, T = 0.8..... 89

47. Nyquist diagram broken in $\beta_c$ channel of system shown in Figure 23, T = 0.8..... 90

## LIST OF TABLES

1. Output Data of Computer Program that Calculates Nyquist Diagram by the New Method..... 105

2. Data for Nyquist in F(z)-Plane..... 107

## LIST OF SYMBOLS

| | |
|---|---|
| C | System output |
| G1BN | Bending-modes transfer function in attitude channel |
| G1R | Rigid body transfer function in attitude channel |
| G2BN | Bending-modes transfer function in attitude rate channel |
| G2R | Rigid body transfer function in attitude rate channel |
| $H_A$ | Averaging parabolic hold transfer function |
| $H_I$ | Ideal hold transfer function |
| $H_o$ | Zero-order hold transfer function |
| $H_p$ | Polygonal hold transfer function |
| R | System input |
| T | Sampling period, seconds |
| $W_{ss}$ | Control engine transfer function |
| $X_n$ | System variable |
| $\beta_c$ | Engine command signal |
| $\beta_e$ | Continuous control engine deflection angle, degrees |
| $\phi$ | Attitude error |
| $\dot{\phi}$ | Attitude rate error |
| $\omega_s$ | Sampling frequency, radians per second |
| * | Sampled signal |

## FOREWORD

This report is a technical summary of the progress made since the May 28, 1965 technical report by the Electrical Engineering Department, Auburn University, toward fulfillment of Contract No. NAS8-11274 granted to Auburn Research Foundation, Auburn, Alabama. The contract was awarded May 28, 1964, by the George C. Marshall Space Flight Center, National Aeronautics and Space Administration, Huntsville, Alabama.

## SUMMARY

A new method of analysis of sampled-data control systems with unsampled inputs is presented. The method is applicable to low-pass systems. The results of an investigation into the accuracy of analysis of sampled-data systems in the w-plane are also presented. Nyquist diagrams of a compensated thrust vector control system which is sampled in the $\phi$ channel are obtained by the describing-function approach. The preliminary results of an investigation into the effects of varing the sampling rate of a sampler in the $\phi$ chnnel are included.

## PERSONNEL

The following named staff members of Auburn University have actively participated on this project.

C. H. Weaver - Head Professor of Electrical Engineering

H. M. Summer - Professor of Electrical Engineering

G. T. Nichols - Associate Professor of Electrical Engineering

C. L. Phillips - Professor of Electrical Engineering

C. L. Rogers - Assistant Professor of Electrical Engineering

R. E. Littleton - Instructor of Electrical Engineering

J. S. Boland - Graduate Assistant in Electrical Engineering

R. K. Cavin - Graduate Assistant in Electrical Engineering

G. V. Evans - Graduate Assistant in Electrical Engineering

# I. INTRODUCTION

A complete analysis of the system shown in Figure 1 requires the determination of the gain and phase margins in each of the three channels. These margins may be determined analytically by breaking the system in each of the three channels, obtaining the open-loop transfer function of the system for each channel respectively, and investigating the Nyquist diagram of each of these transfer functions about the minus one point. An open-loop transfer function can readily be obtained if the input signal is sampled before passing through a continuous-data element. An example is the system shown in Figure 1 broken at the point $\phi$. An open-loop transfer function cannot be written, however, if the input signal is acted upon by a continuous-data element in the system before being sampled. An example is the system shown in Figure 1 broken at the point $\beta_e$ or at the point $\dot{\phi}$.

Chapters II through V of this report are concerned with a new analytical procedure for obtaining a Nyquist diagram for the system shown in Figure 1 broken at $\beta_e$. This method involves inserting a fictitious sampler and a fictitious hold at the point $\beta_e$. The accuracy of this method is investigated and is found to be dependent on the low-pass nature of the system.

Chapter VI of this report is an investigation of the numerical accuracy of analysis of sampled-data systems in the w-plane as compared to analysis in the z-plane. No appreciable increase in accuracy was found using the w-plane.

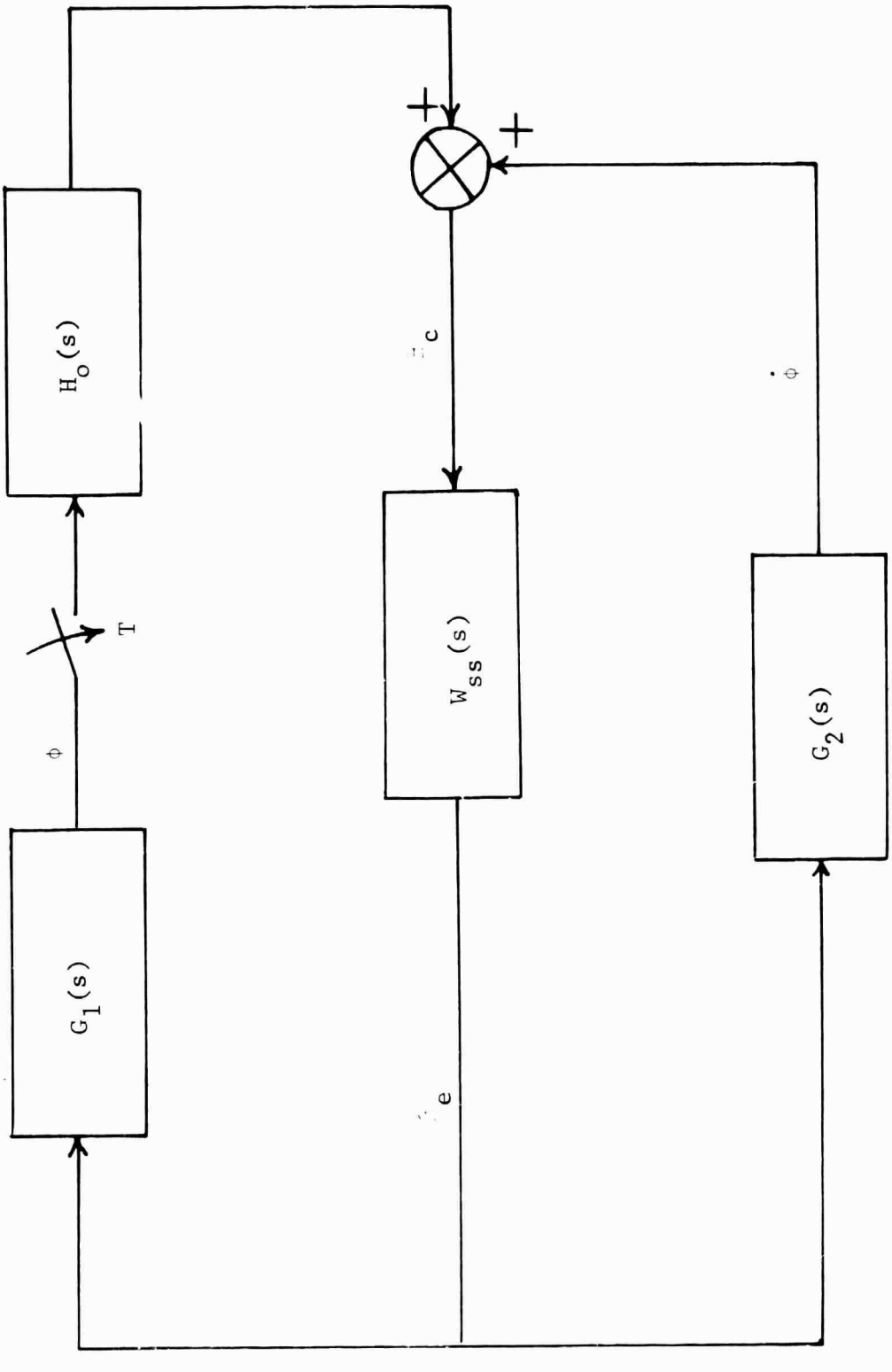


Fig. 1--Sampled-data control system

In Chapter VII the results of an analysis of a sampled, compensated thrust-vector control system are presented. The analysis is based on the describing-function approach. The purpose of this analysis was to obtain results which could be compared with results of an analog simulation.

Chapter VIII presents preliminary results of an investigation of the effects of varying the sampling rate T in the system of Figure 1.

## II. ANALYSIS OF THE SYSTEM

A typical sampled-data control system for a thrust vector control system of a space vehicle is shown in Figure 1. The $\beta_c$ channel is the forward path and the $\psi$ and $\dot{\phi}$ channels are the attitude and attitude rate feedback paths respectively. In Figure 1, $W_{ss}(s)$ is the control engine deflection angle response per control engine command angle, $G_1(s)$ is the attitude error angle response per control engine deflection angle, $G_2(s)$ is the attitude rate angle response per control angine deflection angle, and $H_o(s)$ is the transfer function of the zero-order hold. The switch in the $\phi$ channel is used to symbolize a sampler with a sampling period of T seconds. The sampling frequency, $f_s = 1/T$, of the system in Figure 1 is twenty-five hertz.

Figure 2 is the composite signal flow graph of the system shown in Figure 1 broken at $\phi$. The lower portion of Figure 2 was obtained by assigning a variable, $X_n(s)$, to each node of Figure 1 and then by constructing the "original signal flow graph" of the system.[1] Next, the sampled variables, $X_n^*(s)$, were obtained by applying Mason's gain formula[2] directly to the lower portion of Figure 2 and by taking the pulse transform at the same time. The sampled variables are

$$X_1^*(s) = X_i^*(s)$$

$$X_2^*(s) = \left[\frac{H_o(s)}{1 - G_2W_{ss}(s)}\right]^* X_i^*(s) ,$$

$$X_3^* = \left[\frac{H_oW_{ss}(s)}{1 - G_2W_{ss}(s)}\right]^* X_i^*(s) , \qquad (1)$$

and

$$X_o^* = \left[\frac{G_1H_oW_{ss}(s)}{1 - G_2W_{ss}(s)}\right]^* X_i^*(s) .$$

The sampled signal flow graph, shown in the upper portion of Figure 2, was drawn from Equations (1). The pulsed input, $X_i^*(s)$, to the original flow graph was then obtained directly from the sampled flow graph. The open-loop transfer function was written directly from the composite signal flow graph by using Mason's gain formula and is given by

$$\frac{X_o^*(s)}{X_i^*(s)} = \left[\frac{G_1H_oW_{ss}(s)}{1 - G_2W_{ss}(s)}\right]^* . \qquad (2)$$

The gain and phase margins of the closed-loop system at the point $\phi$ can now be obtained by investigating the Nyquist of (2) about the zero db, 180 degree point.

The gain and phase margins at $\beta_e$ cannot be obtained as readily, however, since an open-loop transfer function independent of the input cannot be obtained. Following the same procedure as outlined

above for the system broken in the $\phi$ channel, the output of the system broken at $\beta_e$ can be obtained and is given below.

$$X_o^*(s) = \left[X_i G_2 W_{ss}(s)\right]^* + \left[X_i G_1(s)\right]^* \cdot \left[H_o W_{ss}(s)\right]^* . \qquad (3)$$

Equation (3) is not a true transfer function since the input, $X_i(s)$, cannot be factored out of the output expression. In general, if the input to a discrete system is acted upon by a continuous-data element before being sampled, it cannot be factored out of the resulting output expression and, therefore, no transfer function can be written.

## III. METHODS OF APPROACH

In Chapter II, it was determined that an open-loop transfer function cannot be written unless the input is sampled before being acted upon by a continuous element in the system. This condition may be satisfied by inserting a fictitious sampler and hold at the input terminal. The possibility of operating the sampler at a much faster rate than the basic sampling rate of the system was first investigated. The higher the sampling frequency of the fictitious sampler, the less effect it has on system performance. Theoretically, as the sampling frequency approaches infinity, the fictitious sampler and hold have characteristics that approach the characteristics of a continuous path.

Figure 3 is the system shown in Figure 1 broken in the $\beta_c$ channel with a fictitious sampler and hold added at the input terminal, $X_i$. If the sampling period of the fictitious sampler is T/N, where T is the sampling period of the sampler in the $\phi$ channel and where N is any positive integer, the fictitious sampler may be represented by the signal flow graph shown in Figure 4. Each of the N samplers in Figure 4 are sampling at the same instant and at the basic sampling rate of the system. The input signal, however, to the $K^{th}$ branch is advanced by KT/N seconds, sampled at the same instant as the signals in all of the other branches, delayed by KT/N seconds, and then

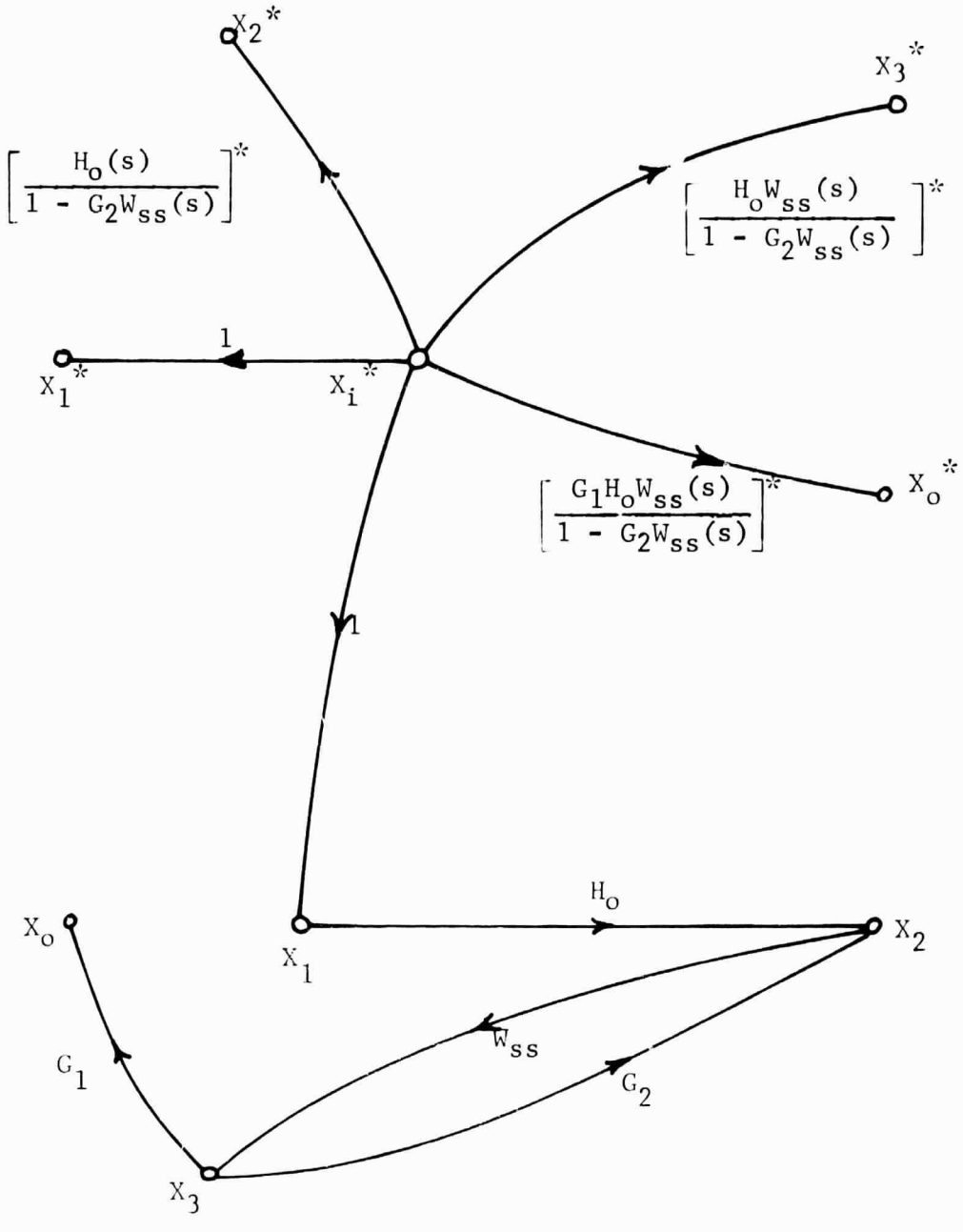


Fig. 2--Composite signal flow graph for system shown in Figure 1

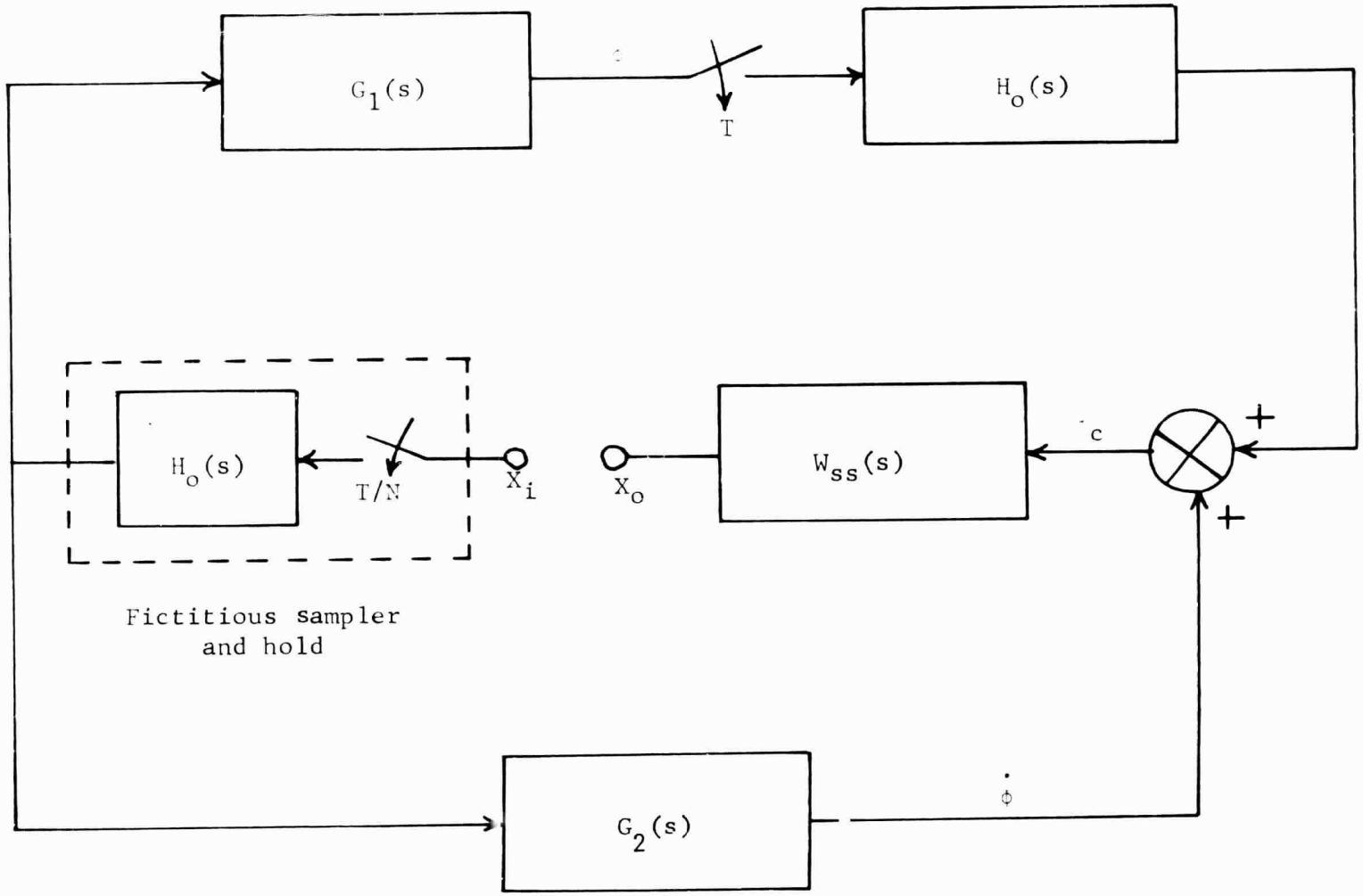


Fig. 3--System broken in $\dot{\phi}_c$ channel with fictitious multirate sampler and hold at input terminal

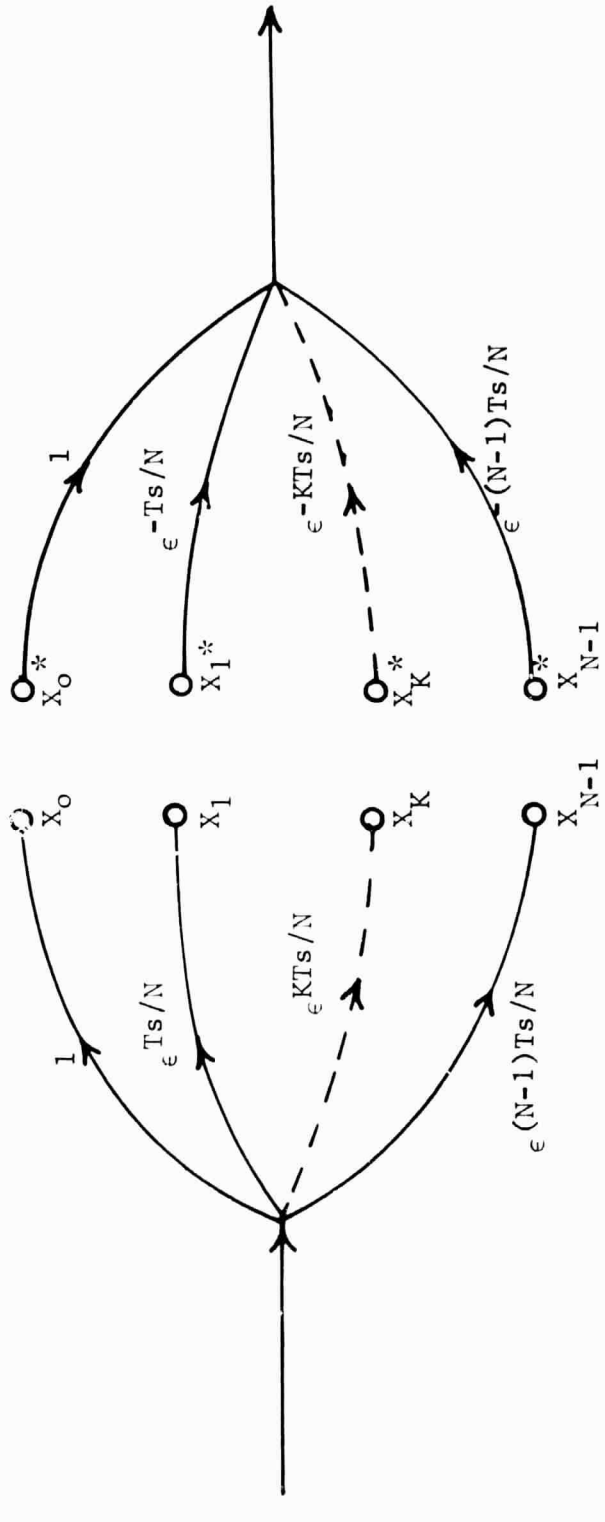


Fig. 4--Equivalent signal flow graph of multirate sampler

added to the other branch output signals. The $K^{th}$ branch, therefore, represents the $K^{th}$ sample of the multirate sampler during each basic sampling period. The sum of the outputs of all branches in Figure 4 represents the N samples of the multirate sampler during each basic sampling period. Representing the fictitious multirate sampler by N samplers, all operating at the basic sampling rate of the system, permits the use of the ordinary z-transform in analyzing the system.

Figure 5 is the composite signal flow graph representing the system of Figure 3, when the sampling rate of the fictitious sampler is twice the rate of the sampler in the $\phi$ channel. By applying Mason's gain formula to Figure 5, the pulsed output, $X_o^*(s)$ can be expressed as

$$X_o^*(s) = X_i^*(s)\left(\left[W_{ss}G_2H_o\right]^*(s) + \left[G_1H_o\right]^*(s)\left[W_{ss}H_o\right]^*(s)\right) \tag{4}$$

$$+ \left[X_i(s)\epsilon^{sT/2}\right]^*\left(\left[W_{ss}G_2H_o\epsilon^{-sT/2}\right]^*(s) + \left[G_1H_o\epsilon^{-sT/2}\right]^*(s)\left[W_{ss}H_o\right]^*(s)\right).$$

In Figure 5,

$$X_{i_o}^*(s) = X_i^*(s)$$

and

$$X_{i_1}^*(s) = \left[X_i(s)\epsilon^{sT/2}\right]^*.$$

Since

$$\left[\epsilon^{sT/2}X_i(s)\right] \neq z^{\frac{1}{2}}X_i(z), \tag{5}$$

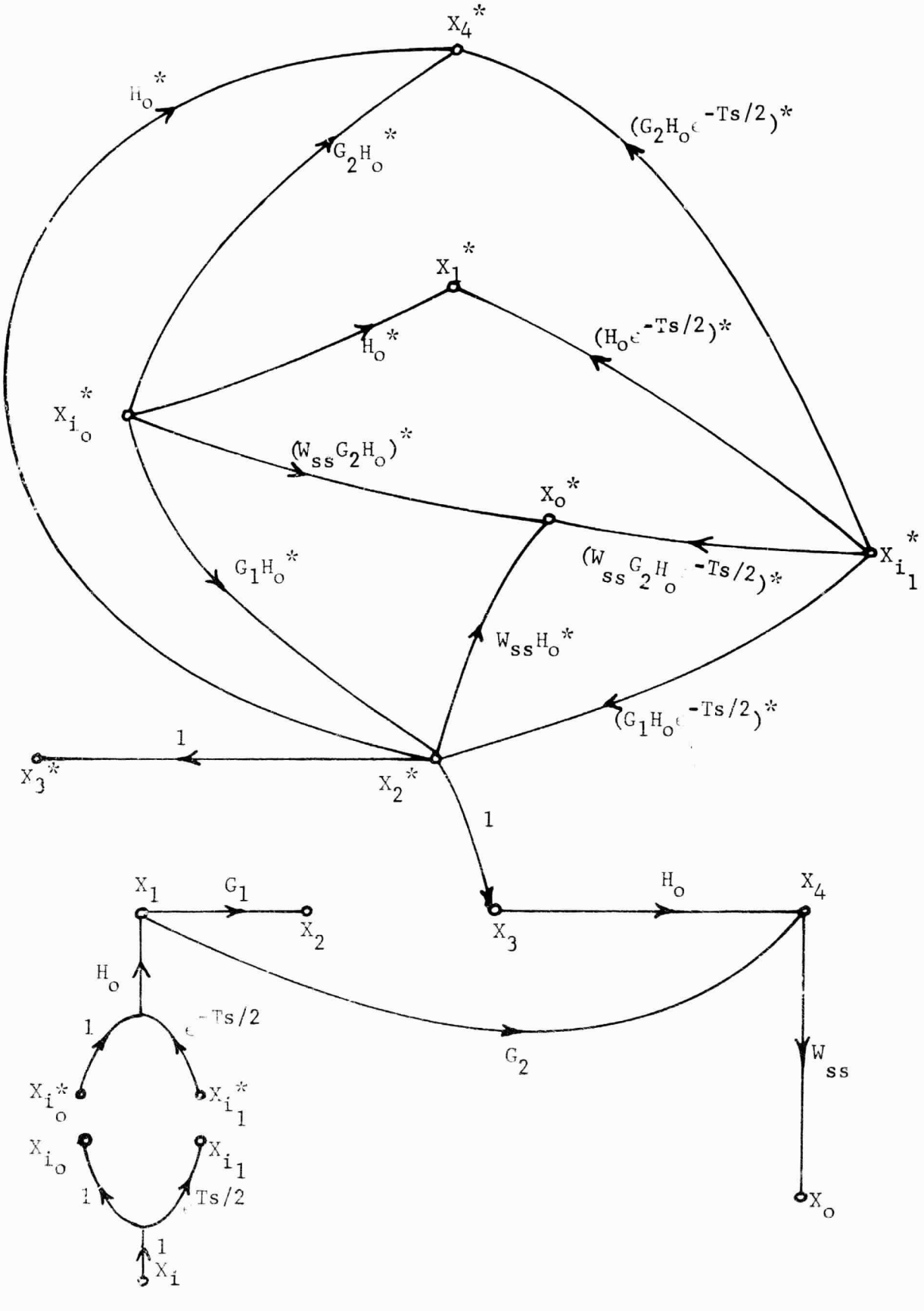


Fig. 5--Composite signal flow graph of Figure 3 (N=2)

the input, $X_i$, cannot be factored out of the second term of (4). Therefore, a transfer function cannot be written when the fictitious sampler is sampling at an integral multiple rate of the basic sampler in the system.

When the rate of the fictitious sampler is T/N, the generalized form of the output, expressed in modified z-transform notation, is[3]

$$X_o(z) = X_i(z)\left(\left[W_{ss}G_2H_o\right](z) + \left[G_1H_o\right](z)\left[W_{ss}H_o\right](z)\right)$$

$$+ z\sum_{P=1}^{N-1} X_i(z,\ P/N)\left(\left[W_{ss}G_2H_o\right](z,\ 1 - P/N)\right. \tag{6}$$

$$\left. + \left[G_1H_o\right](z,\ 1 - P/N)\left[W_{ss}H_o\right](z)\right),$$

where $\left[\epsilon^{PTs/N}X_i(s)\right] = zX_i(z,P/N)$, for $0 < P/N \leq 1$

and $\left[\epsilon^{-PTs/N}X_i(s)\right] = X_i(z,1 - P/N)$, for $0 < P/N \leq 1$.

From the results of Chapter II and the above results of this chapter, it was concluded that no transfer function can be written for the system broken in the $\beta_c$ channel unless a fictitious sampler, operating at the same rate as the sampler in the $\phi$ channel, is in-

serted at the input terminal. The effects on system performance of inserting a fictitious sampler at the input terminal will be investigated in Chapter IV.

## IV. DERIVATION OF TRANSFER FUNCTION USING A FICTITIOUS SAMPLER AND FICTITIOUS HOLD

In Chapter III, a fictitious sampler and a fictitious hold were introduced at the input terminal, $X_i$, as shown in Figure 3. It was determined that in order to write a transfer function, the sampling rate of the fictitious sampler must be the same as the basic sampling rate of the system. In this chapter, the effects of the fictitious sampler on the system will be determined and a transfer function will be written using a fictitious ideal hold.

The fictitious sampler in Figure 3 acts as a pulse modulator, introducing an infinite number of harmonic frequency components in the output in addition to the fundamental frequency component. If the input to the sampler is e(t), the Laplace-transformed, sampled output is given by

$$E^*(s) = \frac{1}{T} \sum_{n=-\infty}^{+\infty} E(s + jn\omega_s) + \frac{e(0^+)}{2} \quad . \tag{7}$$

The $\frac{e(0^+)}{2}$ term[4] is included in (7) to account for the effect at the output of the sampler of an input time function, e(t), that has a jump discontinuity of $e(0^+)$ at $t = 0$. If the Laplace transform, E(s), of the sampled function satisfies the condition

$$\lim_{s \to \infty} sE(s) = 0, \tag{8}$$

the second term of (7) is zero. Since E(s) for the system in Figure 3 has at least two more poles than zeroes, the condition of (8) is satisfied and (7) reduces to

$$E^*(s) = \frac{1}{T} \sum_{n=-\infty}^{+\infty} E(s + jn\omega_s). \tag{9}$$

If the input to the sampler, $E(j\omega)$, contains no frequency component greater than $\omega_c$, where $\omega_c$ is less than one-half the sampling frequency in radians per second, and has the frequency spectrum as shown in Figure 6(a), the output given by (9) is as shown in Figure 6(b). The input signal, E(s), can be completely recovered by an ideal low-pass filter with characteristics as given in Figure 7. The ideal filter can be represented by

$$H_I(j\omega) = A(\omega)\, e^{j\theta(\omega)}, \tag{10}$$

where

$$A(\omega) = T \text{ for } |\omega| \leq |\omega_s/2|, \tag{11}$$

$$A(\omega) = 0 \text{ for } |\omega| > |\omega_s/2|,$$

and $\theta(\omega) = 0$, giving no phase shift through the filter.[5]

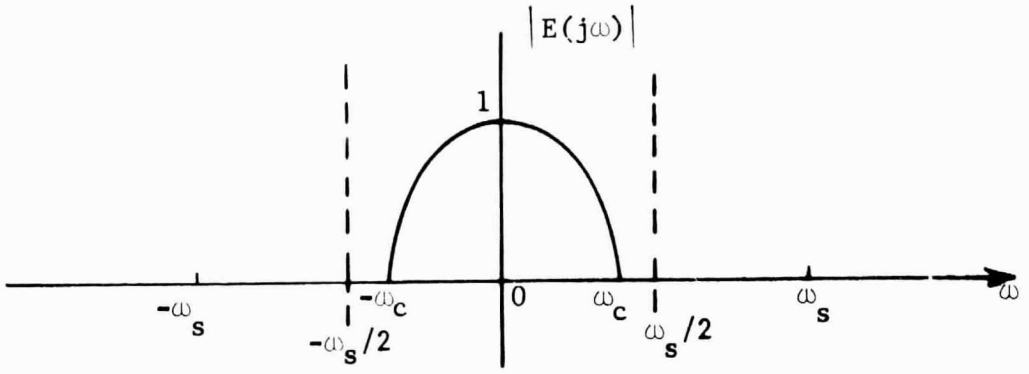


(a)

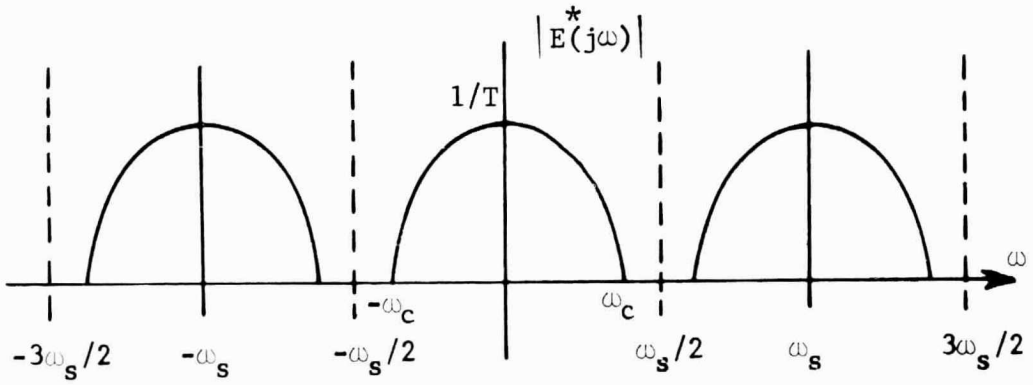


(b)

Fig. 6--Input-output spectrum of ideal sampler (a) Input amplitude frequency spectrum (b) Output frequency spectrum

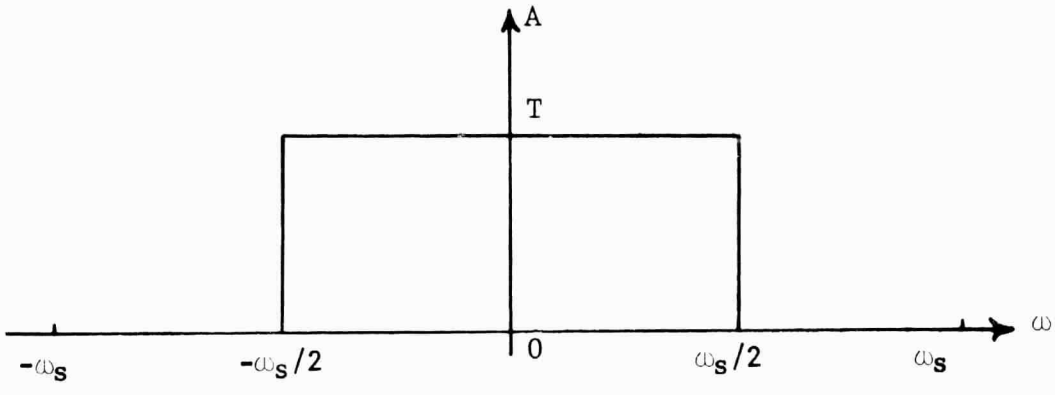


Fig. 7--Gain characteristics of ideal filter

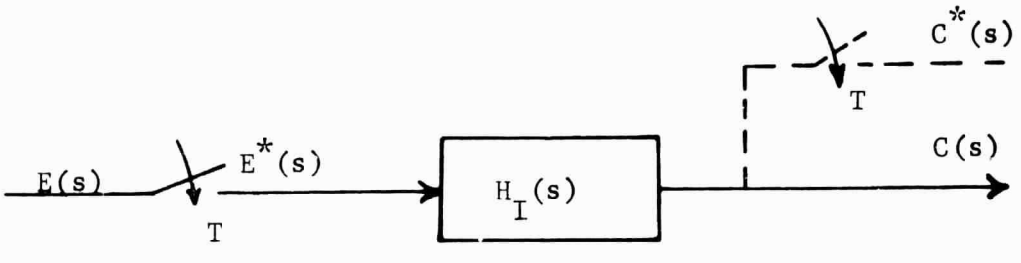


Fig. 8--Sampler followed by ideal hold

The fact that the ideal filter illustrated in Figure 7 cannot be physically realized causes no concern, since it was introduced into the system fictitiously. In fact, as is shown below, no analytic transfer function need be derived for $H_I$ in order to analyze the system.

The output of the sampler in Figure 8 is $E^*(s)$, where $E^*(s)$ is given by

$$E^*(s) = \frac{1}{T} \sum_{n=-\infty}^{+\infty} E(s + jn\omega_s). \tag{12}$$

Or

$$E^*(j\omega) = \frac{1}{T} \left[ E(j\omega) + E(j\omega - j\omega_s) + E(j\omega + j\omega_s) + E(j\omega - 2j\omega_s) + E(j\omega + 2j\omega_s) + \cdots\cdots \right]. \tag{13}$$

Equation (13) is an expression for the input to the ideal hold in Figure 8. The ideal hold, however, as shown in Figure 7, will pass only those components of (13) with frequencies that are less than $\omega_s/2$ and will multiply the magnitude of these components by a factor of T, the sampling period of the sampler. If the input frequency, $\omega$, in (13) is less than $\omega_s/2$, the output will be

$$C(j\omega) = \frac{1}{T} E(j\omega) \left[ \; T \; \right] ,$$

or

$$C(j\omega) = E(j\omega), \tag{14}$$

for

$$\omega < \omega_s/2 \; .$$

Equation (14) shows that if a sampler is followed by an ideal hold, the continuous output wave of the hold is equal to the input wave to the sampler.

From Figure 8

$$C(s) = E^*(s) \; H_I(s) \; . \tag{15}$$

Starring both sides of (15), the following is obtained:

$$C^*(s) = E^*(s) H_I{}^*(s) \; .$$

or

$$\frac{C^*(s)}{E^*(s)} = H_I{}^*(s). \tag{16}$$

Equation (16) is the transfer function of the ideal hold in Figure 8. If (16) is expressed by its equivalent frequency domain expansion, the following relationship results:

$$\frac{C^*(j\omega)}{E^*(j\omega)} = \frac{1}{T} \sum_{n=-\infty}^{+\infty} H_I(j\omega + jn\omega_s) = \frac{1}{T} \left[ H_I(j\omega) + H_I(j\omega - j\omega_s) \right. \tag{17}$$

$$\left. + H_I(j\omega + j\omega_s) + \ldots\ldots \right] .$$

For $\omega$ less than $\omega_s/2$, all the terms in (17) are zero except the first term, which has a value of T. Therefore,

$$\frac{C^*(s)}{E^*(s)} = \frac{1}{T}\left[T\right] = 1$$

and

$$C^*(s) = E^*(s). \tag{18}$$

Equation (18) proves that if the output of the ideal hold in Figure 8 were sampled, the resulting sampled signal would be the same as the sampled input signal to the hold.

The sampled output of Figure 9 is given by

$$C^*(s) = R^*(s)H_IG^*(s). \tag{19}$$

The transfer function of the system shown in Figure 9 is

$$\frac{C^*(s)}{R^*(s)} = H_IG^*(s) = \frac{1}{T}\sum_{n=-\infty}^{+\infty} H_IG(s + jn\omega_s),$$

or

$$\frac{C^*(j\omega)}{R^*(j\omega)} = \frac{1}{T}\Big[H_IG(j\omega) + H_IG(j\omega - j\omega_s) + H_IG(j\omega + j\omega_s) + H_IG(j\omega - 2j\omega_s) + H_IG(j\omega + 2j\omega_s) + \cdots\cdots\Big]. \tag{20}$$

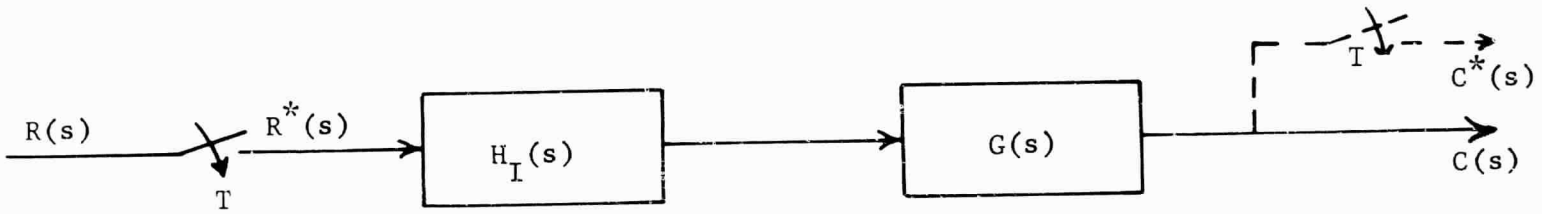


Fig. 9--Open-loop sampled system

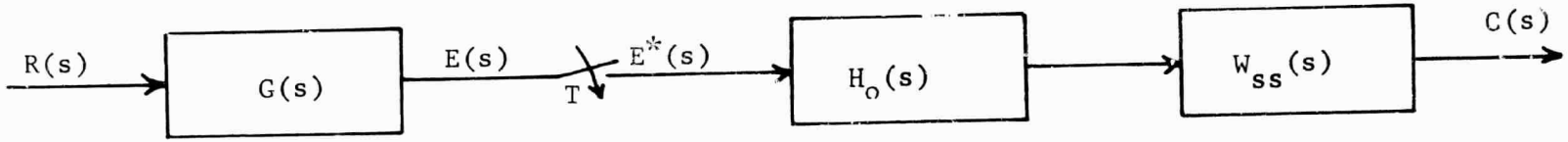


Fig. 10--Sampled system with an unsampled input

If the input frequency, $\omega$, is less than $\omega_s/2$, all of the terms in (20) with the exception of the first term will be zero, since $H_I$ passes only those components with frequencies less than $\omega_s/2$. Under these conditions, (20) becomes

$$\frac{C^*(j\omega)}{R^*(j\omega)} = \frac{1}{T}H_I G(j\omega) = \frac{1}{T}H_I(j\omega)G(j\omega). \tag{21}$$

But, from Figure 7, $H_I(j\omega) = T$ when $\omega$ is less than $\omega_s/2$. Therefore, (20) becomes

$$\frac{C^*(j\omega)}{R^*(j\omega)} = \frac{1}{T}\,(T)G(j\omega),$$

or

$$\frac{C^*(j\omega)}{R^*(j\omega)} = G(j\omega). \tag{22}$$

The output of the ideal hold in Figure 9 is R(s), as was shown by (14). Therefore, the continuous output of Figure 9 can be expressed as

$$C(j\omega) = G(j\omega)\ R(j\omega),$$

or

$$\frac{C(j\omega)}{R(j\omega)} = G(j\omega). \tag{23}$$

Equations (22) and (23) show that for input frequencies less than $\omega_s/2$, there is no effect on the system by the insertion of the fictitious sampler and ideal hold. The results of (22) and (23) are very important when analyzing systems with inputs that are not sampled before passing through a continuous-data element.

As explained in Chapters II and III, a transfer function cannot be written for the system given in Figure 10. However, if a fictitious sampler and a fictitious ideal hold are inserted at the input terminal, as shown in Figure 11, a transfer function can be written and is given by

$$\frac{C^*(s)}{R^*(s)} = H_I G^*(s) H_o W_{ss}{}^*(s). \tag{24}$$

Equation (24) may be written as

$$\frac{C^*(s)}{R^*(s)} = \left[\frac{1}{T}\sum_{n=-\infty}^{+\infty} H_I G(s + jn\omega_s)\right]\left[\frac{1}{T}\sum_{n=-\infty}^{+\infty} H_o W_{ss}(s + jn\omega_s)\right]. \tag{25}$$

From the results shown in (19), (20), (21) and (22), Equation (25) can be reduced to

$$\frac{C^*(j\omega)}{R^*(j\omega)} = G(j\omega)\left[\frac{1}{T}\sum_{n=-\infty}^{+\infty} H_o W_{ss}(j\omega + jn\omega_s)\right]. \tag{26}$$

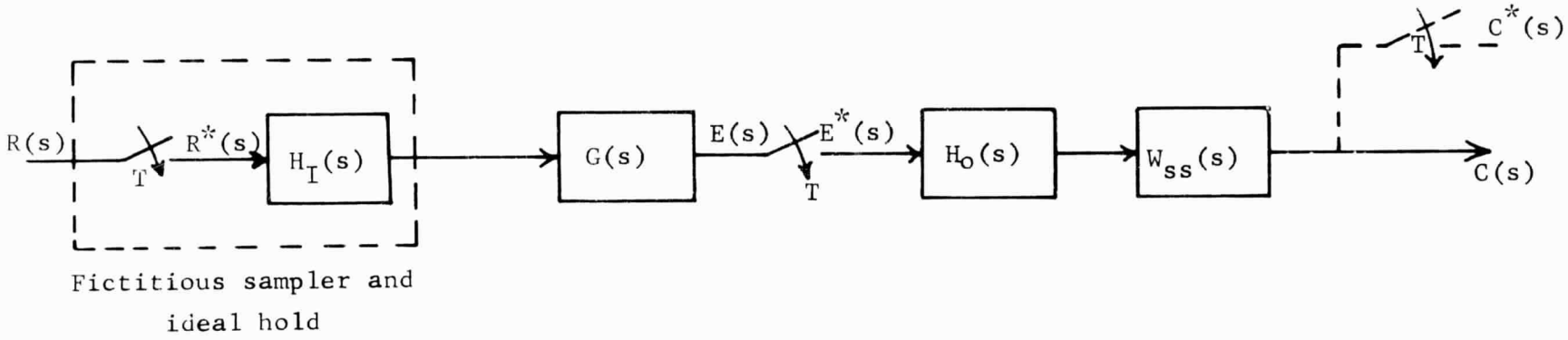


Fig. 11--System shown in Figure 10 with fictitious sampler and ideal hold inserted at the input terminal

Equation (26), however, is only valid for input frequencies less than $\omega_s/2$. For $0 \leq \omega < \omega_s/2$, (26) gives an exact Nyquist diagram of the system in Figure 10.

## V. APPLICATION OF FICTITIOUS SAMPLER AND FICTITIOUS IDEAL HOLD METHOD

The fictitious sampler and ideal hold method of analysis may be applied to the system shown in Figure 1 broken at $\beta_e$. Since the open-loop transfer function is the parallel combination of the upper and lower channels, the complete transfer function is the sum of the upper and lower loop transfer functions. The lower loop, having no sampler, is continuous and has an open-loop transfer function, O.L.T.F., given by

$$\text{O.L.T.F.}_{\text{Lower}} = G_2 W_{ss}(s). \tag{27}$$

The upper loop is identical to the system shown in Figure 10. By using the fictitious sampler and fictitious ideal hold method of analysis, the open-loop transfer function can be obtained and is given by (26) and (28).

$$\text{O.L.T.F.}_{\text{Upper}} = G_1(s)\left[\frac{1}{T}\sum_{n=-\infty}^{+\infty} H_o W_{ss}(s + jn\omega_s)\right]. \tag{28}$$

Therefore, the total open-loop transfer function for the system shown in Figure 1, broken at $\beta_e$, is

$$O.L.T.F. = G_2W_{ss}(s) + G_1(s)\left[\frac{1}{T}\sum_{n=-\infty}^{+\infty} H_oW_{ss}(s + jn\omega_s)\right]. \quad (29)$$

As explained in Chapter IV, (29) is only valid for input frequencies less than $\omega_s/2$.

When the loop is closed at $\beta_e$, the system given in Figure 1 can be redrawn as shown in Figure 12. The closed-loop transfer function of Figure 12 is

$$\frac{X_o}{X_i} = \frac{O.L.T.F.}{1 - O.L.T.F.},$$

or

$$\frac{X_o}{X_i} = \frac{O.L.T.F.}{1 + (- O.L.T.F.)}. \quad (30)$$

The Nyquist of the negative open-loop transfer function can be investigated about the minus one point to determine the stability of the system.

Analysis of a low-pass system

The first system to be analyzed by using the new method of analysis described in Chapter IV, is a system having low-pass characteristics. The transfer functions of the system shown in Figure 1 are given by

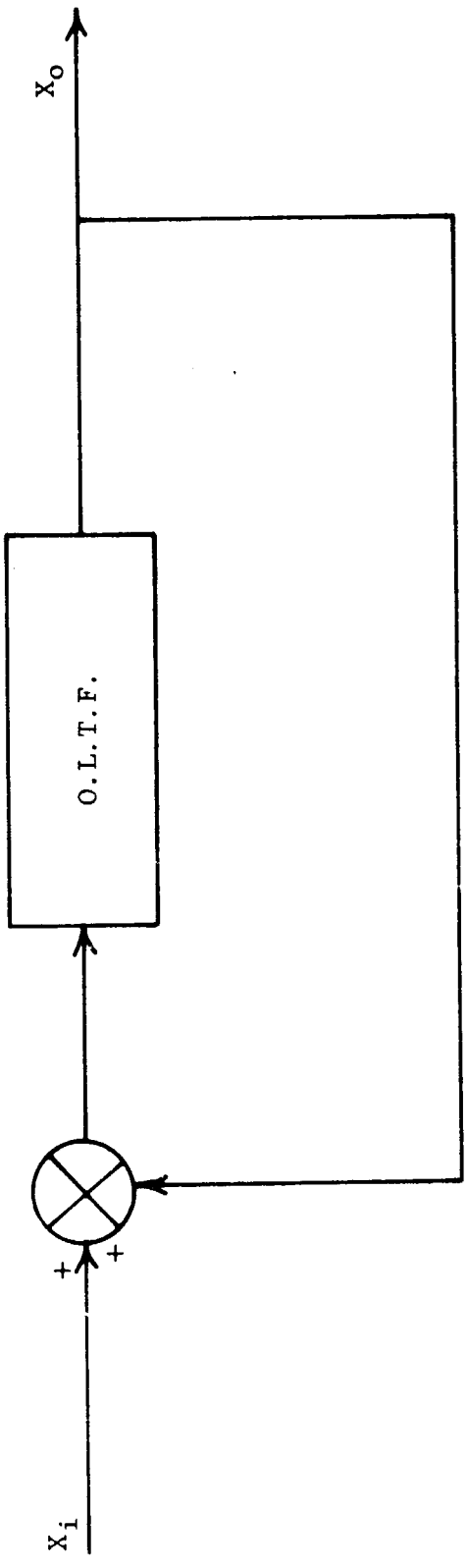


Fig. 12--System shown in Figure 1 redrawn

$$G_1(s) = \frac{-0.94068468}{s^2 - 0.029727836},$$

$$G_2(s) = \frac{-0.94068468\ s}{s^2 - 0.029727836}, \tag{31}$$

$$W_{ss}(s) = \frac{625}{s^2 + 25s + 625},$$

and

$$H_o(s) = \frac{1 - \epsilon^{-sT}}{s}.$$

By substituting (31) into (29) and by using the digital computer program given in Appendix A, the Nyquist diagram shown in Figure 13 was obtained. Figure 13 gives an exact Nyquist for the open-loop system shown in Figure 1.

The effects of the harmonics generated by the sampler in the $\phi$ channel can be investigated by comparing the Nyquist in Figure 13 with the continuous Nyquist. The open-loop transfer function for the continuous system, broken at $\beta_e$, was obtained by deleting the sampler in the $\phi$ channel and is given below.

$$\text{O.L.T.F.} = G_2W_{ss}(s) + G_1H_oW_{ss}(s). \tag{32}$$

The Nyquist for the continuous system was then obtained by plotting

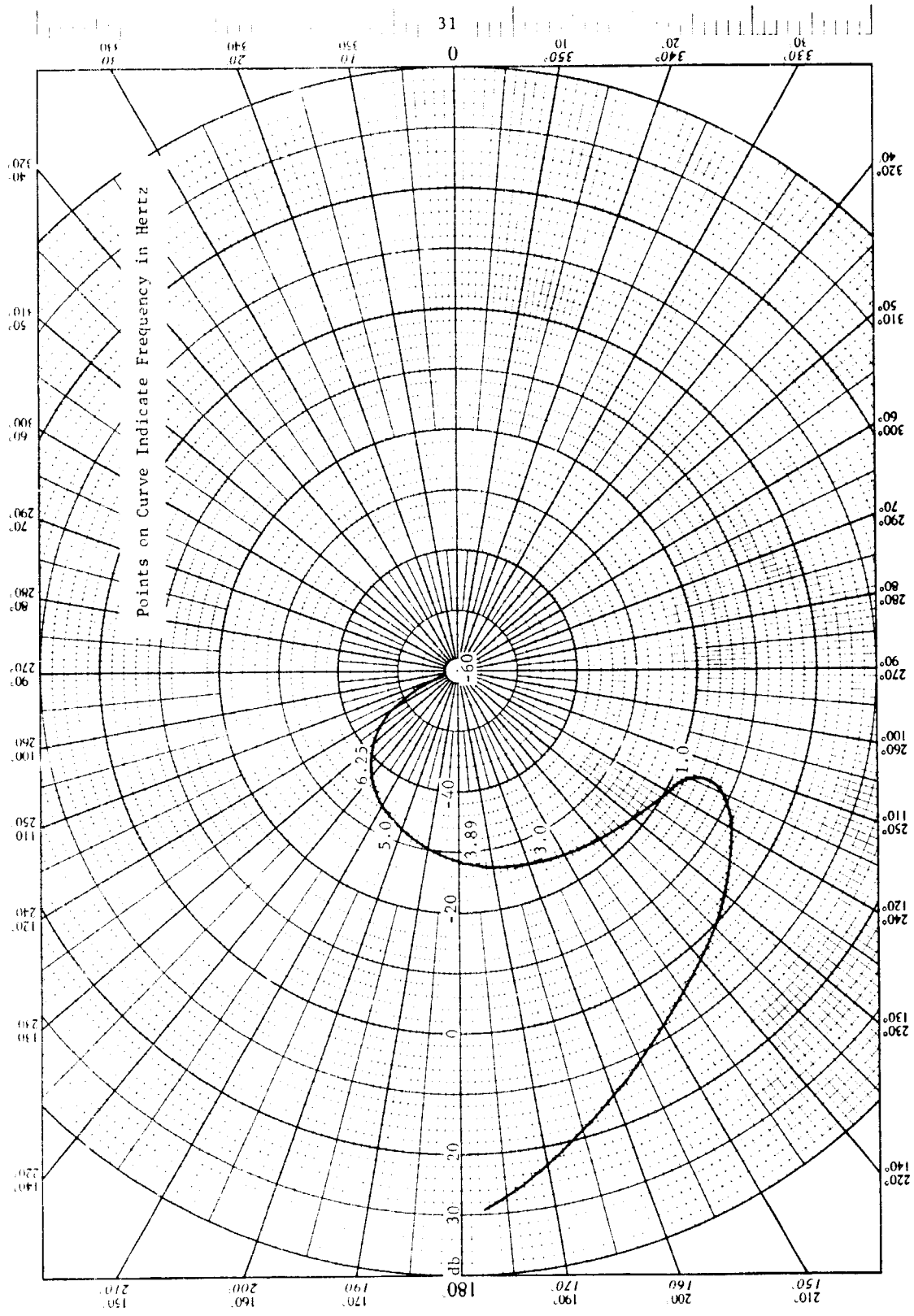


Fig. 13--Nyquist diagram of Figure 3 (with N=1)

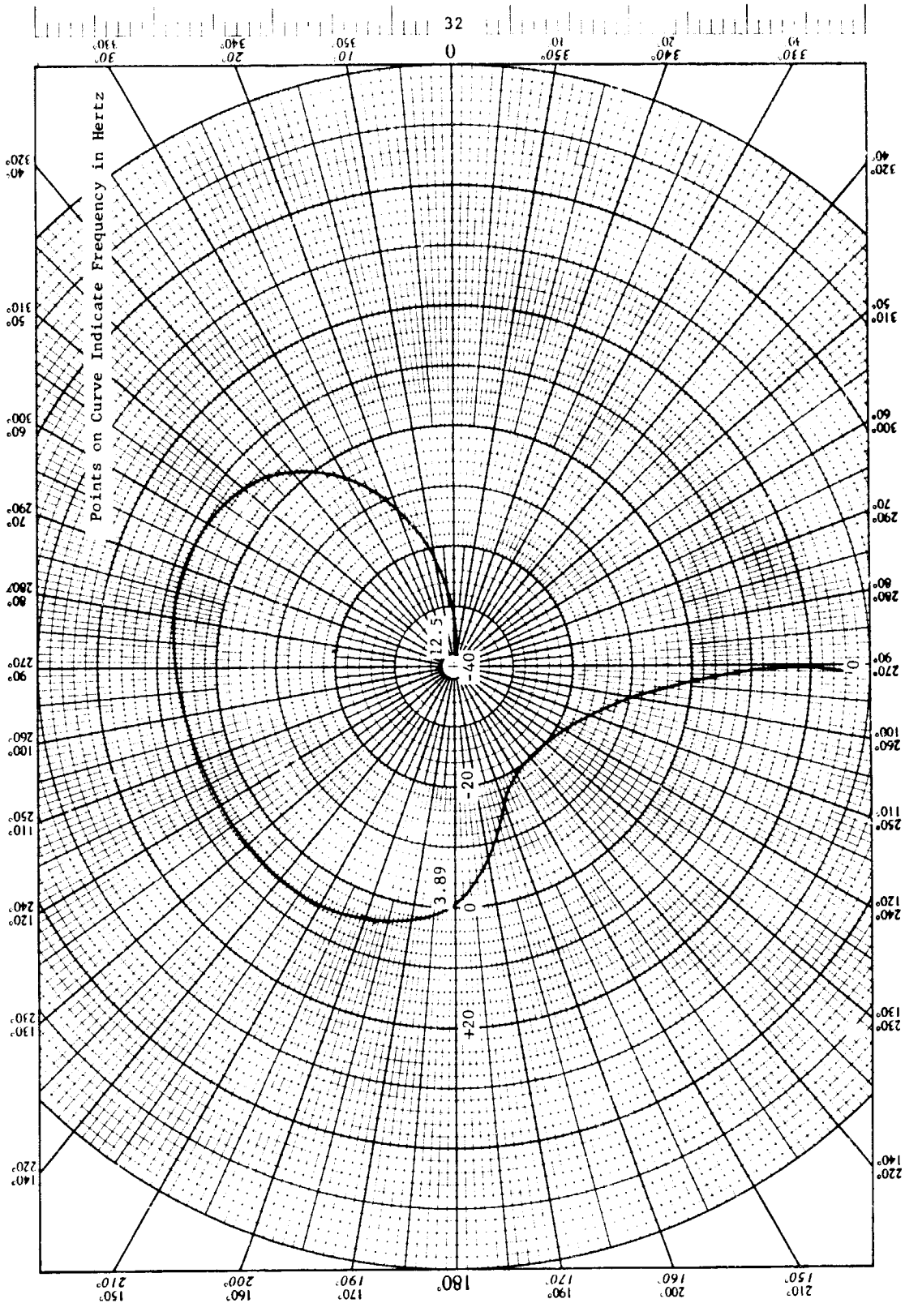


Fig. 14--Nyquist diagram of system broken in $\phi$ channel with marginal gain as determined by system broken in $\beta_c$ channel

the negative of (32) as a function of $\omega$. The Fortran IV computer program given in Appendix B was used. The curve, however, differed from the exact Nyquist by only .05 db and 0.3 degrees at $\omega = \omega_s/2$ and could not be plotted as a separate curve. This indicates that the effects of the harmonics generated by the sampler in the $\Phi$ channel can be considered negligible for the low-pass system described by (31).

The accuracy of the results obtained above can be determined by adjusting the gain of $W_{ss}$ so that the system is marginally stable. Since, as shown in Appendix D, the system of Figure 1 has the same characteristic equation regardless of where it is broken, the open-loop Nyquist diagram of the system broken at $\Phi$ should also show marginal stability at the same gain for $W_{ss}$. The latter marginal gain may be determined by varying the gain of $W_{ss}$ until the Nyquist of the system broken in the $\Phi$ channel is marginally stable. This marginal gain is taken as the correct value because it is obtained by the conventional z-transform method of analysis.

As determined from Figure 13, the marginal gains are +30 db at zero hertz and -28.3 db at 3.9 hertz. By substituting the transfer functions given in (31) into the negative open-loop transfer function of the system broken at $\Phi$, and by increasing the gain of $W_{ss}$ by 28.3 db, the Nyquist diagram in Figure 14 was obtained. This Nyquist diagram, however, shows marginal stability at the same frequency that the system broken in the

$\beta_c$ channel is marginally stable. Therefore, the new method of analysis yields accurate results for low-pass systems.

Analysis of high-pass system

The next system to be analyzed is a system having high-pass characteristics. The transfer functions of the system shown in Figure 1 are given by

$$G_1(s) = \frac{-s}{s^2 - 1000},$$

$$G_2(s) = \frac{-1}{s^2 - 1000},$$

$$W_{ss}(s) = \frac{625s(s + 1)}{(s^2 + s + 2500)(s + 10)}, \tag{33}$$

and

$$H_o(s) = \frac{1 - \epsilon^{-sT}}{s}.$$

The Nyquist diagram shown in curve A of Figure 15 was obtained by substituting (33) into (29) and by using the computer program in Appendix A. It is obvious from the Nyquist diagram that the system described by (33) has high-pass characteristics. Therefore, the harmonics generated by the sampler in the $\phi$ channel must be considered. The effects of these harmonics may be determined by comparing curve A

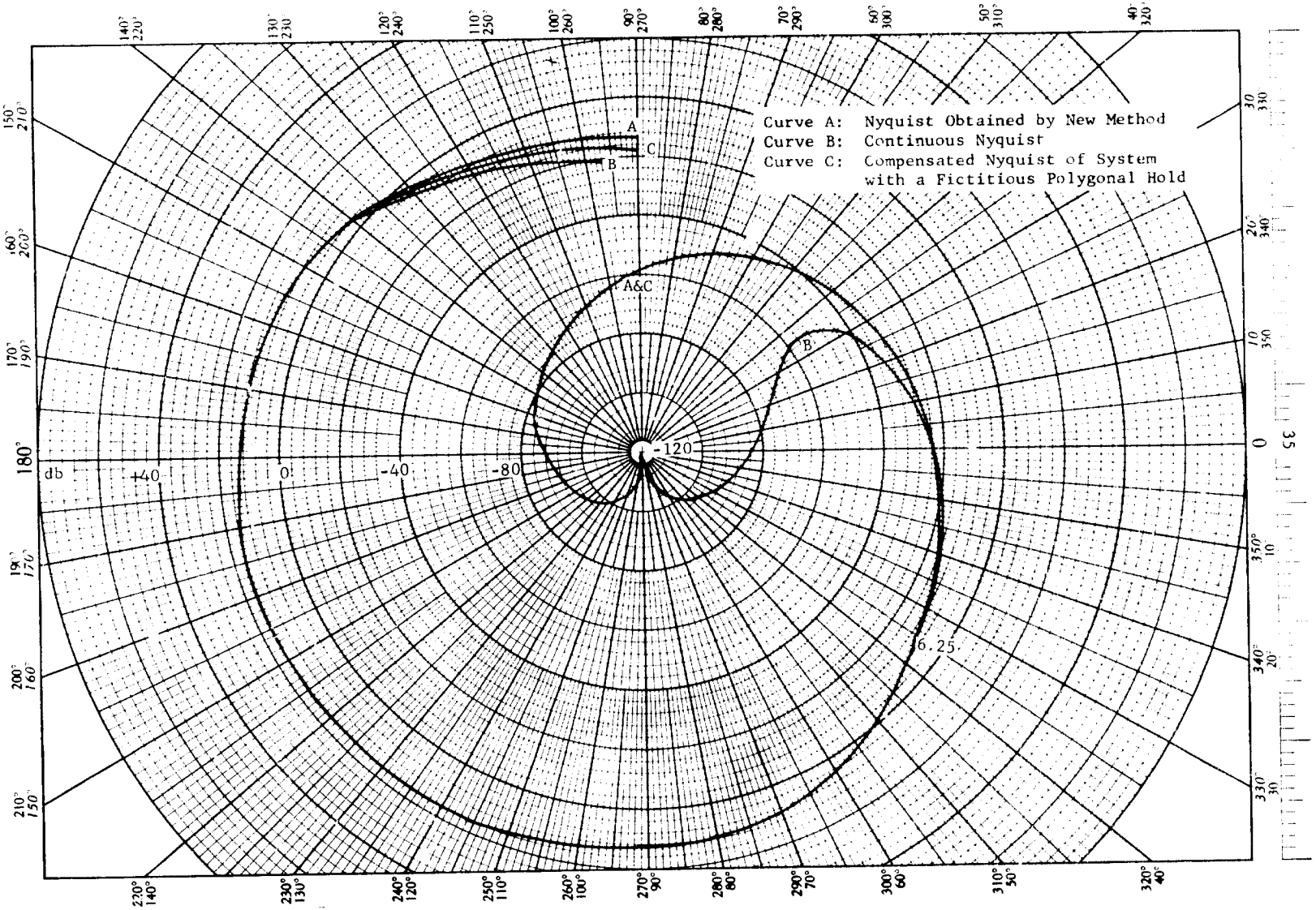


Fig. 15--Nyquist of system given by (33) broken in $\beta_c$ channel

of Figure 15 with the continuous Nyquist. Any difference between the two curves will be caused by the effects of the generated harmonics. By substituting (33) into the negative of (32), curve B of Figure 15 was obtained. The two curves correlate very well for frequencies greater than 6.25 hertz but do not correlate for frequencies below 6.25 hertz.

In order to investigate the accuracy of the Nyquist diagram, as obtained by using the ideal hold method of analysis and as shown by curve A of Figure 15, a Nyquist diagram must be obtained by using a fictitious hold with characteristics that very closely approximate the characteristics of the ideal hold. The zero-order hold, with a transfer function given by (34), is unsatisfactory because of the phase shift introduced and because of the low attenuation of the higher harmonics by the hold. The gain and phase responses of the zero-order hold as a function of the input frequency, $\omega$, are shown by curve A of Figure 16(a) and by Figure 16(b), respectively.[7] The transfer function of the zero-order hold is

$$H_o(s) = \frac{1 - \epsilon^{-sT}}{s} . \tag{34}$$

The polygonal hold, with a transfer function given by

$$H_p = \frac{\epsilon^{sT}(1 - \epsilon^{-sT})^2}{Ts^2}, \tag{35}$$

has characteristics that approximate the characteristics of the ideal hold. The characteristics of the ideal hold are shown in Figure 7

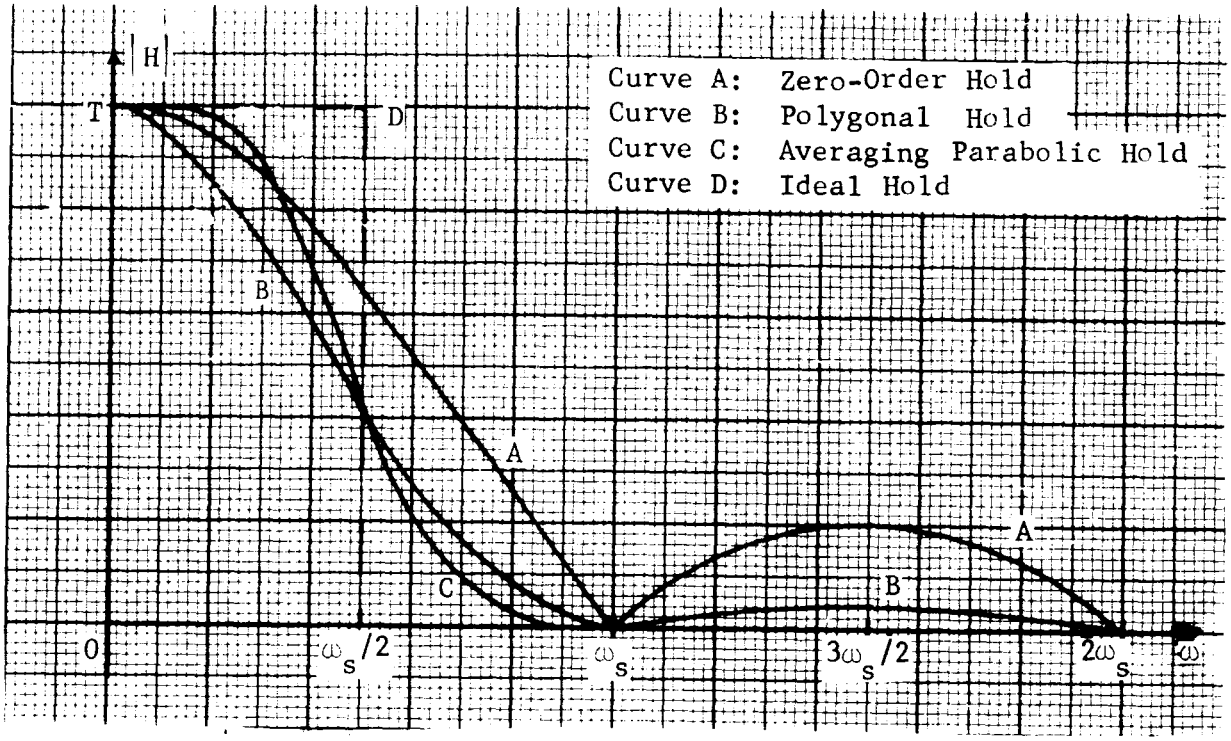


(a)

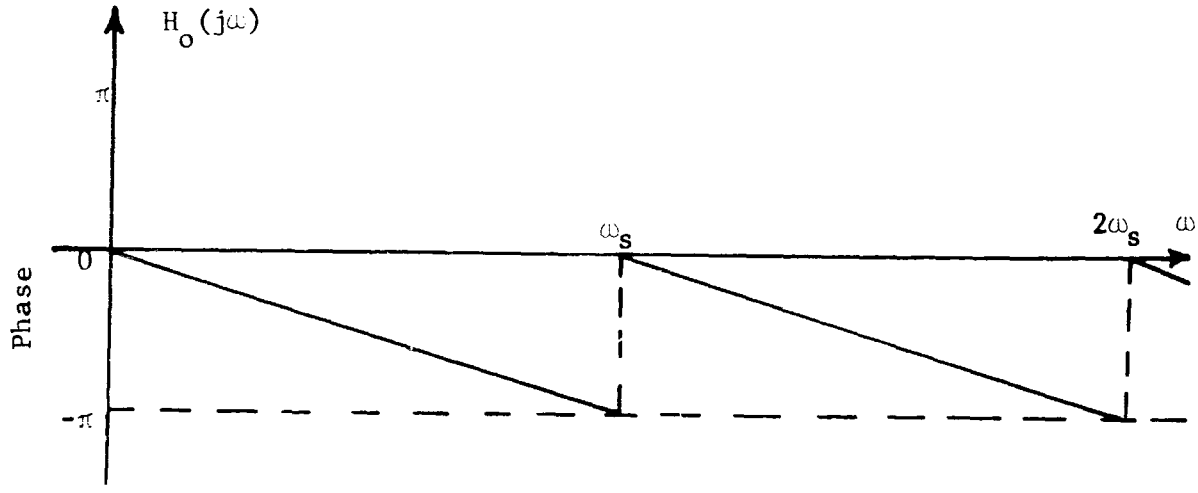


(b)

Fig. 16--Frequency responses of holds (a) Gain characteristics of zero-order hold, polygonal hold, averaging parabolic hold, and ideal hold. (b) Phase characteristics of zero-order hold

and have been redrawn in Figure 16, curve D, for comparison purposes. The polygonal hold, with gain characteristics as shown by curve B of Figure 16(a), introduces no phase shift and greatly attenuates the higher frequency harmonics introduced by the fictitious sampler. The fact that the polygonal hold requires a predictor and, therefore, is not physically realizeable causes no concern, since it is introduced fictitiously and is used only for analytical analysis.

The averaging parabolic hold, with a transfer function given by

$$H_A = \frac{\epsilon^{2sT}(1 - \epsilon^{-sT})\left[2(1 + \epsilon^{-sT}) - sT(1 - \epsilon^{-sT})\right]}{4s^3T^2} \tag{36}$$

and with gain characteristics as shown by curve C of Figure 16(a), gives a better approximation to the characteristics of the ideal hold.[8] Because of the complexity of its transfer function, however, the parabolic hold was not used as the fictitious hold.

Figure 17 shows the system in Figure 1, broken at $\beta_e$, with a fictitious sampler and fictitious polygonal hold in the $\phi$ channel. It is not necessary to introduce the fictitious sampler and hold in the $\dot{\phi}$ channel, because an open-loop transfer function can be written for this channel and is given by (27). The contribution to the output by the upper channel in Figure 17 is

$$X_{o_{Upper}}^*(s) = X_i^*(s)\left[G_1H_p^*(s)\right]\left[H_oW_{ss}^*(s)\right]. \tag{37}$$

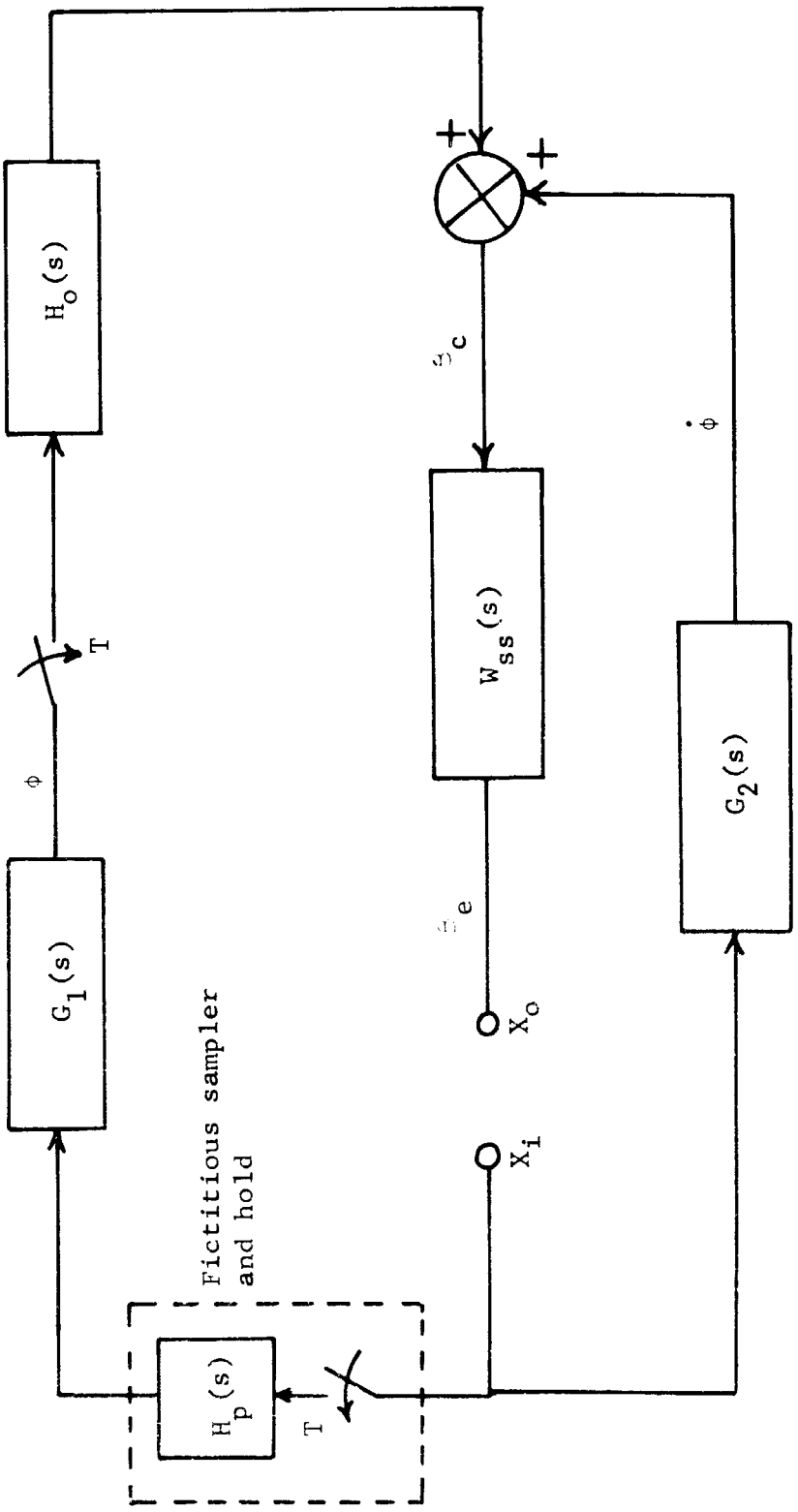


Fig. 17--System broken at $\mathcal{E}_e$ with fictitious sampler and polygonal hold in $\phi$ channel

The transfer function of the upper channel is therefore

$$\frac{X_o^*(s)}{X_i^*(s)} = \left[G_1H_p^*(s)\right]\left[H_oW_{ss}^*(s)\right], \tag{38}$$

which can be expressed in its frequency domain, infinite series representation as

$$\text{O.L.T.F.}_{\text{Upper}} = \left[\frac{1}{T}\sum_{n=-\infty}^{+\infty} G_1H_p(s + jn\omega_s)\right]\left[\frac{1}{T}\sum_{n=-\infty}^{+\infty} H_oW_{ss}(s + jn\omega_s)\right]. \tag{39}$$

The total open-loop transfer function is the sum of the transfer functions of the upper and lower loops and is given by (40).

$$\text{O.L.T.F.} = G_2W_{ss}(s) + \left[\frac{1}{T}\sum_{n=-\infty}^{+\infty} G_1H_p(s + jn\omega_s)\right]\left[\frac{1}{T}\sum_{n=-\infty}^{+\infty} H_oW_{ss}(s + jn\omega_s)\right] \tag{40}$$

Equation (40) will give an accurate Nyquist diagram in the low frequency range of the system in Figure 1 broken at $\beta_e$. A more accurate Nyquist diagram, however, can be obtained by considering the attenuation of the fundamental frequency component introduced by the fictitious polygonal hold. For an input frequency of $\omega_s/4$, for example, the fundamental component of the output of the fictitious sampler is attenuated 1.8 db by the fictitious polygonal hold and at $\omega_s/2$ by 7.5 db. This error can be compensated for by increasing the magnitude

of the fundamental frequency term by an amount equal to the attenuation of the polygonal hold as done by the computer program in Appendix C. The Nyquist diagram of the system expressed by the negative of (40), with the fundamental component of the upper loop compensated, is shown by curve C in Figure 15. For frequencies less than ten hertz, curve C of Figure 15 coorelates with curve A to within four significant figures in db and to within three significant figures in the angle. Therefore, it could not be plotted as a separate curve. The curve separation at frequencies slightly less than $\omega_s/2$ is caused by the second harmonic component, generated by the fictitious sampler, with a frequency slightly greater than $\omega_s/2$. The magnitude of this harmonic component is not negligible compared with the magnitude of the fundamental component.

Since the characteristics of the polygonal hold, with its fundamental output component compensated,closely approximate the characteristics of the ideal hold, curve C of Figure 15 is a good analytical check on the accuracy of the open-loop Nyquist diagram obtained by the new method of analysis. From the above results, it is concluded that the new method of analysis yields accurate results for both high and low-pass, open-loop systems.

Limitations of the new method of analysis

The accuracy of the new method in obtaining closed-loop Nyquist diagrams will be investigated in this section. In the first section of this chapter, the new method of analysis was shown to be very

accurate in determining gain and phase margins of low-pass systems. This section is concerned with the accuracy of the new method of analysis in determining gain and phase margins of systems that are not low-pass.

The transfer functions of the system in Figure 1 are given by

$$G_1(s) = \frac{-\ 0.94068468}{s^2\ -\ 0.02972784}\ ,$$

$$G_2(s) = \frac{-\ 0.94068468\ s}{s^2\ -\ 0.02972784}\ , \tag{41}$$

and

$$W_{ss}(s) = \frac{s}{s^2\ -\ 25{,}000}\ .$$

By substituting (41) into (29), the open-loop Nyquist diagram for the system broken at $\beta_e$ is obtained. This Nyquist, however, does not intersect the 180 degree axis. Therefore, the system has no gain margin. If $W_{ss}(s)$ is given by

$$W_{ss}(s) = \frac{s\ \epsilon^{j\pi/3}}{s^2\ -\ 25{,}000} \tag{42}$$

and if $G_1(s)$ and $G_2(s)$ are given by (41), the open-loop Nyquist diagram is shifted by sixty degrees, as shown by curve A of Figure 18. The continuous Nyquist for this system, obtained by substituting the

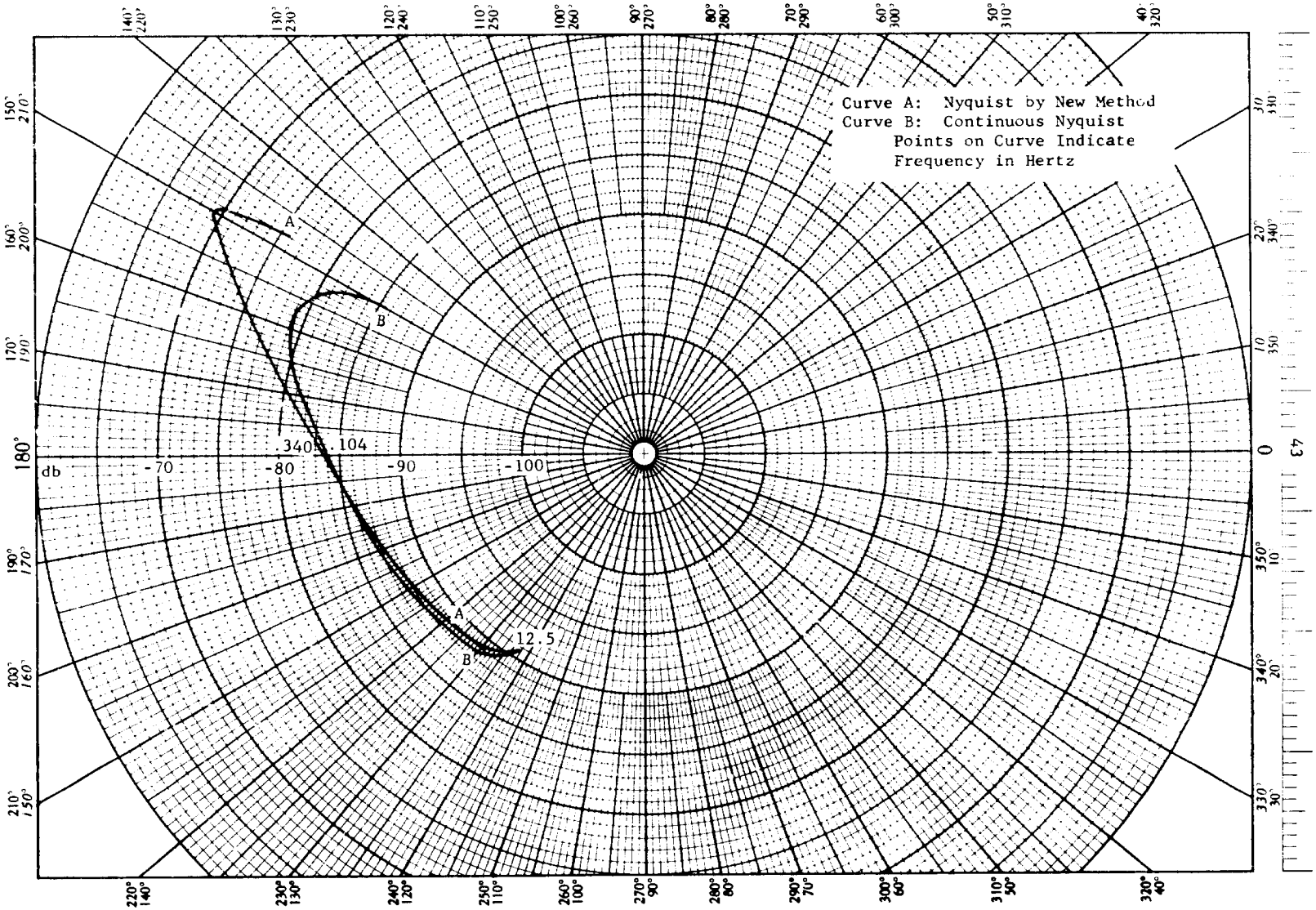


Fig. 18--Nyquist diagrams of system shown in Figure 1 broken in $\theta_c$ channel and described by (41) and (42)

above transfer functions into (32), is given in curve B of Figure 18. Both curves have a gain margin of approximately 88.6 db. The frequencies at which these gain margins are measured, however, are .104 hertz for the continuous system and .340 hertz for the sampled system.

The correct frequency at which the system will oscillate, when it is marginally stable, is obtained by increasing the gain of $W_{ss}(s)$ by 88.6 db and then by obtaining the Nyquist diagram of the system broken in the $\phi$ channel. This Nyquist, shown in Figure 19, is obtained by substituting the gain of $W_{ss}(s)$ and the transfer functions given by (41) and (42) into the negative of (2) and by using the digital computer program in Appendix A. From Figure 19, the correct frequency at which the system will oscillate, when it is marginally stable, is .104 hertz.

The above results indicate that, although both the continuous Nyquist and the Nyquist obtained by the new method of analysis give the correct gain margin, only the continuous Nyquist gives the correct frequency at which the gain margin is measured. This inaccuracy in the new method of analysis is caused by the high-pass nature of $W_{ss}(s)$. The sampler preceding $W_{ss}(s)$ generates harmonic frequency components that are not filtered out entirely by $H_o(s)$ and $W_{ss}(s)$. These components are present at the output of the open-loop system. The new method of analysis presented in this paper includes the effects of these components whereas the continuous analysis does not. When

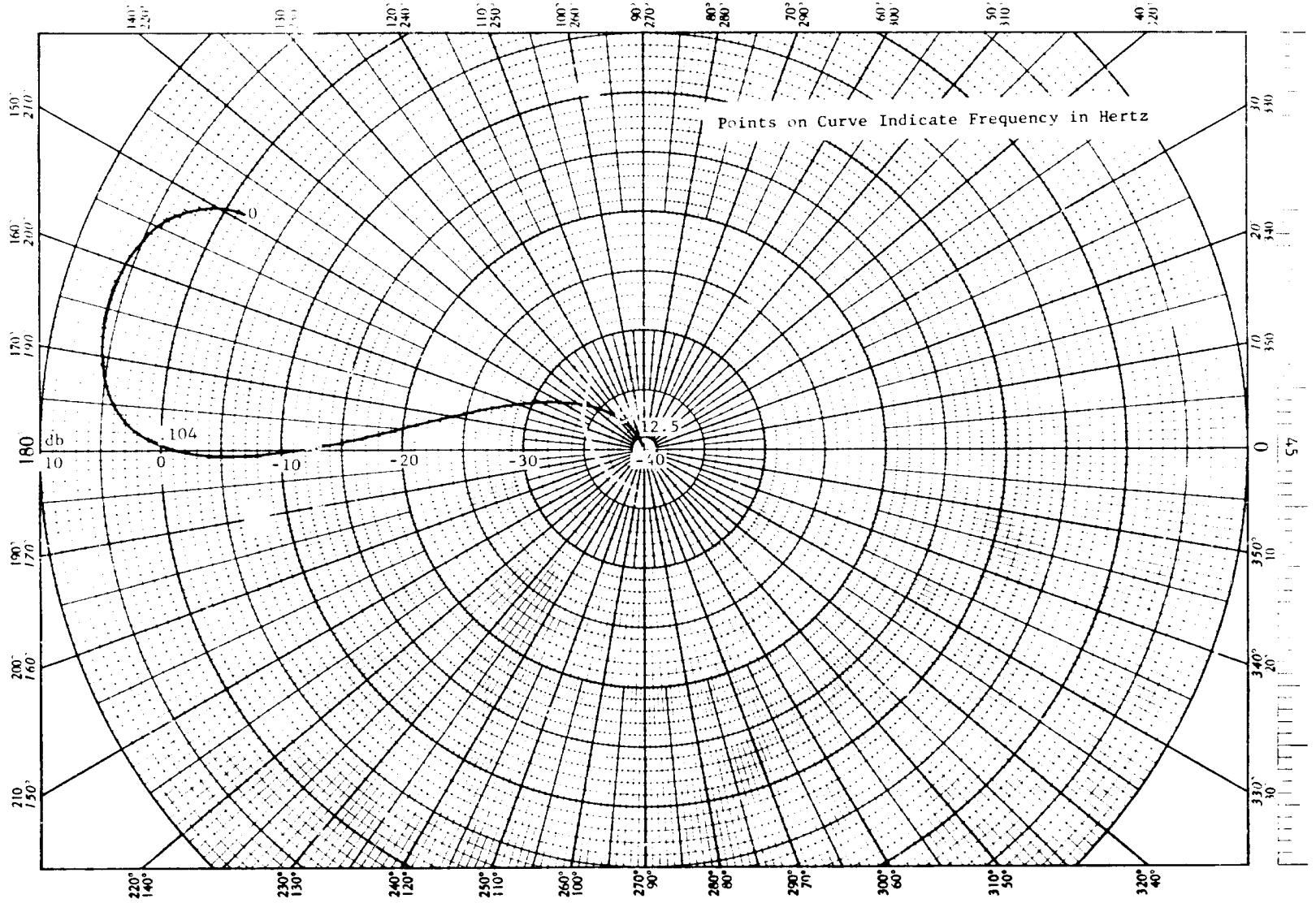


Fig. 19--Nyquist of system described by (41) and (42), broken at $\Phi$

the system is closed, however, all of the harmonic components are filtered out by the ideal hold, leading to inaccuracies in the new method of analysis when analyzing closed-loop, high-pass systems. The continuous Nyquist yields accurate results for this particular example because, when the open-loop system is closed, all of the harmonic components are filtered out by the low-pass transfer functions in the remainder of the system. If the remainder of the system were high-pass, the continuous Nyquist would also have led to inaccurate results.

# VI. INVESTIGATION OF NUMERICAL ACCURACY OF ANALYSIS IN W-PLANE

In this chapter an investigation is made of the accuracy of Nyquist diagrams obtained from a contour in the z-plane as compared to those obtained from a contour in the w-plane. The sampled-data control system chosen for the investigation is shown in Figure 21. The particular transfer functions shown below along with the polygonal hold were chosen because the Nyquist diagram obtained from the path around the unit circle in the z-plane became erratic at frequencies above 3 hertz. It was felt that if more accurate results can be obtained by using a Nyquist path in the w-plane, the increased accuracy would become evident in this example.

$$G_1(s) = \frac{-.94068468}{s^2 - 0.029727836},$$

$$G_2(s) = \frac{-\ 0.94068468\ s}{s^2 - 0.029727836}, \qquad (43)$$

$$W_{ss}(s) = \frac{625}{s\ \ + 25s + 625},$$

and

$$H_p(s) = \frac{\epsilon^{sT}(1 - \epsilon^{-sT})^2}{Ts^2}$$

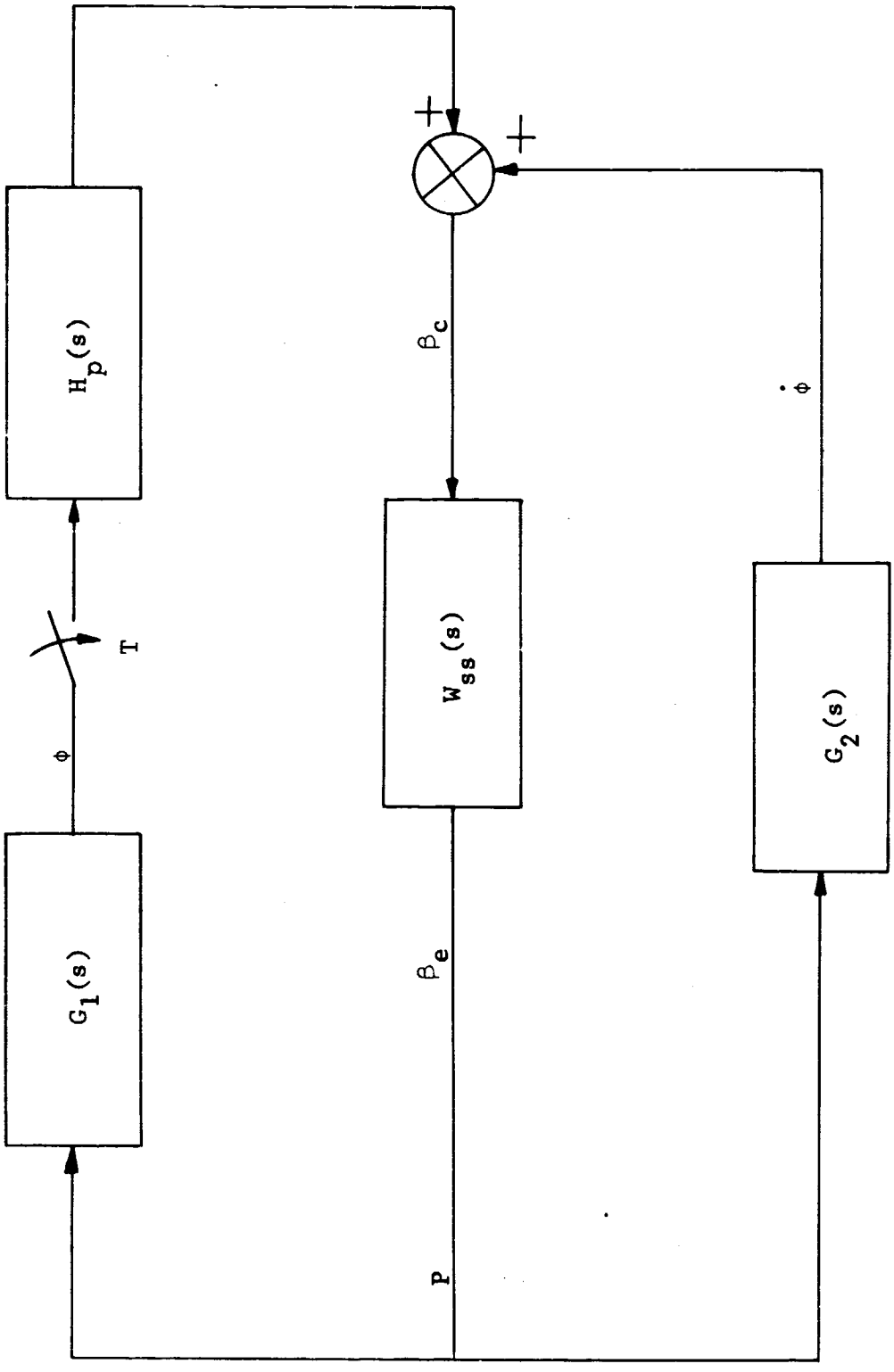


Fig.21--Sampled-data control system.

The open-loop transfer function of the system in Figure 21 broken at $\phi$ was derived in Chapter II, and, from (2), is

$$O.L.T.F.^{*}(s) = \left[\frac{H_p G_1 W_{ss}(s)}{1 - G_2 W_{ss}(s)}\right]^{*} . \tag{44}$$

Substituting (43) into (44) and simplifying yields

$$O.L.T.F.^{*}(s) = \left[\frac{14{,}698.198(\epsilon^{sT} - 2 + \epsilon^{-sT})}{s^2(s^4+25s^3+ 624.97027s^2+587.1847s-18.579900)}\right] \tag{45}$$

The z-transform of (45) is

$$O.L.T.F.(z) = HOLD\ (z)\Big[ RTOT1\ (z) + RTOT2\ (z) + RTOT3\ (z) + RTOT4\ (z) + RTOT5\ (z)\Big] \tag{46}$$

where

$$HOLD(z) = \frac{(z - 1)^2}{zT} ,$$

$$RTOT1(z) = \frac{- 791.08032Tz}{(z - 1)^2}$$

$$RTOT2(z) = \frac{- 25000.679z}{z - 1},$$

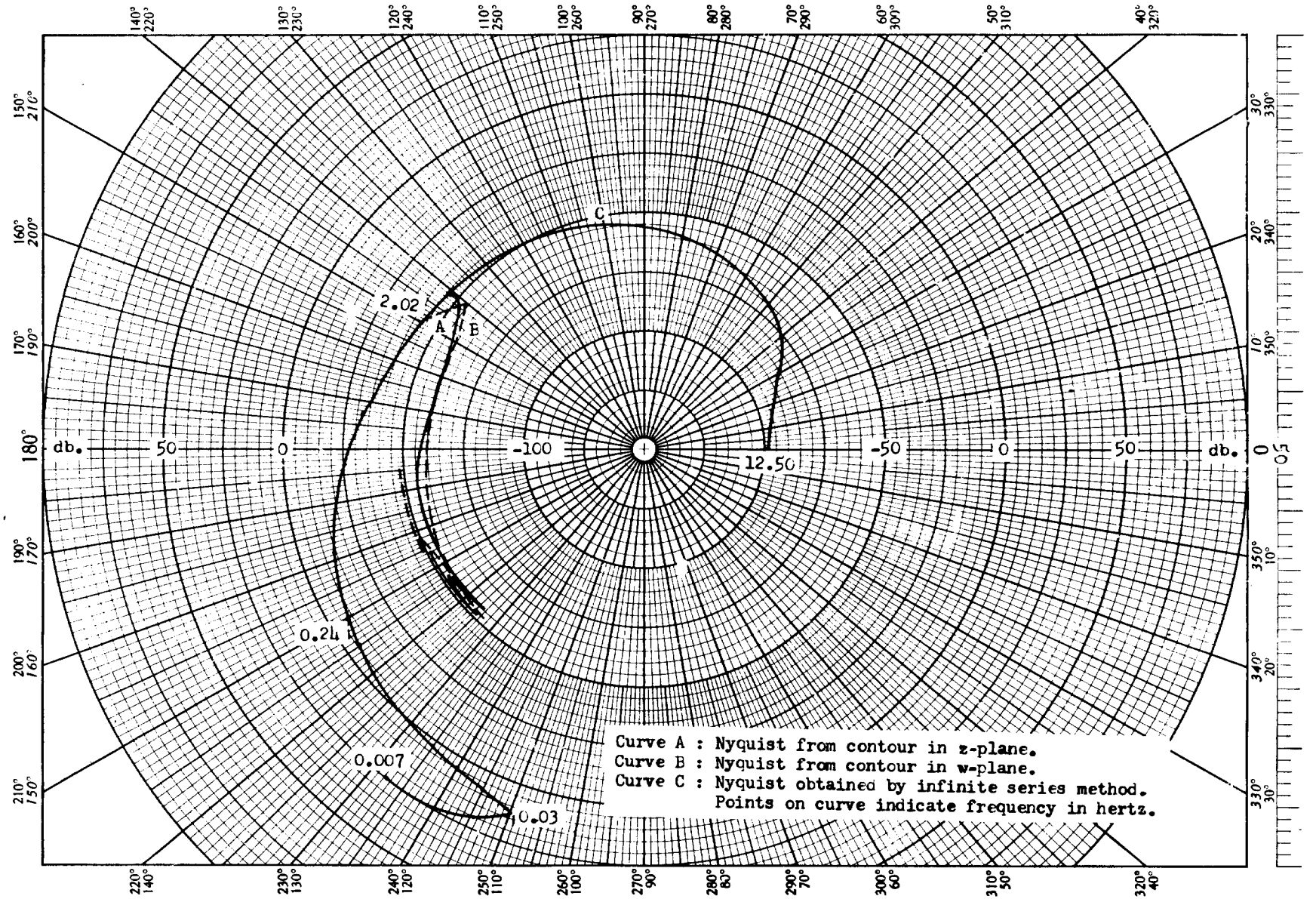


Fig. 22 - - Nyquist diagrams of system shown in Figure 21, broken at ø.

$$\text{RTOT3}(z) = \frac{25024.761z}{z - 1.0012264} \quad ,$$

$$\text{RTOT4}(z) = \frac{- 24.079914z}{z - 0.96048047} \quad , \tag{47}$$

and

$$\text{RTOT5}(z) = \frac{- .0017510774(z^2 + 0.62627080z)}{z^2 - 0.81143327z + 0.38254692} \quad .$$

The Nyquist diagram of (47) substituted into (46) is shown by curve A in Figure 22. The Nyquist diagram, however, became so erratic at frequencies above 3 hertz that it could not be plotted.

Making the bilateral substitution

$$z = \frac{1 + w}{1 - w} \quad , \tag{48}$$

(47) becomes

$$\text{HOLD}(w) = \frac{4w^2}{(1 - w^2)T} \quad ,$$

$$\text{RTOT1}(w) = \frac{- 791.08032(1 - w^2)T}{4w^2} \quad ,$$

$$RTOT2(w) = \frac{-25000.679(1+w)}{2w},$$

$$RTOT3(w) = \frac{25024.761(1+w)}{2.0012264w - 0.0012264} \tag{49}$$

$$RTOT4(w) = \frac{-24.079914(1+w)}{1.9604805w + 0.03951953},$$

and

$$RTOT5(w) = \frac{-0.0017510774\left[(1+w)^2 + 0.62627080(1-w^2)\right]}{(1+w)^2 - 0.81143327(1-w^2) + 0.38254692(1-w)^2}.$$

The Nyquist diagram of (49) substituted into (46) agrees very closely with the Nyquist diagram of (47) substituted into (46) in the low frequency range and is just as erratic above 3 hertz. This Nyquist diagram is shown in curve B of Figure 22.

In order to investigate the relative accuracy of the two Nyquist diagrams obtained above, the terms in (47) and (49) were broken down into their real and imaginary parts and printed out in a digital computer program. Table 2, page 107, gives this data for frequencies of 0.34722222 hertz, 6.250 hertz, and 12.50 hertz. As can be seen from the data at 0.34722222 hertz, the real and imaginary parts of the HOLD and RTOT terms correlate out to the eighth significant figure except for the imaginary parts of RTOT1 and HOLD and except for the real part of RTOT3 which does not correlate in the sixth significant

figure because the constant in the denominator of RTOT3(w) contains only five significant figures. The imaginary parts of RTOT1 and HOLD should be zero. It is seen that in cases where the imaginary part of the function is zero, the w-plane Nyquist gives the most accurate results. It is pointed out that in this program and in other programs used in the accuracy investigation of the w-plane Nyquist, the case where the imaginary part of the function is zero is the only case where the w-plane Nyquist yielded more accurate results. This is not to say, however, that if the investigation were continued, more cases could not be found.

The reason for the erratic behavior of the Nyquist diagram above 3 hertz can be determined by investigating the sum of the real and imaginary parts of the RTOT terms at 6.25 hertz. The sum of the real parts of the RTOT terms is 0.0023 and the sum of the imaginary parts of the RTOT terms is 0.0012. The first significant figure of the sum corresponds to the last significant figure of several of the individual terms. Since the last significant figures of these terms were rounded off by the computer, it is easy to see that the erratic behavior of the Nyquist diagrams is due to lack of significant figures.

In order to obtain a more accurate Nyquist diagram by the z-transform method, it is necessary to increase the number of significant figures in the Nyquist program, in the s-plane to z-plane transformation program, and in the partial fraction and root solving program in the s-plane. This represents a considerable amount of time and effort.

A more accurate method of computing the Nyquist diagram without having to increase the number of significant figures is given below.

Expressing (44) in its infinite series-frequency domain expansion yields

$$\text{O.L.T.F.}^*(s) = \frac{1}{T}\sum_{n=-\infty}^{\infty} \text{O.L.T.F.}\ (s + jn\omega_s)$$

$$= \frac{1}{T}\sum_{n=-\infty}^{+\infty} \frac{H_p G_1 W_{ss}(s + jn\omega_s)}{1 - G_2 W_{ss}(s + jn\omega_s)} \quad . \tag{50}$$

If the system under consideration is low-pass, only a few terms of (50) will be necessary in order to obtain accurate results. Substituting (43) into (50) and taking twenty terms of (50) yield the Nyquist diagram shown in curve C of Figure 22. This Nyquist diagram correlates with the z-plane and w-plane Nyquists up to approximately 2.1 hertz. It is pointed out that the Nyquist obtained by the infinite series method does not become erratic in the upper frequency range. The accuracy of the infinite series Nyquist was checked by using eighty terms of (50). The output obtained was identical to the output using only twenty terms of (50) out to eight significant figures in the magnitude expressed in db and to eight significant figures in the angle. It was therefore concluded that the Nyquist diagram shown in curve C of Figure 22 is accurate.

From the above results it is concluded that only a very slight increase in accuracy, if any, can be realized by going to the w-plane. The Nyquist diagram can, however, be accurately computed in single precision by using the infinite series-frequency domain method of analysis.

## VII. APPROXIMATE TRANSFER FUNCTION USING THE DESCRIBING FUNCTION

The describing function approach was used to obtain Nyquist diagrams for the system of Figure 23 which has compensation in the $\phi$ channel. The describing function approach was described in the Second Technical report, dated May 28, 1965. The object of this investigation was to obtain data which can be compared with results obtained by the Marshall Space Flight Center in order to determine the accuracy of the describing function approach. Two cases were considered. For the first case, $a_o$ and $a_1$ were equal to one. For the second case, $a_o$ and $a_1$ were equal to 0.5. The transfer functions used were

$$H_o = \frac{1}{T}(1 - e^{-Ts})/s \tag{51}$$

$$G1R(s) = \frac{-0.94068468}{s^2 - 0.02972784} \tag{52}$$

$$G1B1(s) = \frac{0.0065323138(s^2 + 498.59362)}{s^2 + 0.064905305s + 42.126986} \tag{53}$$

$$G1B2(s) = \frac{-0.0040378959(s^2 + 485.48033)}{s^2 + 0.12013450s + 144.32299} \tag{54}$$

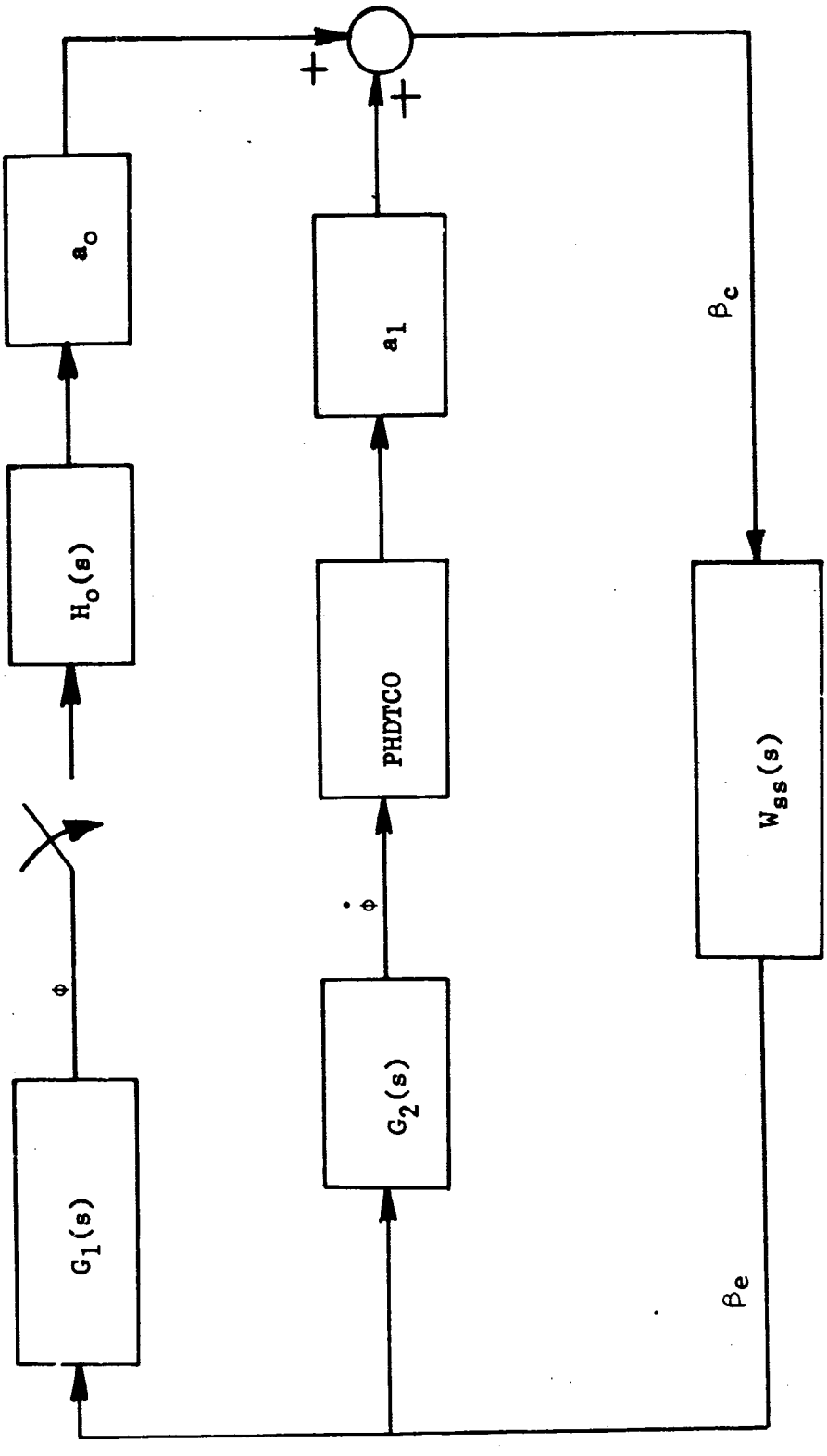


Fig. 23--Sampled-data control system with compensation

$$G1B3(s) = \frac{-0.0053896739(s^2 + 470.36052)}{s^2 + 0.1837817s + 337.76255} \quad (55)$$

$$G1B4(s) = \frac{0.0058368238(s^2 + 469.03256)}{s^2 + 0.22481237s + 505.40603} \quad (56)$$

$$G2R(s) = s(G1R(s)) \quad (57)$$

$$G2B1(s) = s(G1B1(s)) \quad (58)$$

$$G2B2(s) = s(G1B2(s)) \quad (59)$$

$$G2B3(s) = s(G1B3(s)) \quad (60)$$

$$G2B4(s) = s(G1B4(s)) \quad (61)$$

$$W_{ss} = \frac{625}{s^2 + 25s + 625} \quad (62)$$

$$PHDTC0 = \frac{0.33747 \times 10^{-8}s^8 + 0.57852 \times 10^{-7}s^7 + 0.32159 \times 10^{-5}s^6}{0.31188 \times 10^{-10}s^9 + 0.30536 \times 10^{-7}s^8 + 0.13131 \times 10^{-5}s^7} \text{ con't}$$

$$= \frac{+ 0.38442 \times 10^{-4}s^5 + 0.727818 \times 10^{-3}s^4 + 0.0069727s^3}{+ 0.33399 \times 10^{-4}s^6 + 0.59308 \times 10^{-3}s^5 + 0.0068924s^4} \text{ con't}$$

$$\frac{+ 0.055606s^2 + 0.38360s + 1.0}{+ 0.056518s^3 + 0.30188s^2 + 0.87623s + 1.0} \quad (63)$$

$$\phi \text{ open-loop} = \frac{a_o(G1R + G1B1 + G1B2 + G1B3 + G1B4)\ H_o W_{ss}}{1 - a_1 W_{ss}(G2R + G2B1 + G2B2 + G2B3 + G2B4)PHDTCO}\ (s) \qquad (64)$$

$$\dot{\phi} \text{ open-loop} = \frac{a_1 W_{ss}(G2R + G2B1 + G2B2 + G2B3 + G2B4)\ PHDTCO}{1 - a_o W_{ss}(G1R + G1B1 + G1B2 + G1B3 + G1B4)H_o}\ (s) \qquad (65)$$

$$\beta_c \text{ open-loop} = W_{ss}\left[a_1(G2R + G2B1 + G2B2 + G2B3 + G2B4)\ PHDTCO + a_o(G1R + G1B1 + G1B2 + G1B3 + G1B4)H_o\right]\ (s) \qquad (66)$$

The compensation in the $\dot{\phi}$ channel (PHDTCO) was furnished by D. P. Vallely, George C. Marshall Space Flight Center, National Aeronautics and Space Administration, R-ASTR-F, Huntsville, Alabama.

Figures 24, 25 and 26 are Nyquist diagrams of the system broken in the $\phi$, $\dot{\phi}$ and $\beta_c$ channels respectively, for $a_o$ and $a_1$ equal to one. The poles of the system broken in the $\phi$ channel are

$$s_1 = 0$$

$$s_2 = 0.5725$$

$$s_3 = -15.27$$

$$s_4 = 935.5$$

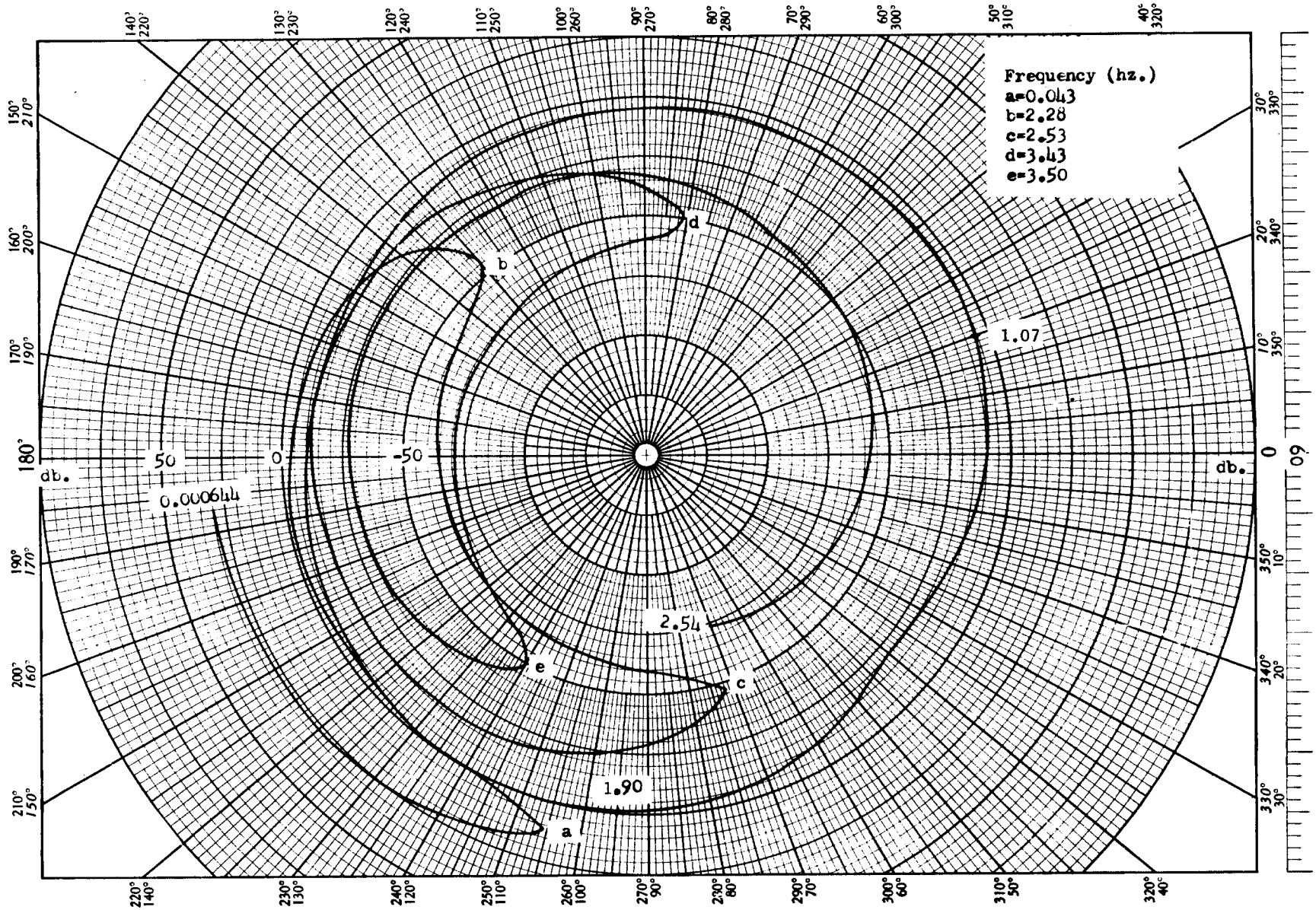


Fig. 24--Nyquist Diagram Broken in Φ Channel of the system shown in Fig. 23 with $a_o = a_1 = 1$

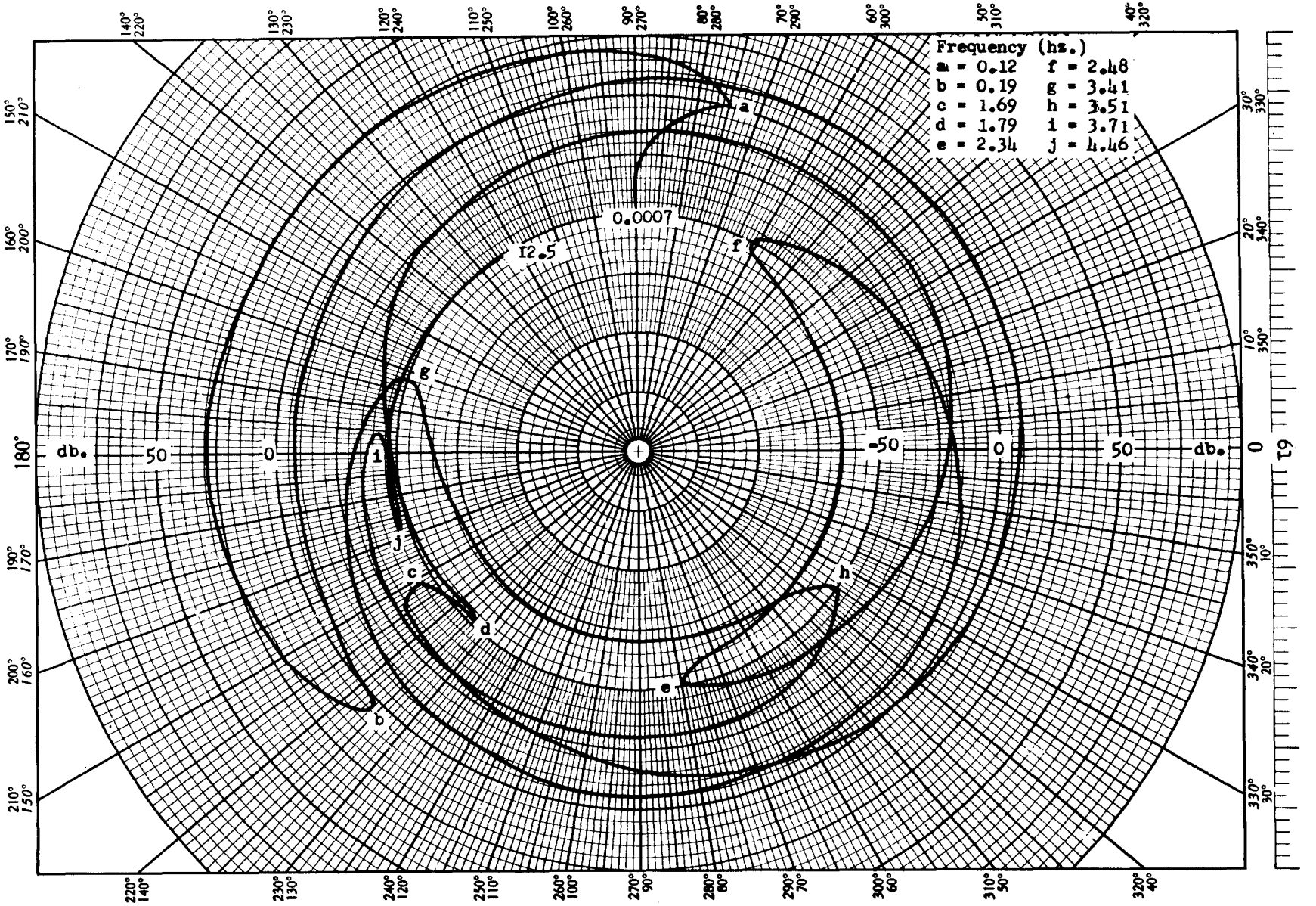


Fig. 25--Nyquist Diagram Broken in $\Phi$ Channel of the system shown in Fig. 23 with $a_o = a_1 = 1$

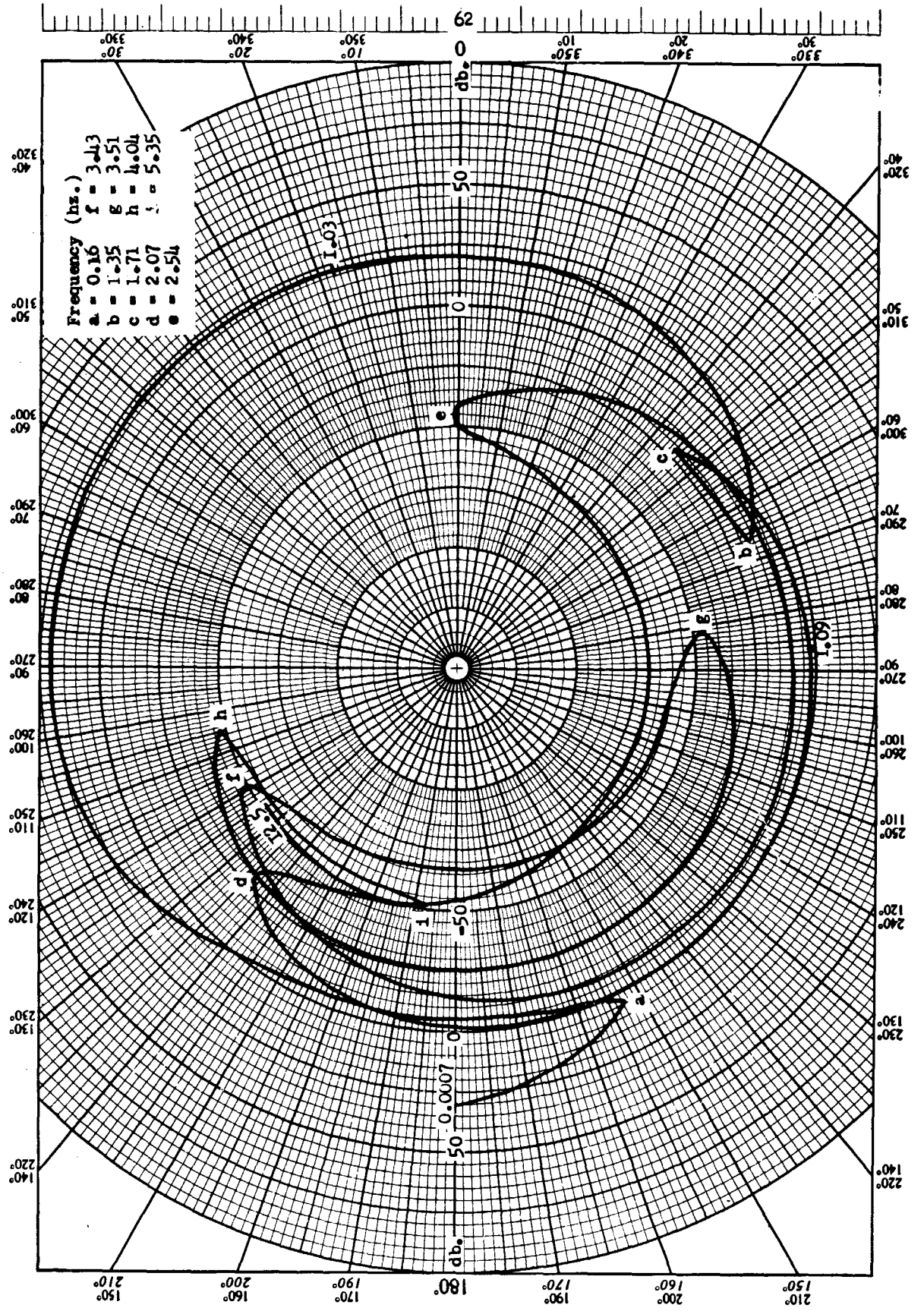


Fig. 26-- Nyquist Diagram Broken in $\beta_c$ Channel of the system shown in Fig. 23 with $a_o = a_1 = 1$

$s_5 = - 0.06310 + j12.01$

$s_6 = - 0.06310 - j12.01$

$s_7 = 0.09854 + j18.41$

$s_8 = - 0.09854 - j18.41$

$s_9 = - 0.1117 + j22.48$

$s_{10} = - 0.1117 - j22.48$

$s_{11} = - 0.5688 + j6.275$

$s_{12} = - 0.5688 - j6.275$

$s_{13} = - 1.278 + j2.230$

$s_{14} = - 1.278 - j2.230$

$s_{15} = - 3.244 + j8.660$

$s_{16} = - 3.244 - j8.660$

$s_{17} = - 3.890 + j16.29$

$s_{18} = - 3.890 - j16.29$

$s_{19} = - 5.412 + j1.241$

$s_{20} = - 5.412 - j1.241$

$s_{21} = -12.58 + j21.77$

$s_{22} = -12.58 - j21.77$

As can be seen from Figure 24, there is one encirclement of the 0 DB-180° point in the counterclockwise direction. From the above roots it is seen that there is one root in the right-half of the s-plane; this result was also checked with the Routh - Hurwitz criterion. This means that there are no poles of the closed-loop system in the right-half of the s-plane and that the system is stable.

Figures 27, 28 and 29 are Nyquist diagrams of the system broken in the $\phi$, $\dot{\phi}$ and $\beta_c$ channels respectively, for $a_o$ and $a_1$ equal to 0.5. The poles of the system broken in the $\phi$ channel are

$s_1 = 0.6106$

$s_2 = 0.0$

$s_3 = -15.71$

$s_4 = -935.4$

$s_5 = -0.06378 + j12.01$

$s_6 = -0.06278 - j12.01$

$s_7 = -0.09592 + j18.39$

$s_8 = -0.09592 - j18.39$

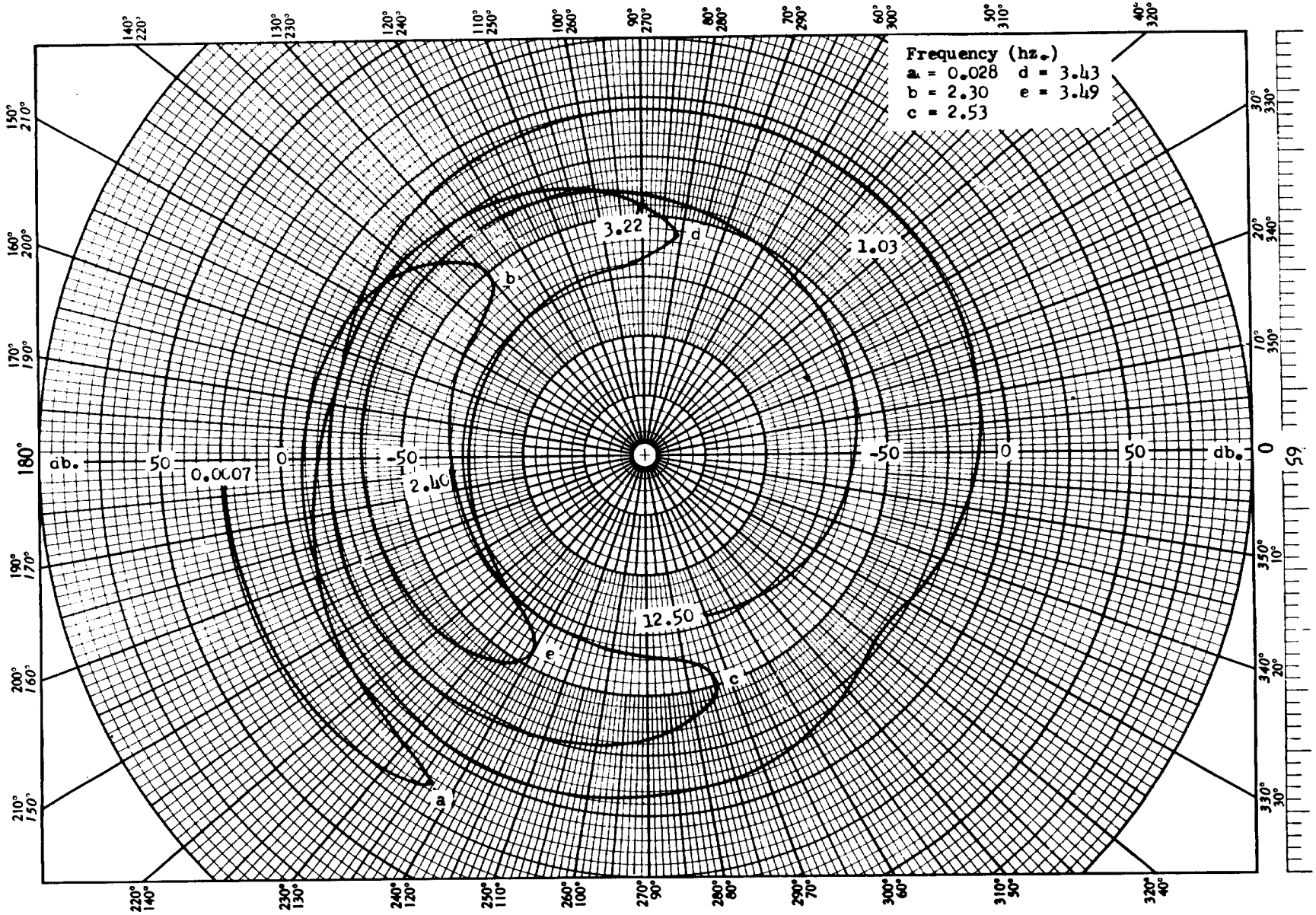


Fig. 27--Nyquist diagram broken in $\phi$ channel of the system shown in Figure 23 with $a_o = a_1 = 0.5$.

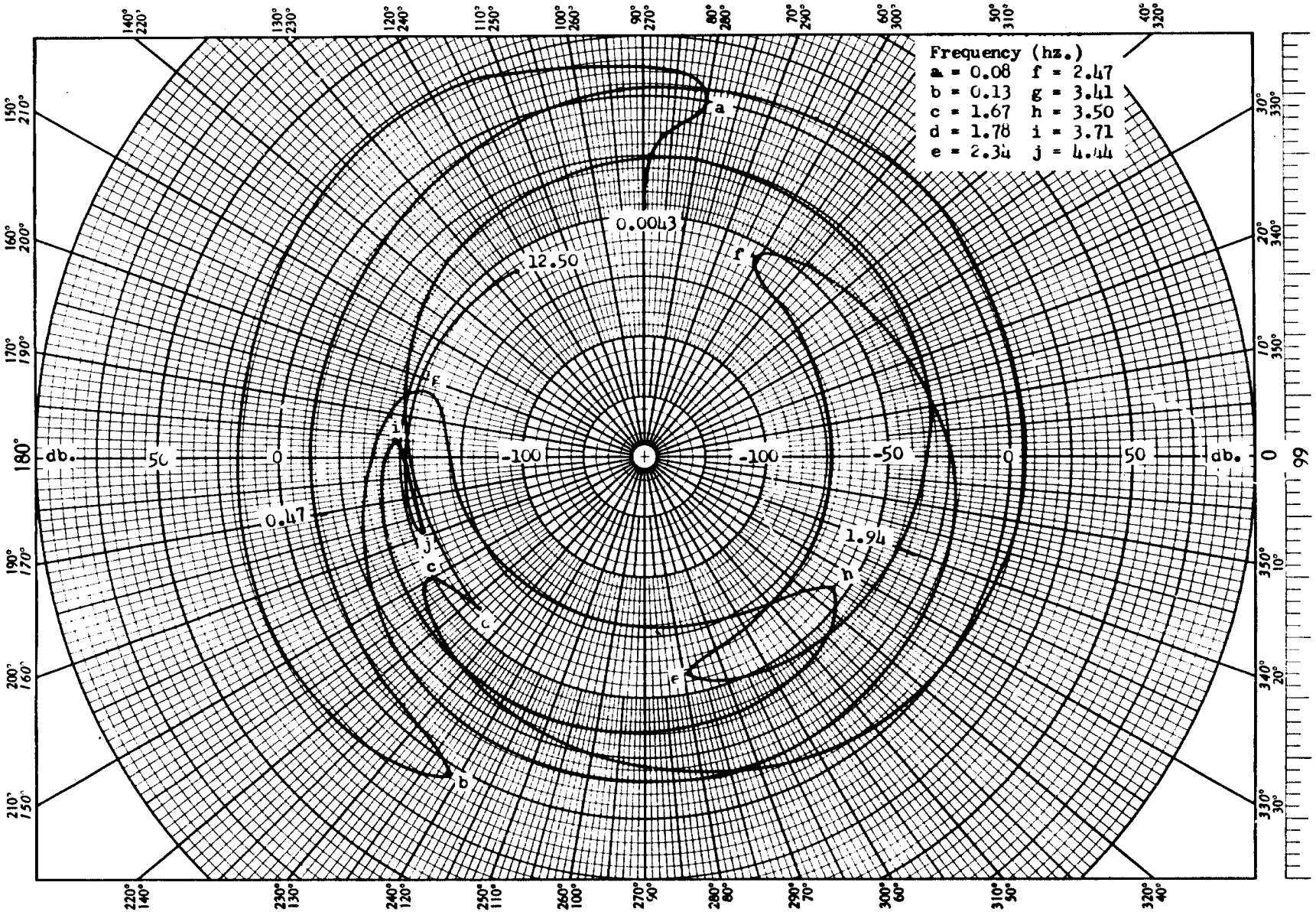


Fig. 28--Nyquist diagram broken in $\dot{\phi}$ channel of the system shown in Figure 23 with $a_o = a_1 = 0.5$.

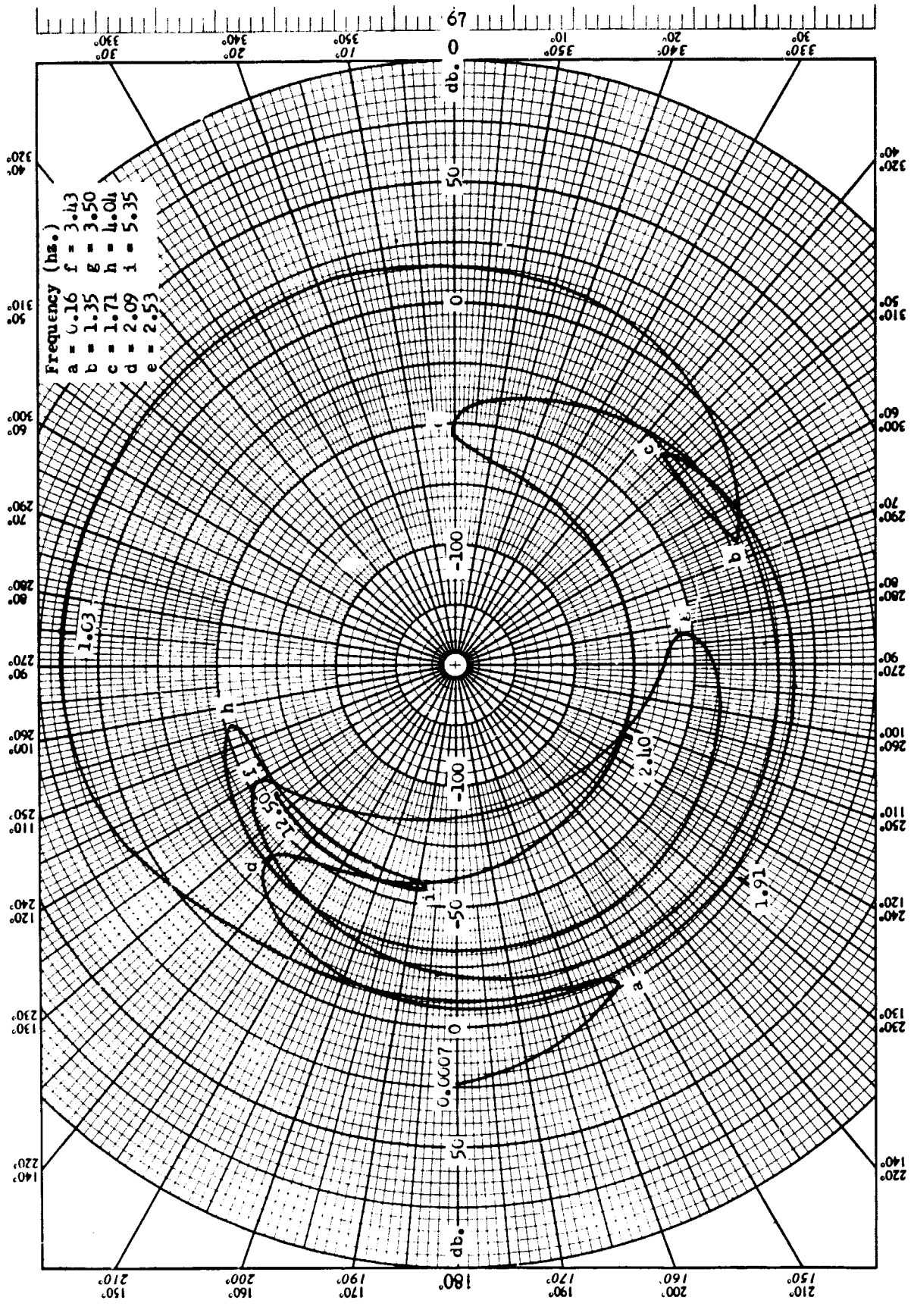


Fig. 29--Nyquist diagram broken in $\beta_c$ channel of the system shown in Figure 23 with $a_o = a_1 = 0.5$.

$s_9 = -0.1118 + j22.48$

$s_{10} = -0.1118 - j22.48$

$s_{11} = -0.2755 + j6.386$

$s_{12} = -0.2755 - j6.386$

$s_{13} = -1.420 + j1.620$

$s_{14} = -1.420 - j1.620$

$s_{15} = -3.261 + j8.885$

$s_{16} = -3.261 - j8.885$

$s_{17} = -3.928 + j16.32$

$s_{18} = -3.928 - j16.32$

$s_{19} = -5.408 + j1.182$

$s_{20} = -5.408 - j1.182$

$s_{21} = -12.54 + j21.71$

$s_{22} = -12.54 - j21.71$

As can be seen from Figure 27, there is one encirclement of the 0 db-180° point in the counterclockwise direction. From the above roots it is seen that there is one root in the right-half of the

s-plane. This result was also checked with the Routh-Hurwitz criterion. Thus, there are no poles of the closed-loop system in the right-half of the s-plane and that the system is stable. The gain margin is 8 db and the phase margin is 35 degrees in the $\phi$ channel.

## VIII. AN INVESTIGATION OF THE EFFECTS OF VARYING THE SAMPLING RATE IN THE $\phi$ CHANNEL

The describing function approach was used to investigate the effects of varying the sampling rate of the sampler in the $\phi$ channel of the system of Figure 23. For the investigation, $a_o$ and $a_1$ were chosen equal to 0.5, and PHDTCO, the compensating function, was set equal to one. The system functions used were those of (51) through (62). For the $\phi$ channel,

$$\phi_{\text{open-loop}} = \frac{(1/T)(1 - e^{-Ts})(0.919s^{10} + 0.464s^9 + 864.0s^8 + 382.8s^7}{s(s^{12} + 24.66^{11} + 167.0s^{10} + 0.2577x\ 10^5s^9 + 0.987 \times 10^6s^8} \text{ con't}$$

$$\frac{+ 0.354 \times 10^6s^6 + 0.107 \times 10^6s^5 + 0.925 \times 10^8s^4}{+ 0.833 \times 107s7 + 0.248 \times 10^9s^6 + 0.833 \times 10^9s^5 + 0.242 \times 10^{11}s^4} \text{ con't}$$

(67)

$$\frac{+ 0.912 \times 10^{10}s^2 - 0.103 \times 10^{10}s - 0.306 \times 10^{12}}{+ 0.190 \times 10^{11}s^3 + 0.649 \times 10^{12}s^2 + 0.305 \times 10^{12}s - 0.193 \times 10^{11})}$$

This transfer function was obtained by substituting (51) through (62) into into (64), with PHDTCO set equal to one.

Figures 30 through 47 are the Nyquist diagrams for the system broken in the $\phi$, $\dot{\phi}$, and $\beta_c$ channels for different values of T. It is

noted that the Nyquist diagrams of values of T of 0.01, 0.04, 0.08, and 0.1 seconds are approximately of the same form. It is also to be noted that since the describing function approach was used in this investigation, the accuracy of the Nyquist diagrams for $T > 0.1$ seconds is doubtful. For $T > 0.1$ seconds, $f_s/2$ is less than five cycles-per-second and the system is no longer low-pass with respect to $f_s/2$.

The roots of the denominator of $\phi_{open\text{-}loop}$ are

$s_1 = 0.4446$

$s_2 = 0.4556 - j6.381$

$s_3 = 0.4556 - j6.381$

$s_4 = 10.88 + j20.56$

$s_5 = 10.88 - j20.56$

$s_6 = 0.0$

$s_7 = - 0.6439$

$s_8 = - 0.2213 + j18.61$

$s_9 = - 0.2213 - j18.61$

$s_{10} = - 0.2402 + j12.13$

$s_{11} = - 0.2402 - j12.13$

$$s_{12} = -23.11 + j6.604$$

$$s_{13} = -23.11 - j6.604$$

As can be seen from (67) the poles of $\phi_{open\text{-}loop}$ do not change as T is changed so the above five roots of $\phi_{open\text{-}loop}$ in the right-half of the s-plane do not change. From Figures 7 through 24, it is seen that varying T does not give the needed encirclements of the 0 db-$180^{\circ}$ point necessary to stabilize the system. This investigation is not complete. Further work will be performed during the next month.

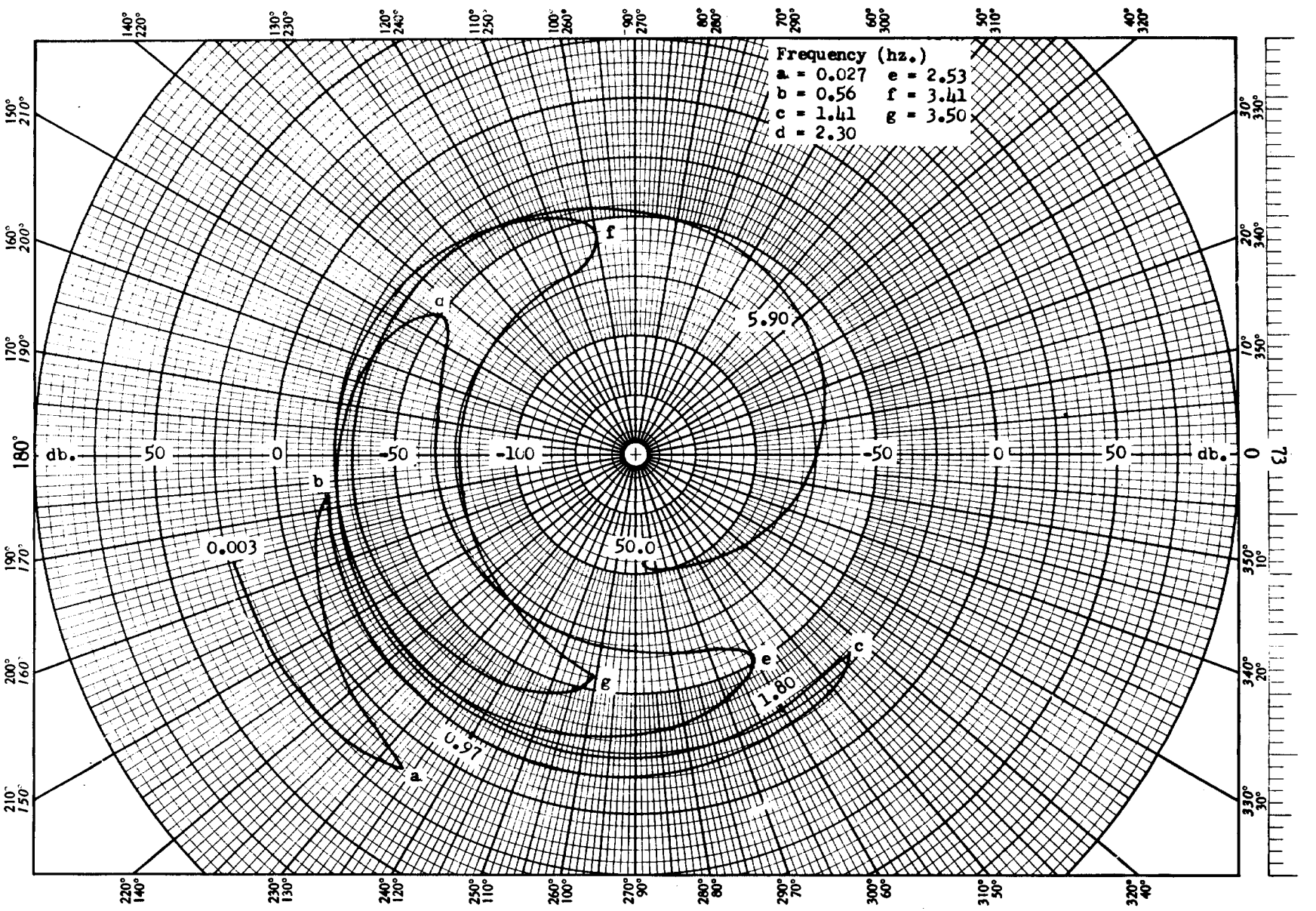


Fig. 30--Nyquist diagram broken in $\phi$ channel of system shown in Fig. 23, T = 0.01

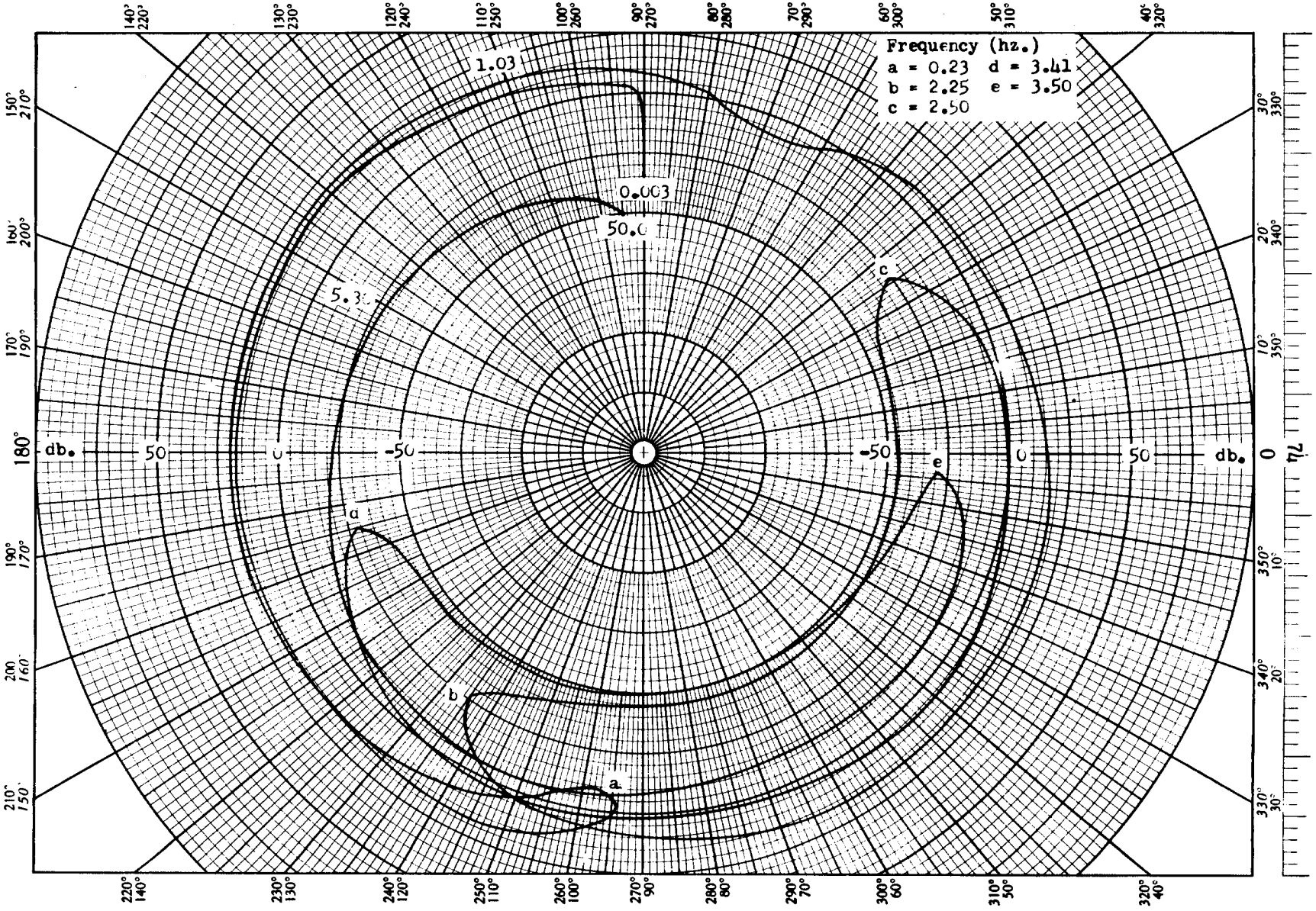


Fig. 31--Nyquist diagram broken in $\phi$ channel of system shown in Fig. 23, T = 0.01

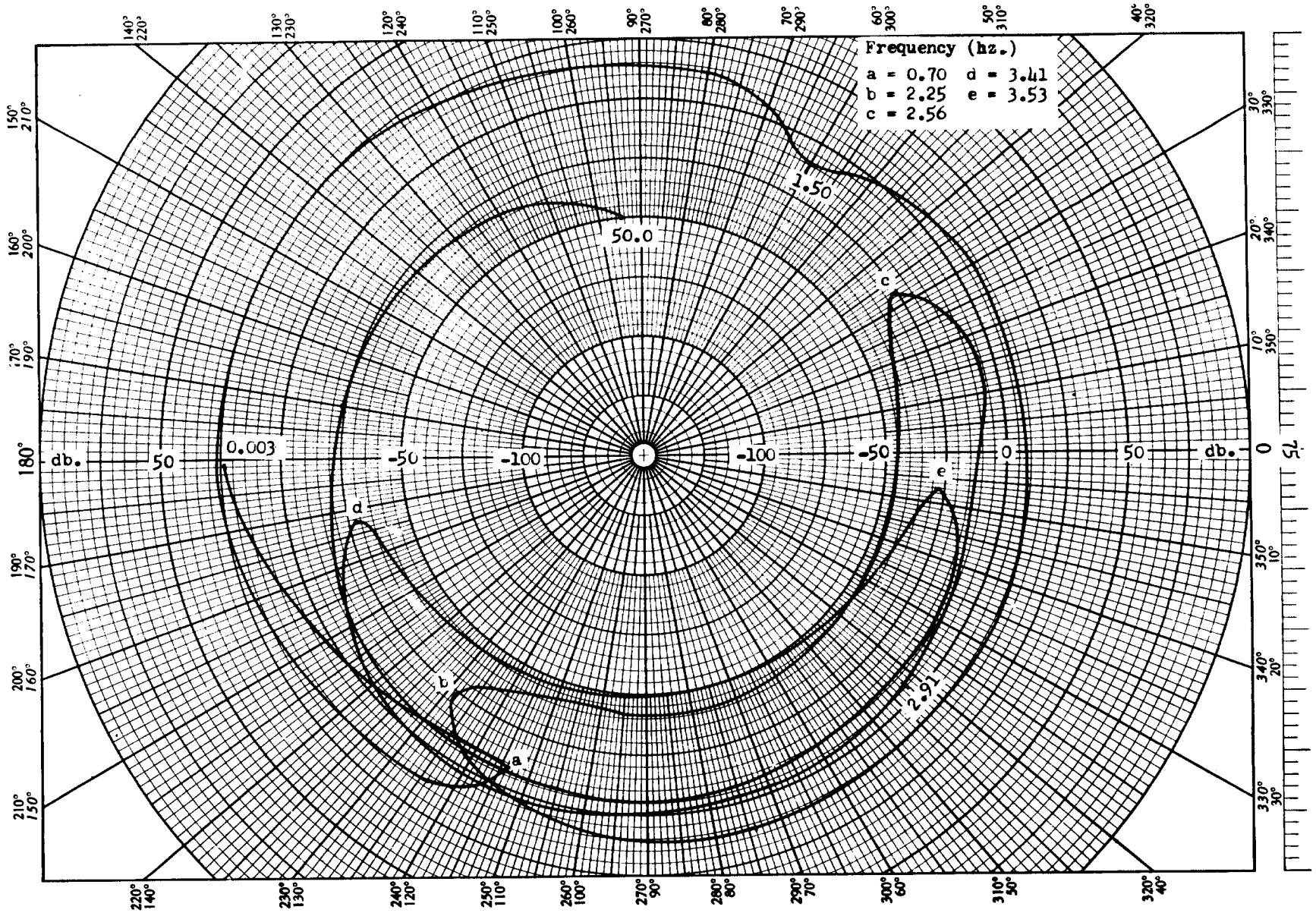


Fig. 32 --Nyquist diagram broken in $\beta_c$ channel of system shown in Fig. 23, T = 0.01

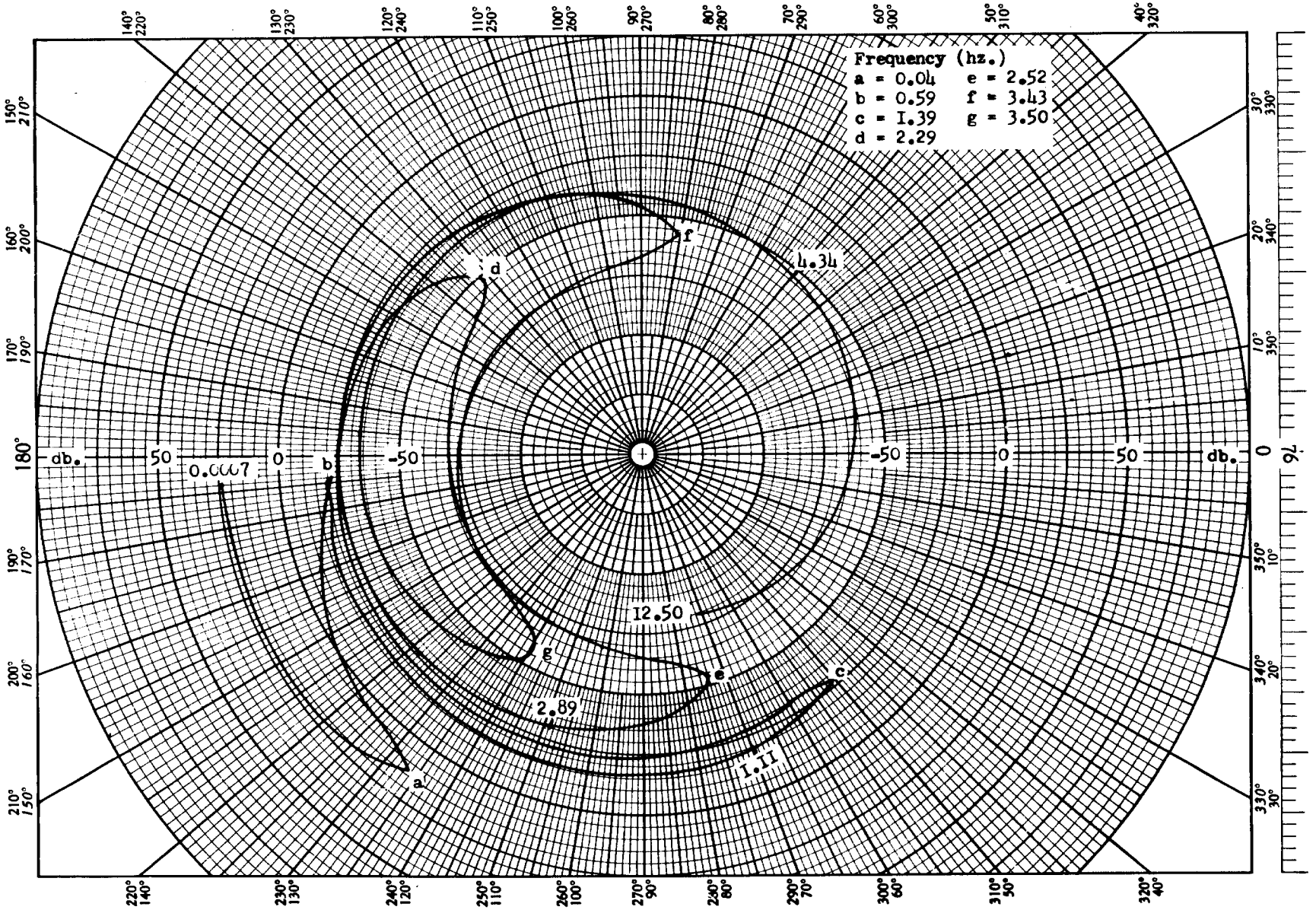


Fig. 33--Nyquist diagram broken in Φ channel of system shown in Fig. 23, T = 0.04

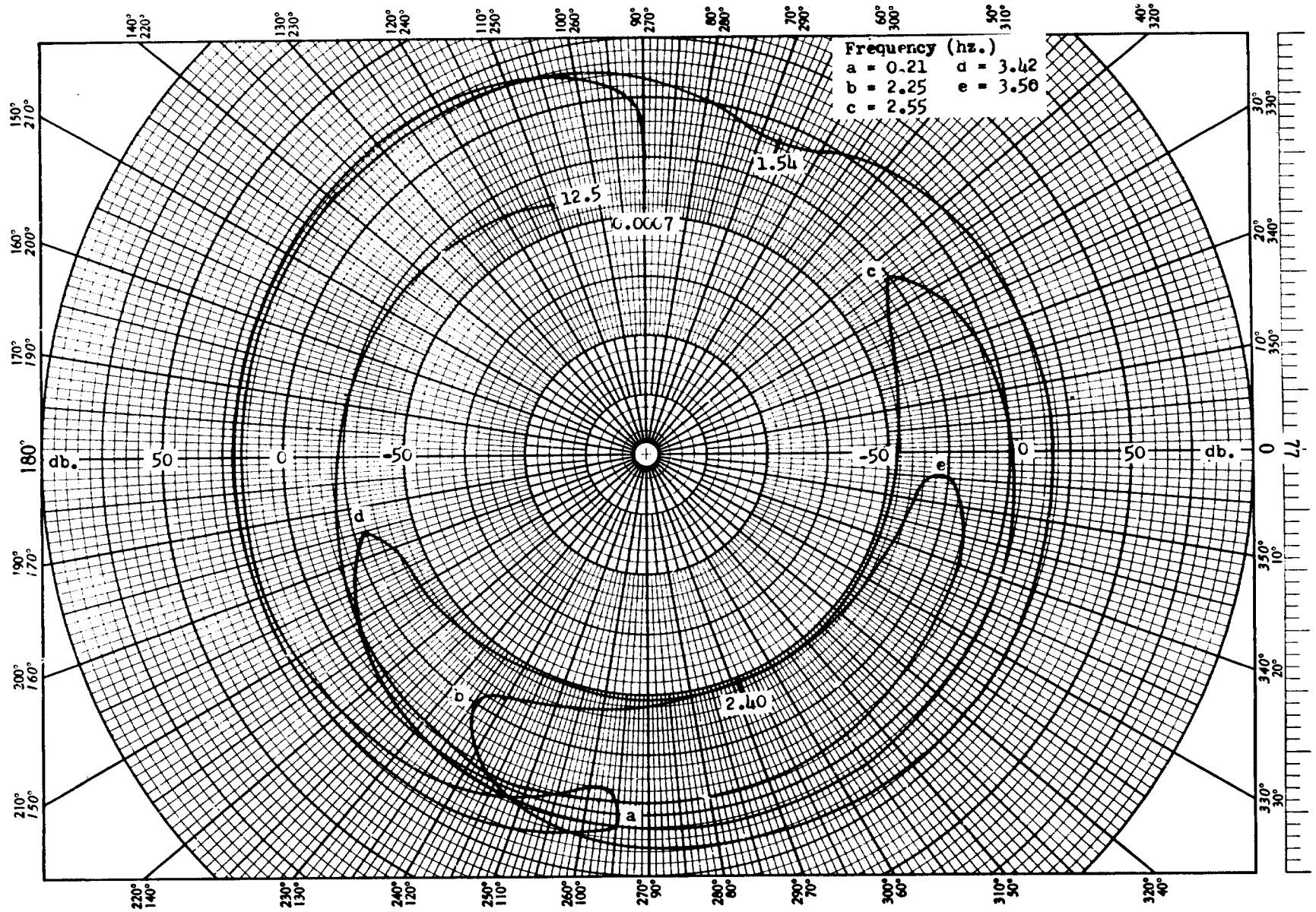


Fig. 34--Nyquist diagram broken in $\phi$ channel of system shown in Fig. 23, T = 0.04

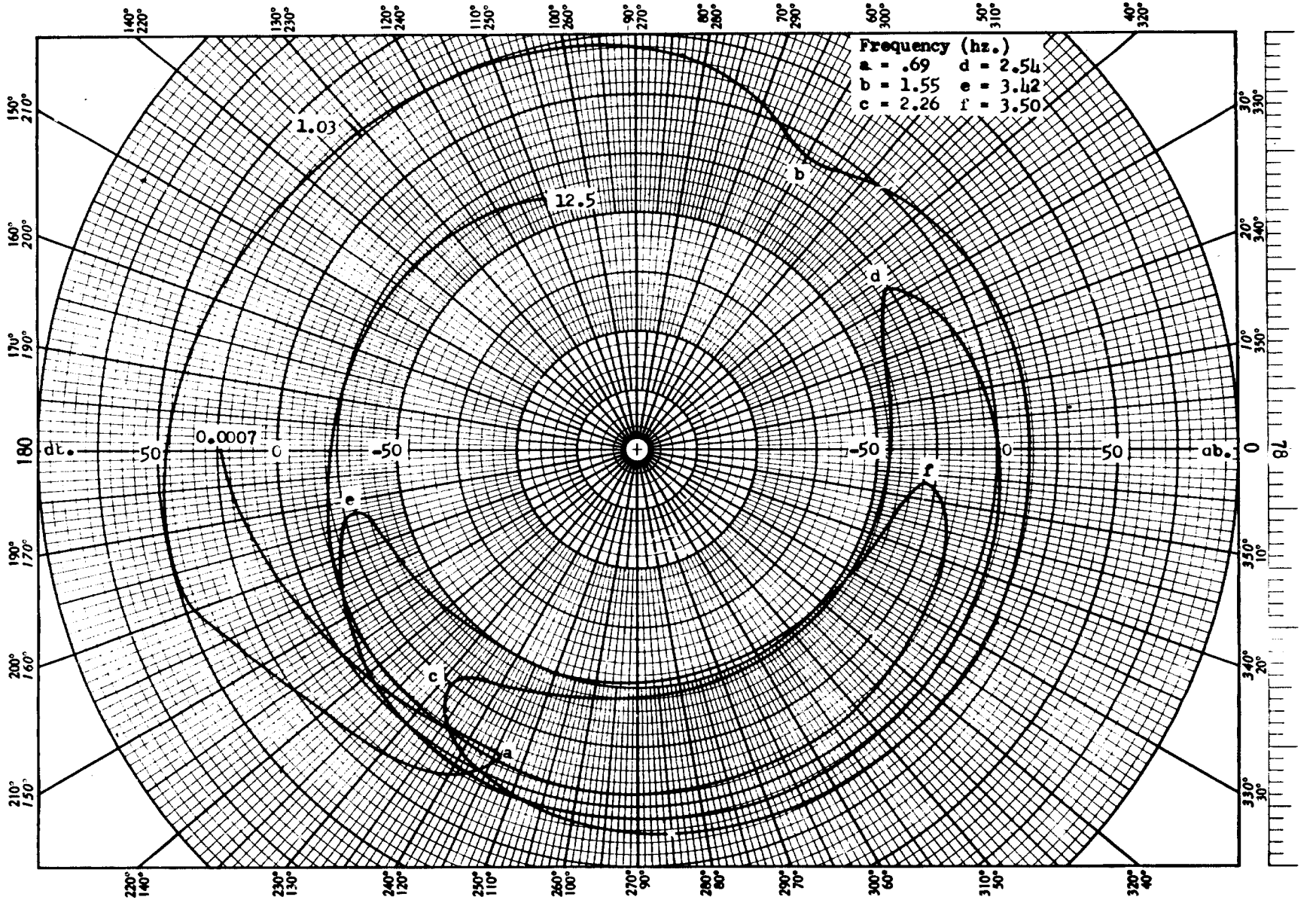


Fig. 35--Nyquist diagram broken in $\beta_c$ channel of system shown in Fig. 23, T = 0.04

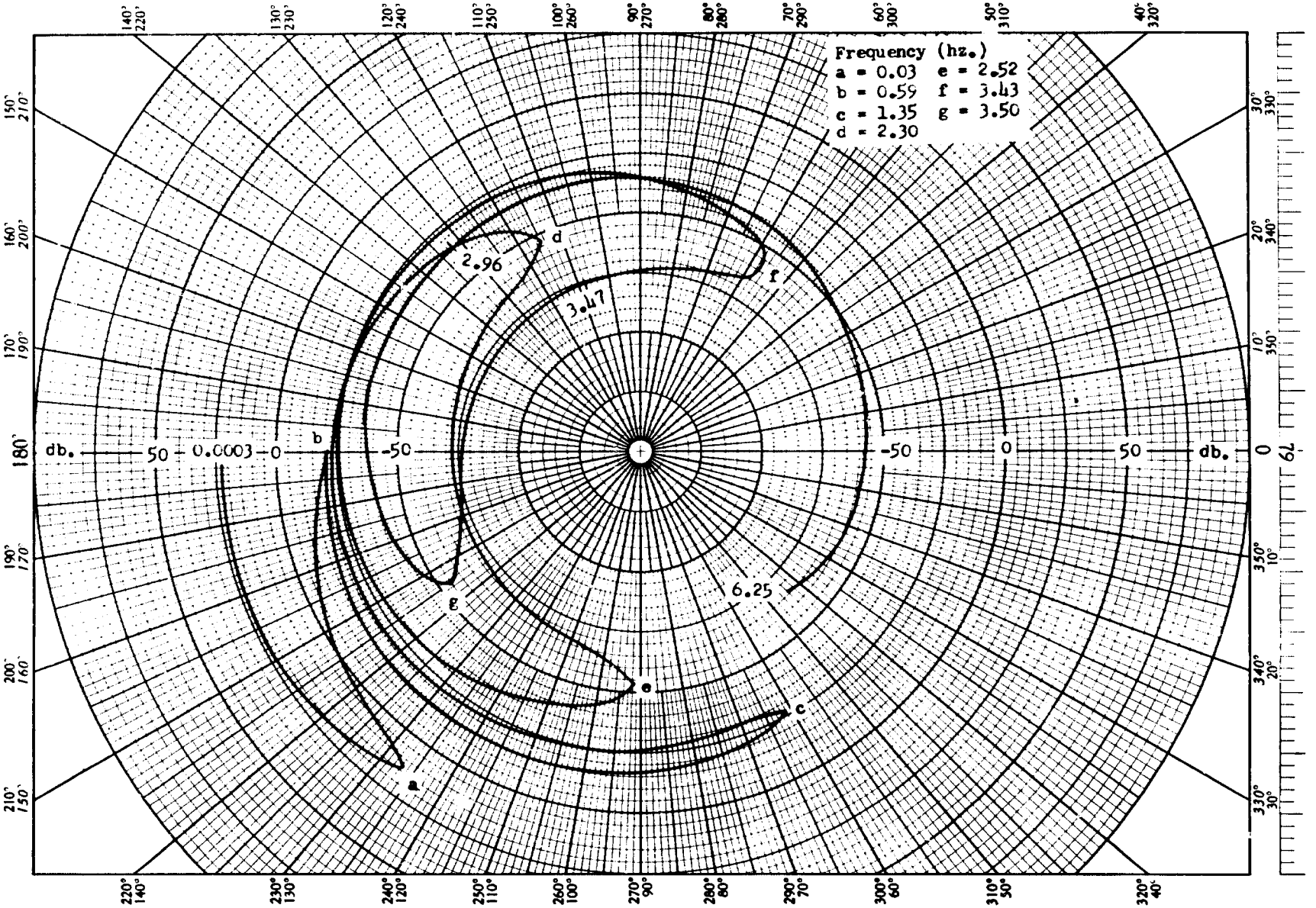


Fig. 36--Nyquist diagram broken in Φ channel of system shown in Fig. 23, T = 0.08

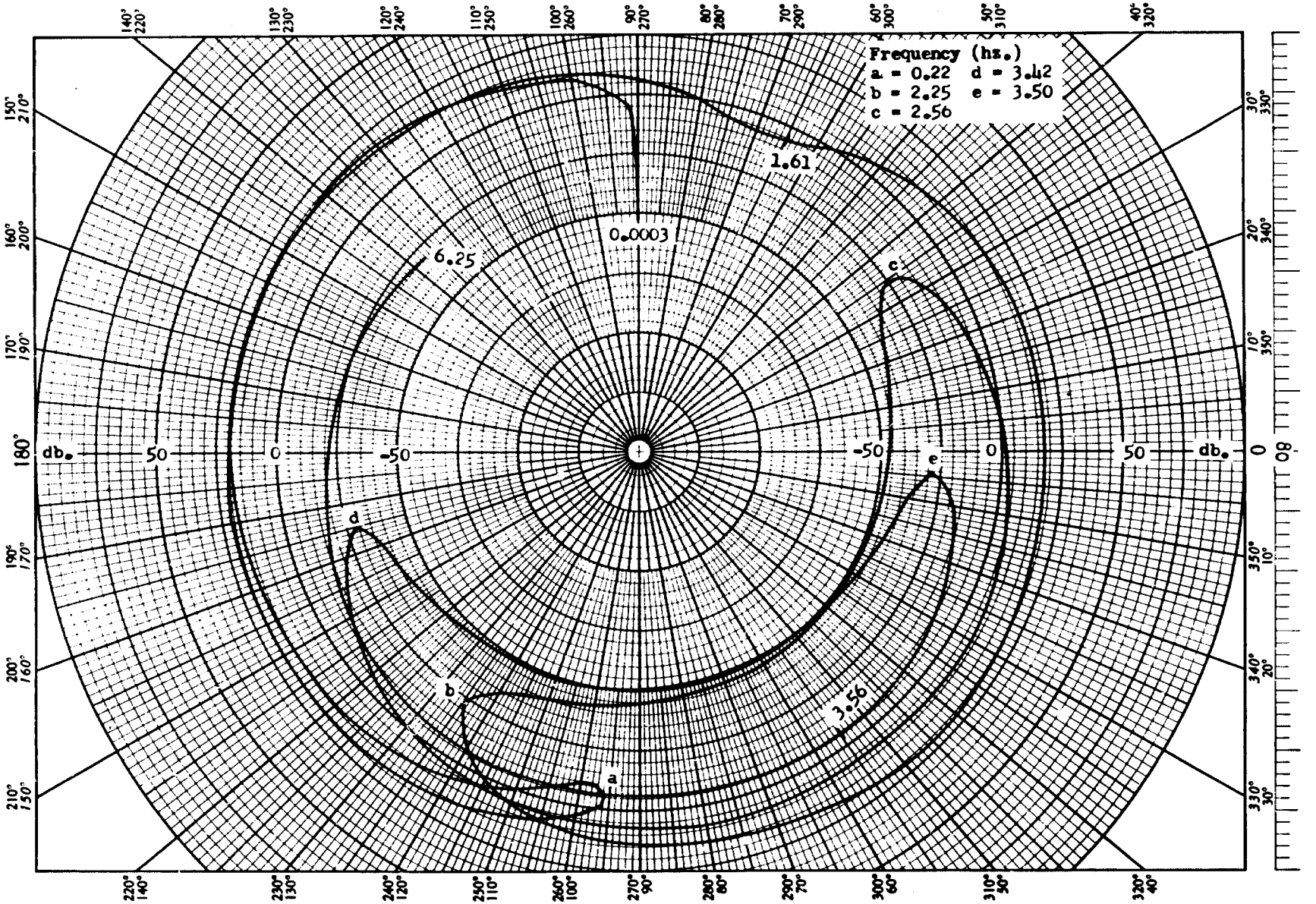


Fig. 37--Nyquist diagram broken in $\phi$ channel of system shown in Fig. 23, T = 0.08

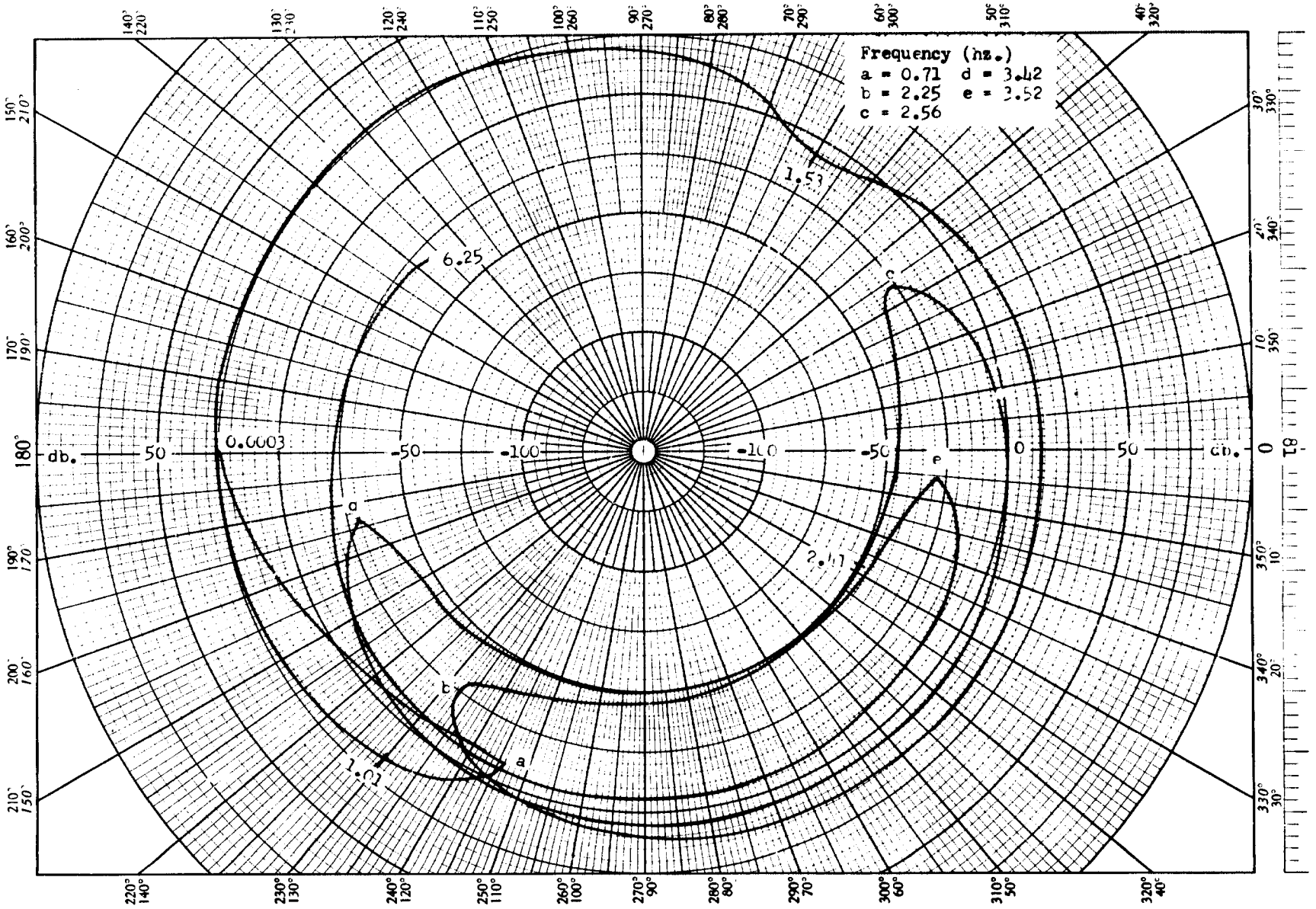


Fig. 38--Nyquist diagram broken in $\beta_c$ channel of system shown in Fig. 23, T = 0.08

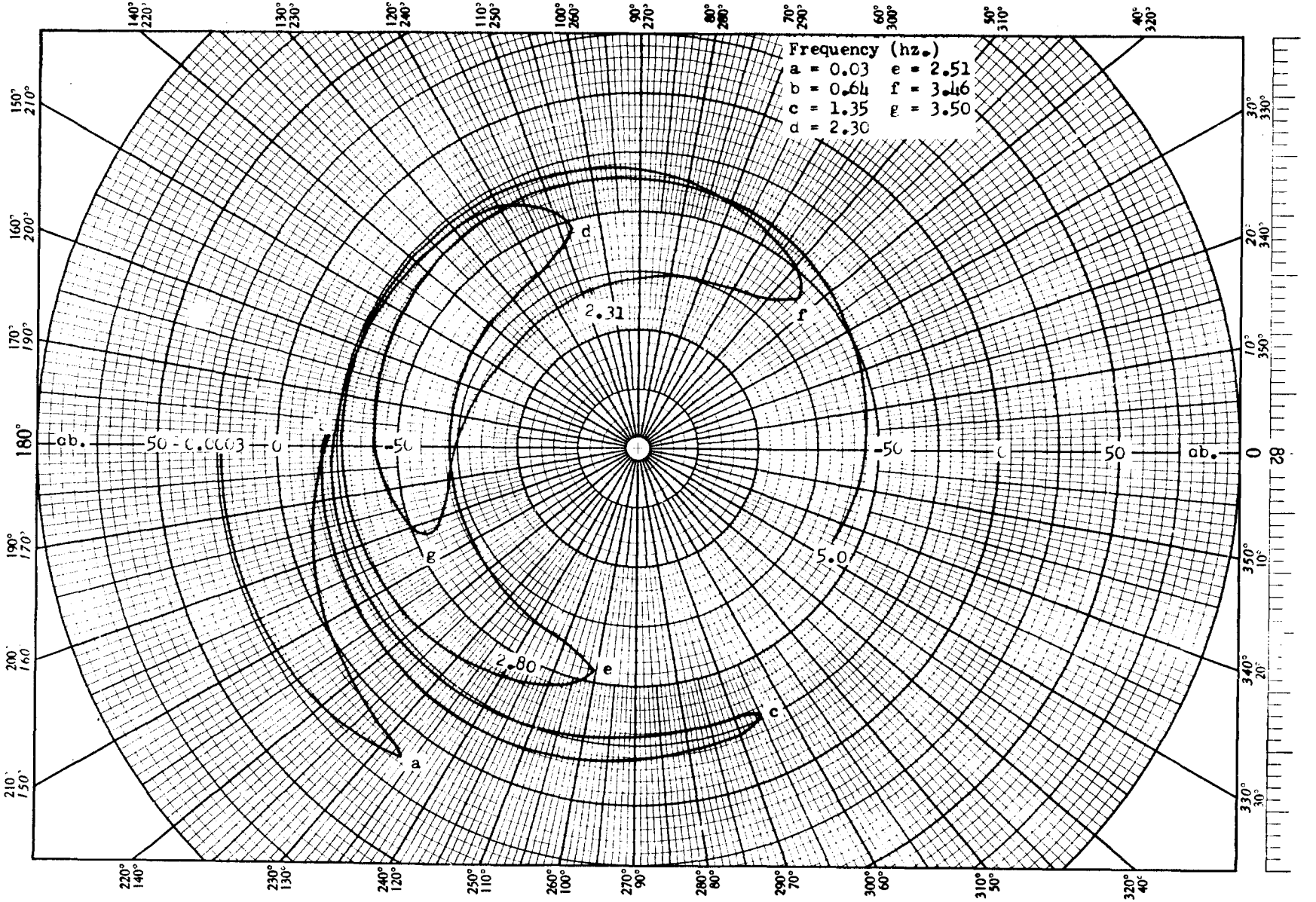


Fig. 39--Nyquist diagram broken in $\Phi$ channel of system shown in Fig. 23, T = 0.1

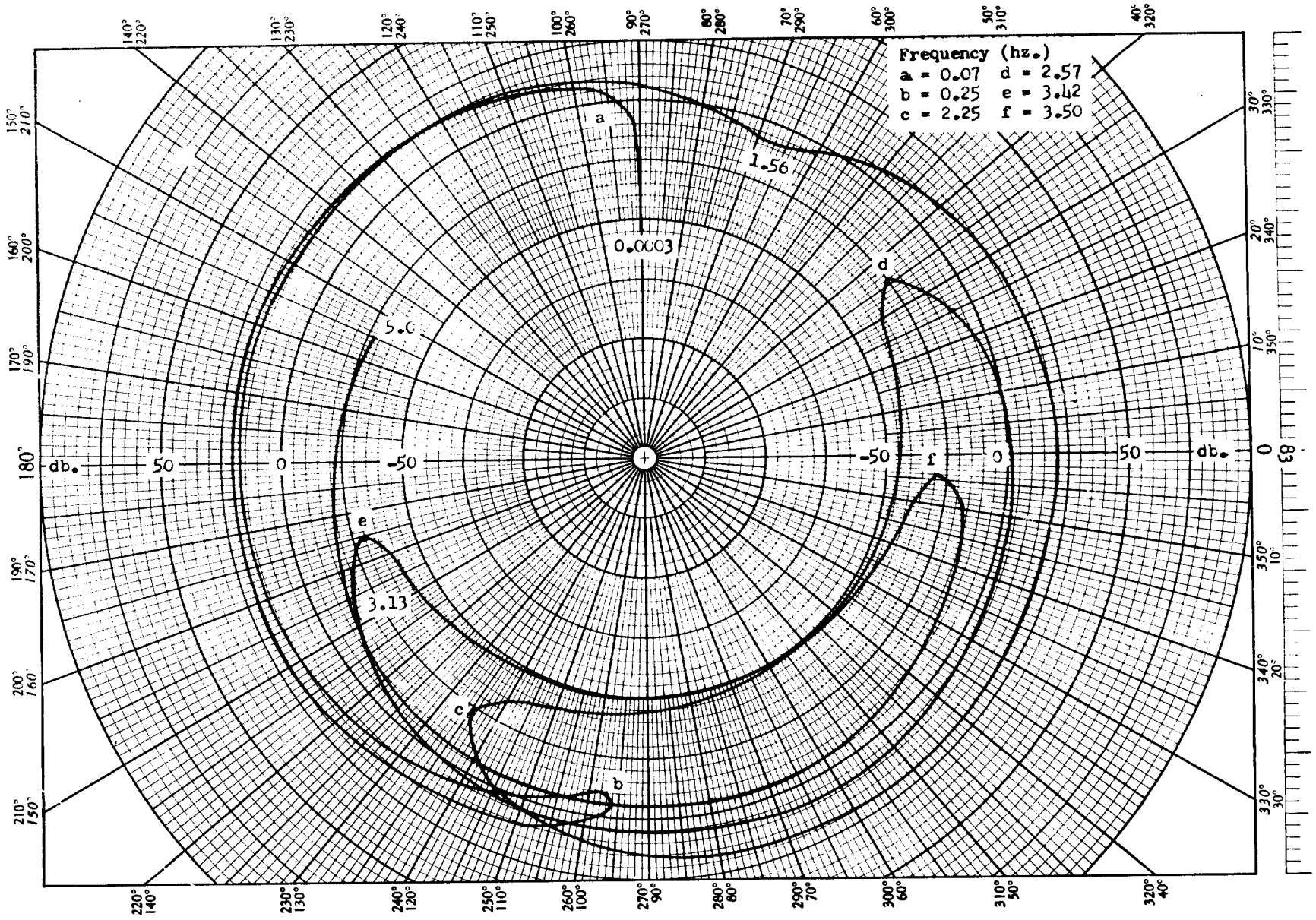


Fig. 40--Nyquist diagram broken in $\phi$ channel of system shown in Fig. 23, T = 0.1

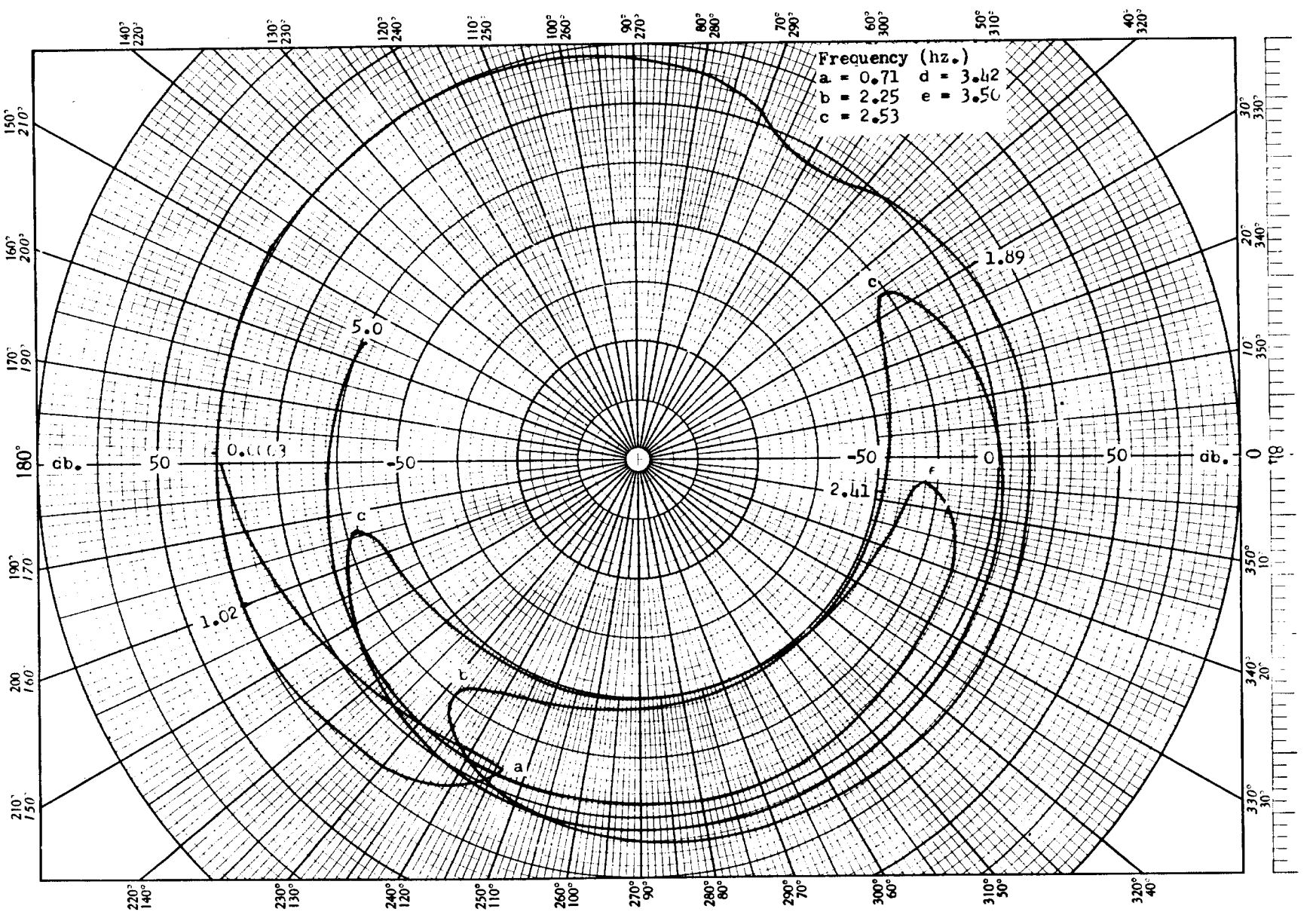


Fig. 41--Nyquist diagram broken in $\beta_c$ channel of system shown in Fig. 23, T = 0.1

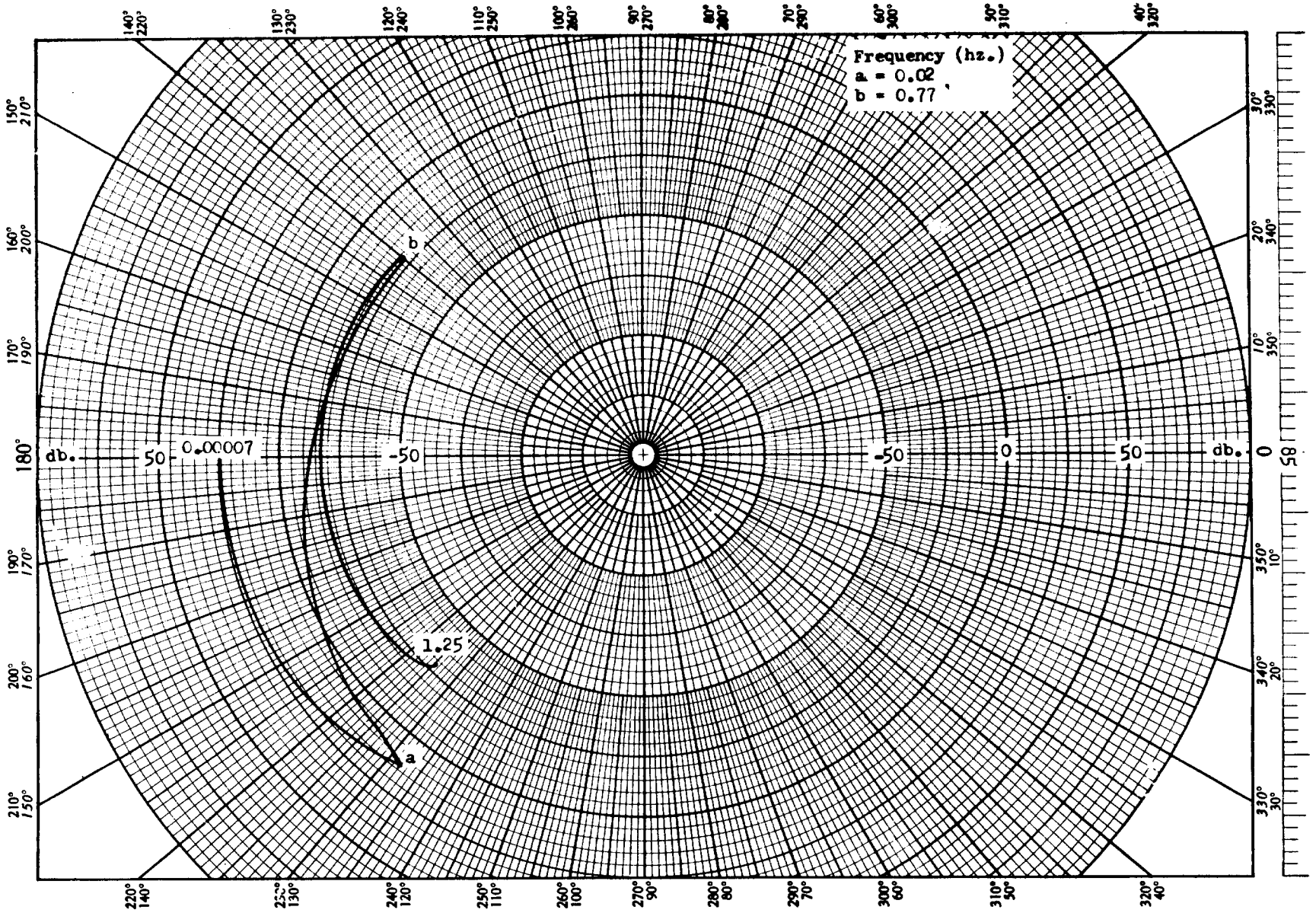


Fig. 42--Nyquist diagram broken in $\Phi$ channel of system shown in Fig. 23, T = 0.4

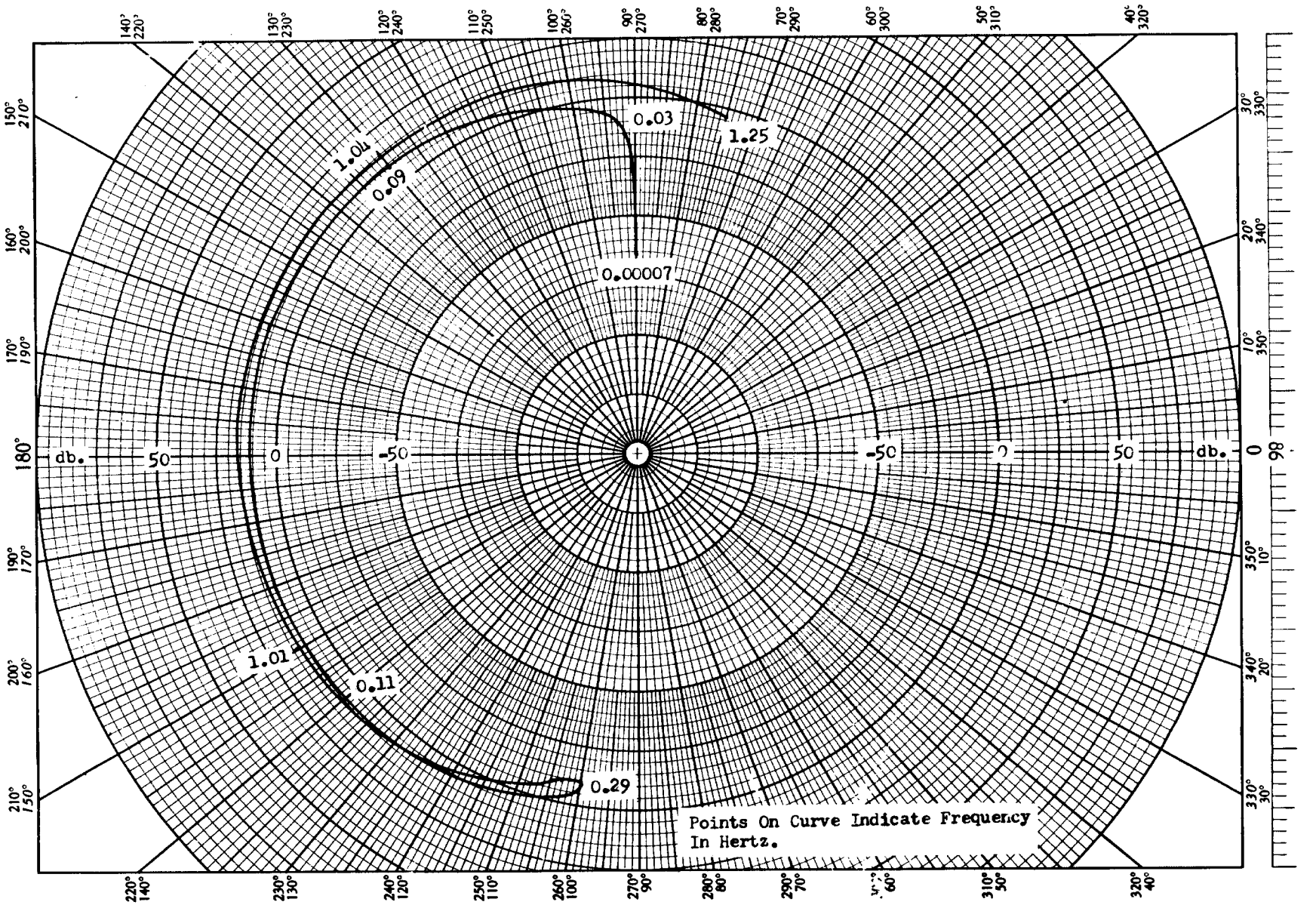


Fig. 43 --Nyquist diagram broken in $\phi$ channel of system shown in Fig. 23, T = 0.4

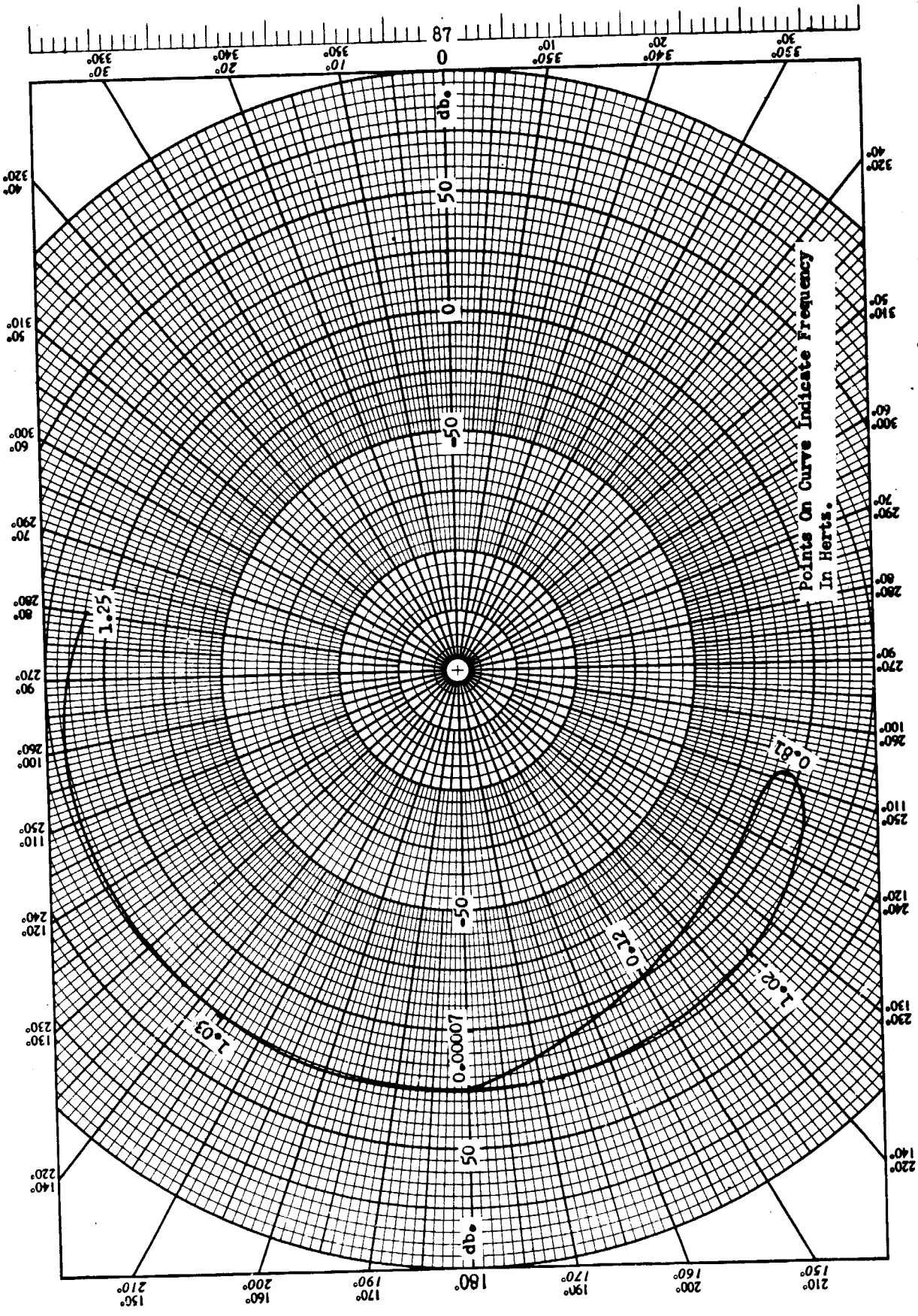


Fig. 44 --Nyquist diagram broken in $\beta_c$ channel of system shown in Fig. 23, T = 0.4

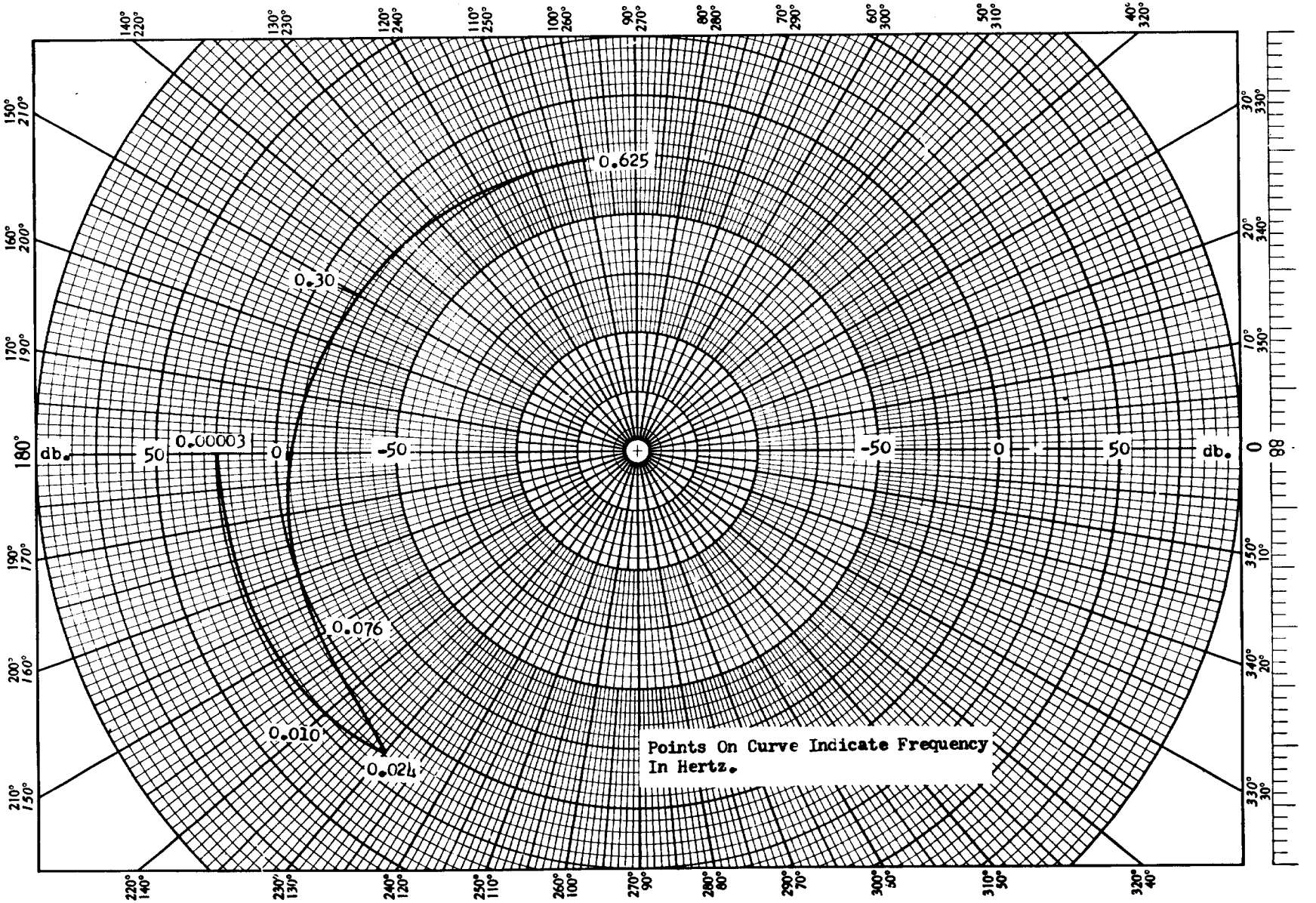


Fig. 45--Nyquist diagram broken in Φ channel of system shown in Fig. 23, T = 0.8

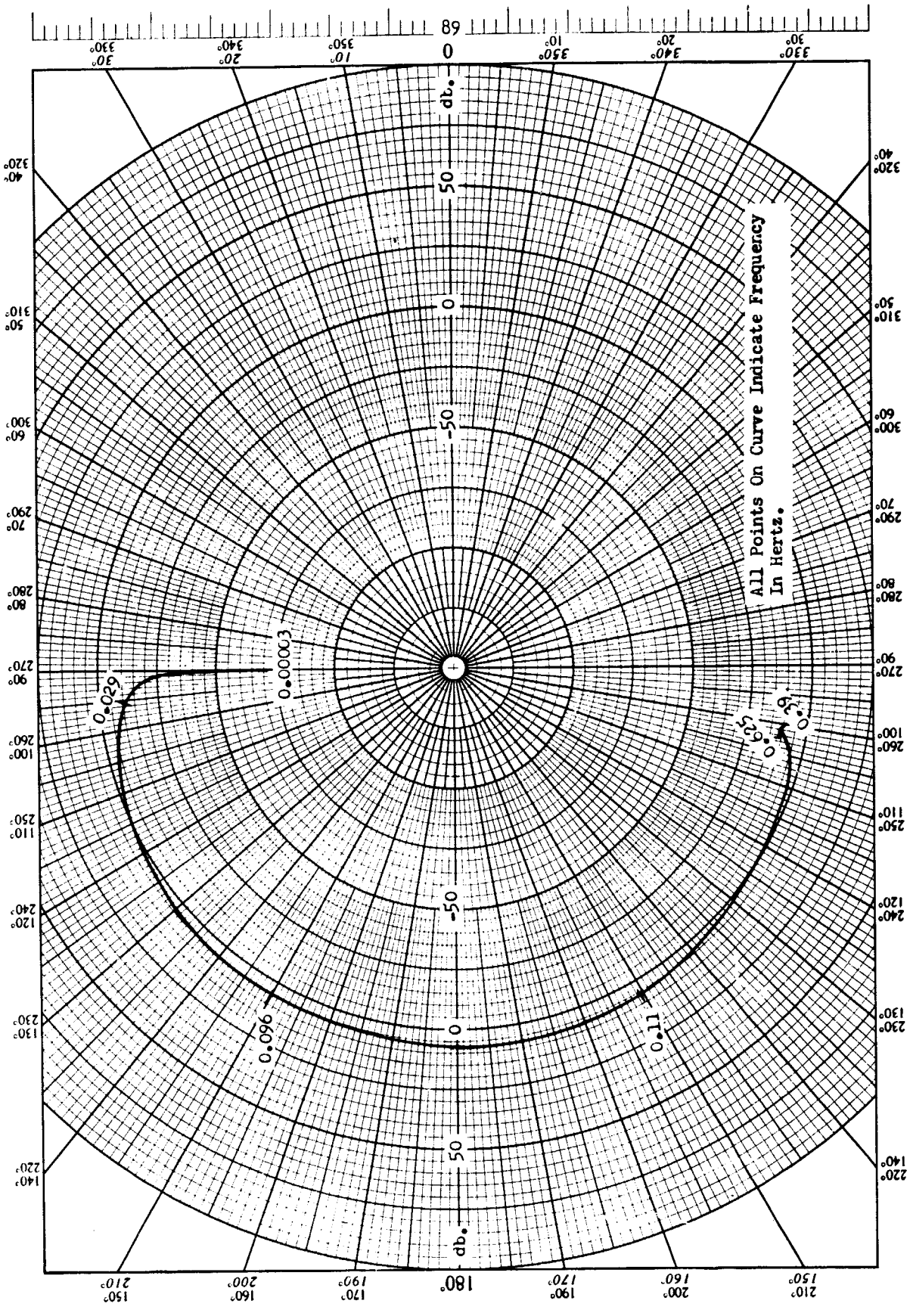


Fig. 46--Nyquist diagram broken in $\dot{\Phi}$ channel of system shown in Fig. 23, T = 0.8

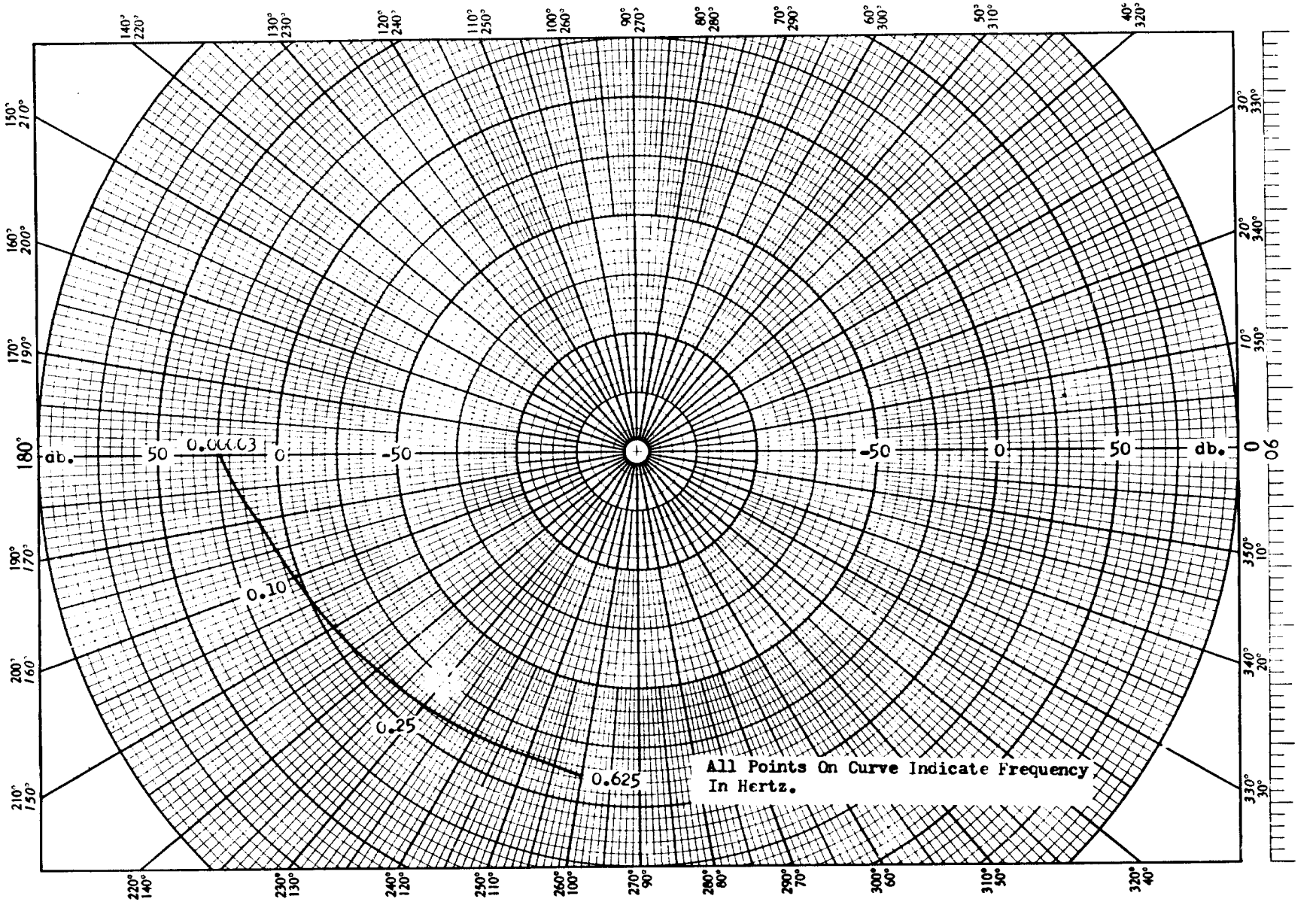


Fig. 47--Nyquist diagram broken in $\beta_c$ channel of system shown in Fig. 23, T = 0.8

# IX. CONCLUSIONS

The new method, presented in Chapers II through V, of analyzing sampled systems that have unsampled inputs yields accurate results for open-loop systems at frequencies less than $\omega_s/2$. When analyzing closed-loop systems by using the open-loop Nyquist diagram, however, the new method of analysis is accurate only for systems that are low-pass. Thus, at the present time, it appears that there is little added advantage to this method as compared to the describing function approach. The principal advantage is due to the fact that the new method considers to some degree the effects of the higher frequencies generated by the sampler.

An investigation was made of the accuracy of Nyquist diagrams obtained from a contour in the z-plane as compared to those obtained from a contour in the w-plane. It was concluded that very little, if any, increase in accuracy can be realized by going to the w-plane.

Nyquist diagrams were obtained for a sampled, compensated thrust-vector control system using the describing-function techniques. These results may now be compared to the results obtained by an analog simulation to determine the accuracy of the describing-function approach. Progress is being made in constructing an analog simulation at Auburn University.

Investigations have been initiated into the effects of varying the sampling rate of the sampler in the $\phi$ channel of the thrust-vector control system. No definite conclusions have been reached.

## REFERENCES


1. B. C. Kuo, "Analysis and Synthesis of Sampled-Data Control Systems," Prentice-Hall, Inc., Englewood Cliffs, N.J., pp. 112-121; 1963.

2. S. J. Mason, "Feedback theory-some properties of signal flow graphs," Proc. IRE, Vol. 41, pp. 1144-1156; September, 1953.

3. B. C. Kuo, "Analysis and Systhesis of Sampled-Data Control Systems," Prentice-Hall, Inc., Englewood Clifts, N.J., pp. 353-364; 1963.

4. Pierre and Kolb,"Concerning the Laplace transform of sampled signals," IEEE Trans. on Automatic Control, Vol. AC-9, pp. 191-192; April, 1964.

5. M. Schwartz, "Information Transmission, Modulation, and Noise," McGraw-Hill Book Co., Inc., New York, N.Y., pp. 41-55; 1959.

6. R. M. Oliver, J. R. Pierce, C. E. Shannon, "The philosophy of pulse code modulation," Proc. IRE, 36, No. 11, pp. 1324-1331; November, 1948.

7. B. C. Kuo, "Analysis and Synthesis of Sampled-Data Control Systems." Prentice-Hall, Inc., Englewood Clifts, N.J., p. 44; 1963.

8. D. A. Pierre, "Sampled-data representative system: an effective concept for use in the analysis and design of distributed-parameter systems," 18th Annual ISA Conference, Preprint No. 30.4.63, pp. 3-11; September, 1963.

APPENDIX A

Digital Computer Program for Calculating
Nyquist Diagram by the New Method

```
 0 $IBFTC          NODECK
 1     10 FORMAT(5(5X,E15.8))
 2     20 FORMAT(7X,92HFREQ(HERTZ)        FREQ(RADIANS)          MAGNITUDE
       1      MAGNITUDE IN DB        ANGLE IN DEG,//)
 3     30 FORMAT (1H1)
 4        PIE = 3.1415926
 5        T = 0.04
 6        COMPLEX S,HELP,C(5)
 7        DEM = PIE/(T*180.0)
10        K = 1
11      9 DEG = 0.0
12        PRINT 20
13        WS = (2.0*PIE)/T
14      1 IF (DEG.GT.5.0) GO TO 11
17        DEG = DEG + 0.1
20        GO TO 12
21     11 DEG = DEG + 1.0
22     12 W = DEG*DEM
23        S = CMPLX(0.0,W)
24        C(1) = 625.0*S*0.94068468/((S**2+25.0*S+625.0)*(S**2-0.02972784))
25        C(2) = 0.94068468/(S**2-0.02972784)
26        C(3) = (0.0,0.0)
```

```
27          DO 34 J=1,21
30          N = -11+J
31          XN = N
32          W1 = W + XN*WS
33          S = CMPLX(0.0,W1)
34          C(4) = (1.0-CEXP(-S*T))*625.0/(S*(S**2+25.0*S+625.0))
35       34 C(3) = C(3) + C(4)*25.0
37          C(K) = C(1) + C(2)*C(3)
40          HELP = C(K)
41          XREAL = REAL(HELP)
42          XIMAG = AIMAG(HELP)
43          XMAG = SQRT(XREAL**2+XIMAG**2)
44          ANGLE = ATAN(XIMAG/XREAL)
45          IF(XREAL.EQ.0.0) IF(XIMAG) 3,4,5
50          IF(XREAL.GT.0.0) GO TO 6
53          IF(XREAL.LT.0.0) IF(XIMAG) 2,2,8
56        8 ANGLE = ANGLE+ PIE
57          GO TO 6
60        2 ANGLE = ANGLE - PIE
61          GO TO 6
62        3 ANGLE = -PIE/2.0
63        4 GO TO 6
64        5 ANGLE = PIE/2.0
65        6 ANGLE = ANGLE*180.0/PIE
66          FREQ = W/(2.0*PIE)
67          DB = 20.0*ALOG10(XMAG)
70          PRINT 10 ,FREQ,W,XMAG,DB,ANGLE
71          IF(W-78.80) 1,1,7
72        7 K = K+1
73          IF (K.EQ.2) STOP
76          PRINT 30
77          GO TO 9
100         END
```

APPENDIX B

Digital Computer Program for Calculating Nyquist Diagram for a Continuous System

```
C $IBFTC          NCDECK
1     1C FCRMAT(5(5X,E15.8))
2     2C FCRMAT(7X,92HFREQ(HERTZ)          FREQ(RADIANS)          MAGNITUDE
        1     MAGNITUDE IN DB        ANGLE IN DEG,//)
3     3C FCRMAT (1H1)
4        PIE = 3.1415926
5        T = C.C4
6        CCMPLEX S,HELP,C(5)
7        DEM = PIE/(T*18C.C)
1C       K = 1
11     9 DEG = C.C
12       PRINT 2C
13       WS = (2.C*PIE)/T
14     1 IF (DEG.GT.5.C) GC TC 11
17       DEG = DEG + C.1
2C       GC TC 12
21    11 DEG = DEG + 1.C
22    12 W = DEG*DEM
23       S = CMPLX(C.C,W)
24       C(1) = 625.C*S*C.94C68468/((S**2+25.0*S+625.0)*(S**2-0.029727841)
25       C(2) = 625.C*25.C*0.94C68468*(1.C-CEXP(-S*T))/(S*(S**2-0.02972784)
        1*(S**2+25.C*S+625.C))
26       C(K) = C(1) + C(2)
```

```
27      37 HELP = C(K)
30         XREAL = REAL(HELP)
31         XIMAG = AIMAG(HELP)
32         XMAG = SQRT(XREAL**2+XIMAG**2)
33         ANGLE = ATAN(XIMAG/XREAL)
34         IF(XREAL.EQ.0.0) IF(XIMAG) 3,4,5
37         IF(XREAL.GT.0.0) GO TO 6
42         IF(XREAL.LT.0.0) IF(XIMAG) 2,2,8
45       8 ANGLE = ANGLE+ PIE
46         GO TO 6
47       2 ANGLE = ANGLE - PIE
50         GO TO 6
51       3 ANGLE = -PIE/2.0
52       4 GO TO 6
53       5 ANGLE = PIE/2.0
54       6 ANGLE = ANGLE*180.0/PIE
55         FREQ = W/(2.0*PIE)
56         DB = 20.0*ALOG10(XMAG)
57         PRINT 10 ,FREQ,W,XMAG,DB,ANGLE
60         IF(W-78.8) 1,1,7
61       7 K = K+1
62         IF (K.EQ.2) STOP
65         PRINT 30
66         GO TO 9
67         END
```

APPENDIX C

## Digital Computer Program for Calculating the Compensated Nyquist Diagram of a Sampled System with a Fictitious Polygonal Hold

```
 0 $IBFTC          NODECK
 1     10 FORMAT(5(5X,E15.8))
 2     20 FORMAT(7X,92HFREQ(HERTZ)        FREQ(RADIANS)          MAGNITUDE
       1      MAGNITUDE IN DB       ANGLE IN DEG,//)
 3     30 FORMAT (1H1)
 4        PIE = 3.1415926
 5        T = 0.04
 6        COMPLEX S,HELP,C(5)
 7        DEM = PIE/(T*180.0)
10        K = 1
11      9 DEG = 0.0
12        PRINT 20
13        WS = (2.0*PIE)/T
14      1 IF (DEG.GT.5.0) GO TO 11
17        DEG = DEG + 0.1
20        GO TO 12
21     11 DEG = DEG + 1.0
22     12 W = DEG*DEM
23        S = CMPLX(0.0,W)
24        C(1) = 625.0*S*0.94068468/((S**2+25.0*S+625.0)*(S**2-0.02972784))
25        C(5) = 25.0*CEXP(S*T)*(1.0-CEXP(-S*T))**2/(S**2*T)
26        C(2) = (0.0,0.0)
```

```
 27        DO 34 J=1,21
 30        N = -11+J
 31        XN = N
 32        W1 = W + XN*WS
 33        S = CMPLX(0.0,W1)
 34        C(3) =(25.0*CEXP(S*T)*(1.0-CEXP(-S*T))**2*0.94068468)/(T*S**2*
          1(S**2-0.02972784))
 35        IF (N.EQ.0) GO TO 33
 40     32 C(2) = C(2) + C(3)
 41        GO TO 34
 42     33 C(2) = C(2) +C(3)/C(5)
 43     34 CONTINUE
 45        C(3) = (0.0,0.0)
 46        DO 35 J=1,21
 47        N = -11+J
 50        XN = N
 51        W1 = W + XN*WS
 52        S = CMPLX(0.0,W1)
 53        C(4) = 25.0*(1.0-CEXP(-S*T))*625.0/(S*(S**2+25.0*S+625.0))
 54     35 C(3) = C(3) +C(4)
 56     36 C(K) = C(1) + C(2)*C(3)
 57     37 HELP = C(K)
 60        XREAL = REAL(HELP)
 61        XIMAG = AIMAG(HELP)
 62        XMAG = SQRT(XREAL**2+XIMAG**2)
 63        ANGLE = ATAN(XIMAG/XREAL)
 64        IF(XREAL.EQ.0.0) IF(XIMAG) 3,4,5
 67        IF(XREAL.GT.0.0) GO TO 6
 72        IF(XREAL.LT.0.0) IF(XIMAG) 2,2,8
 75      8 ANGLE = ANGLE+ PIE
 76        GO TO 6
 77      2 ANGLE = ANGLE - PIE
100        GO TO 6
```

```
101       3 ANGLE = -PIE/2.0
102       4 GO TO 6
103       5 ANGLE = PIE/2.0
104       6 ANGLE = ANGLE*180.0/PIE
105         FREQ = W/(2.0*PIE)
106         DB = 20.0*ALOG10(XMAG)
107         PRINT 10 ,FREQ,W,XMAG,DB,ANGLE
110         IF(W-78.80) 1,1,7
111       7 K = K+1
112         IF (K.EQ.2) STOP
115         PRINT 30
116         GO TO 9
117         END
```

# APPENDIX D

## Derivation of Closed-Loop Transfer Function for Systems with Unsampled Inputs

A closed-loop transfer function for the system shown in Figure 1, with an input at $\beta_e$, cannot be obtained by the ordinary starring and block diagram manipulation procedure, because the input is not sampled. If a fictitious sampler and a fictitious ideal hold are inserted between the input, R, and the summer, as shown in Figure 20, however, the input at the summer will not be altered and a closed-loop transfer function can be written.

From Figure 20, the signals at C and at $\beta_c$ are given by

$$C = R^*H_I + \beta_e \tag{43}$$

and

$$\beta_c = \phi^*H_o + G_2C \ . \tag{44}$$

But,

$$\beta_e = W_{ss}\beta_c \ . \tag{45}$$

Substituting (43) and (44) into (45) and simplifying, the following is obtained:

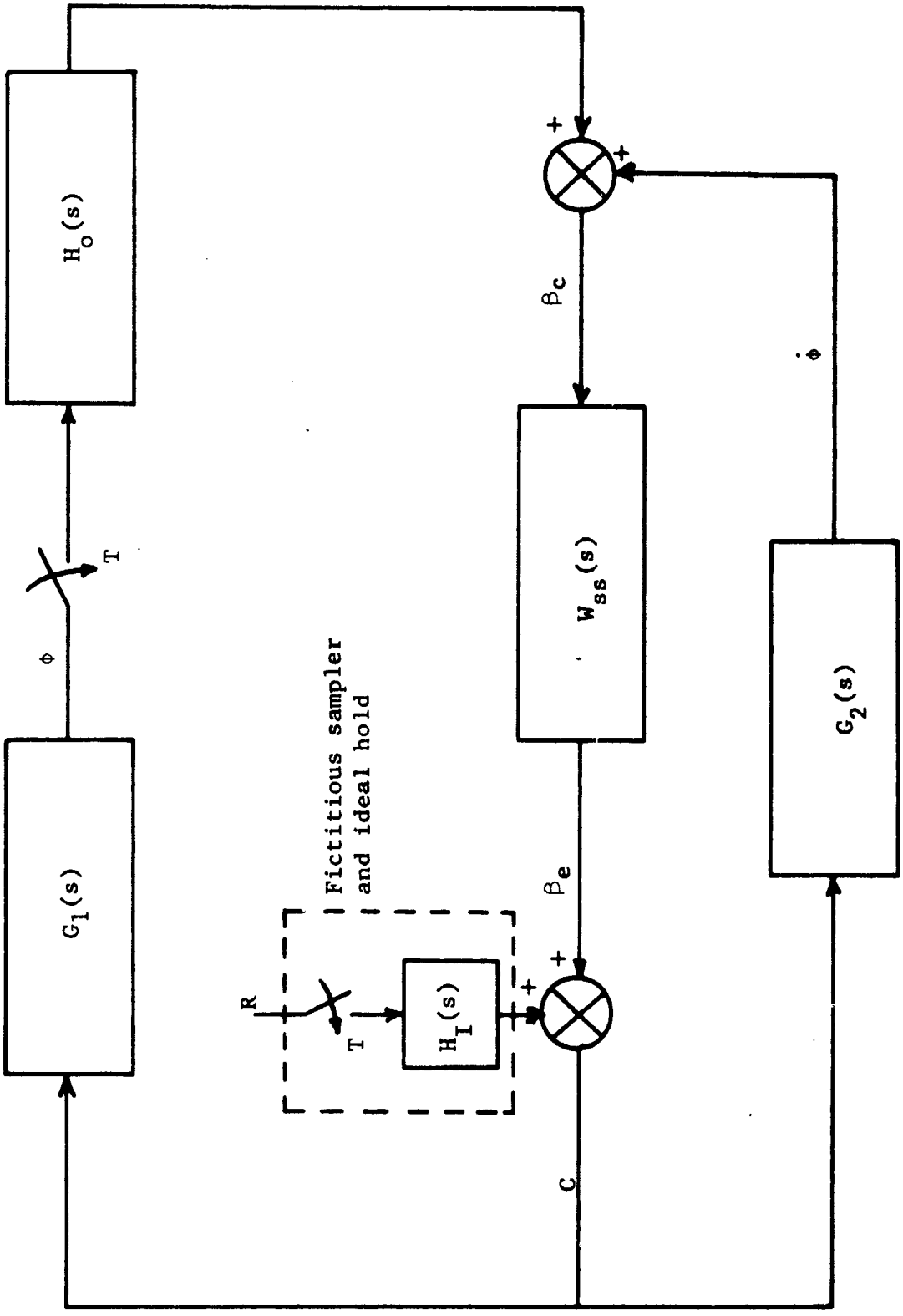


Fig. 20--System in Figure 1 with an input at $\beta_e$

$$\beta_e = \frac{\phi^* H_o W_{ss} + R^* G_2 W_{ss} H_I}{1 - G_2 W_{ss}} \quad . \tag{46}$$

Also,

$$\phi = R^* G_1 H_I + G_1 \beta_e \quad . \tag{47}$$

Substituting (46) into (47), starring the resulting equation, and then solving for $\phi^*$, the following is obtained:

$$\phi^* = \frac{(G_1 H_I)^* R^* + \left(\frac{G_1 G_2 W_{ss} H_I}{1 - G_2 W_{ss}}\right)^* R^*}{1 - \left(\frac{G_1 H_o W_{ss}}{1 - G_2 W_{ss}}\right)^*} \quad . \tag{48}$$

Substituting (48) into (46) and solving for the closed-loop transfer function, the following is obtained:

$$\frac{\beta_e^*}{R^*} = \left(\frac{W_{ss} H_o}{1 - G_2 W_{ss}}\right)^* \left[\frac{(G_1 H_I)^* + \left(\frac{G_1 G_2 W_{ss} H_I}{1 - G_2 W_{ss}}\right)^*}{1 - \left(\frac{G_1 H_o W_{ss}}{1 - G_2 W_{ss}}\right)^*}\right] \tag{49}$$

$$+ \left(\frac{G_2 W_{ss} H_I}{1 - G_2 W_{ss}}\right)^* \quad .$$

Using the results of (19), (20), (21), and (22), Equation (49) can be reduced to

$$\frac{\beta_e^*}{R^*} = \frac{\left(\frac{G_1}{1 - G_2W_{ss}}\right)\left(\frac{H_oW_{ss}}{1 - G_2W_{ss}}\right)^*}{1 - \left(\frac{G_1H_oW_{ss}}{1 - G_2W_{ss}}\right)^*} \tag{50}$$

$$+ \frac{\left(\frac{G_2W_{ss}}{1 - G_2W_{ss}}\right)\left[1 - \left(\frac{G_1H_oW_{ss}}{1 - G_2W_{ss}}\right)^*\right]}{1 - \left(\frac{G_1H_oW_{ss}}{1 - G_2W_{ss}}\right)^*} .$$

Equation (50) is valid only for input frequencies less than $\omega_s/2$.

The denominator of (50) is the characteristic equation of the system broken at $\beta_e$. The denominator of (30), where the O.L.T.F., open-loop transfer function, is given by (2), is the characteristic equation of the system broken at $\phi$ and is the same as the characteristic equation of the system broken at $\beta_e$. This was expected, however, since the characteristic equation should be the same regardless of the point at which the system is broken.

Using the fictitious sampler and the fictitious ideal hold to obtain closed-loop transfer functions for sampled systems that have unsampled inputs, is one application of the new method of analysis presented in Chapter IV.

TABLE 1

OUTPUT DATA OF COMPUTER PROGRAM THAT CALCULATES
NYQUIST DIAGRAM BY THE NEW METHOD

| FREQ(HERTZ) | FREQ(RADIANS) | MAGNITUDE IN DB | ANGLE IN DEG |
|---|---|---|---|
| 0.69444444E-01 | 0.43633230E 00 | 0.13346105E 02 | -0.15784856E 03 |
| 0.13888889E 00 | 0.87266460E 00 | 0.38904066E 01 | -0.14146018E 03 |
| 0.20833333E 00 | 0.13089969E 01 | -0.11226460E 01 | -0.13093227E 03 |
| 0.27777778E 00 | 0.17453292E 01 | -0.43325159E 01 | -0.12430728E 03 |
| 0.34722222E 00 | 0.21816615E 01 | -0.66465238E 01 | -0.12006578E 03 |
| 0.41666666E 00 | 0.26179938E 01 | -0.84443017E 01 | -0.11730456E 03 |
| 0.48611111E 00 | 0.30543261E 01 | -0.99110164E 01 | -0.11550269E 03 |
| 0.55555555E 00 | 0.34906584E 01 | -0.11148309E 02 | -0.11435126E 03 |
| 0.62499999E 00 | 0.39269907E 01 | -0.12217269E 02 | -0.11365955E 03 |
| 0.69444444E 00 | 0.43633230E 01 | -0.13157285E 02 | -0.11330503E 03 |
| 0.76388888E 00 | 0.47996553E 01 | -0.13995190E 02 | -0.11320608E 03 |
| 0.83333332E 00 | 0.52359876E 01 | -0.14750083E 02 | -0.11330670E 03 |
| 0.90277777E 00 | 0.56723199E 01 | -0.15436054E 02 | -0.11356743E 03 |
| 0.97222221E 00 | 0.61086522E 01 | -0.16063811E 02 | -0.11395985E 03 |
| 0.10416667E 01 | 0.65449845E 01 | -0.16641695E 02 | -0.11446315E 03 |
| 0.11111111E 01 | 0.69813168E 01 | -0.17176344E 02 | -0.11506184E 03 |
| 0.11805555E 01 | 0.74176491E 01 | -0.17673140E 02 | -0.11574432E 03 |
| 0.12500000E 01 | 0.78539814E 01 | -0.18136524E 02 | -0.11650176E 03 |
| 0.13194444E 01 | 0.82903137E 01 | -0.18570210E 02 | -0.11732749E 03 |
| 0.13888889E 01 | 0.87266460E 01 | -0.18977351E 02 | -0.11821640E 03 |

TABLE I (continued)

| | | | |
|---|---|---|---|
| 0.14583333E 01 | 0.91629782E 01 | -0.19360659E 02 | -0.11916462E 03 |
| 0.18055556E 01 | 0.11344640E 02 | -0.20993537E 02 | -0.12471554E 03 |
| 0.21527778E 01 | 0.13526301E 02 | -0.22297604E 02 | -0.13152684E 03 |
| 0.25000000E 01 | 0.15707963E 02 | -0.23422524E 02 | -0.13955451E 03 |
| 0.28472222E 01 | 0.17889624E 02 | -0.24491414E 02 | -0.14870872E 03 |
| 0.31944444E 01 | 0.20071286E 02 | -0.25610018E 02 | -0.15873314E 03 |
| 0.35416666E 01 | 0.22252947E 02 | -0.26855044E 02 | -0.16916352E 03 |
| 0.38888888E 01 | 0.24434609E 02 | -0.28257443E 02 | -0.17941384E 03 |
| 0.42361111E 01 | 0.26616270E 02 | -0.29800002E 02 | 0.17104482E 03 |
| 0.45833332E 01 | 0.28797932E 02 | -0.31434982E 02 | 0.16254119E 03 |
| 0.49305555E 01 | 0.30979593E 02 | -0.33108211E 02 | 0.15518074E 03 |
| 0.52777777E 01 | 0.33161255E 02 | -0.34774969E 02 | 0.14891095E 03 |
| 0.56249999E 01 | 0.35342916E 02 | -0.36404839E 02 | 0.14360200E 03 |
| 0.59722221E 01 | 0.37524578E 02 | -0.37980073E 02 | 0.13910371E 03 |
| 0.63194443E 01 | 0.39706239E 02 | -0.39492012E 02 | 0.13527474E 03 |
| 0.66666666E 01 | 0.41887901E 02 | -0.40937817E 02 | 0.13199365E 03 |
| 0.70138888E 01 | 0.44069562E 02 | -0.42318073E 02 | 0.12916051E 03 |
| 0.73611110E 01 | 0.46251224E 02 | -0.43635240E 02 | 0.12669479E 03 |
| 0.77083332E 01 | 0.48432885E 02 | -0.44892702E 02 | 0.12453212E 03 |
| 0.80555554E 01 | 0.50614547E 02 | -0.46094207E 02 | 0.12262102E 03 |
| 0.84027776E 01 | 0.52796208E 02 | -0.47243543E 02 | 0.12092025E 03 |
| 0.87499998E 01 | 0.54977870E 02 | -0.48344374E 02 | 0.11939654E 03 |
| 0.90972220E 01 | 0.57159531E 02 | -0.49400147E 02 | 0.11802287E 03 |
| 0.94444442E 01 | 0.59341193E 02 | -0.50414065E 02 | 0.11677710E 03 |
| 0.97916665E 01 | 0.61522854E 02 | -0.51389067E 02 | 0.11564098E 03 |
| 0.10138889E 02 | 0.63704515E 02 | -0.52327848E 02 | 0.11459927E 03 |
| 0.10486111E 02 | 0.65886176E 02 | -0.53232868E 02 | 0.11363920E 03 |
| 0.10833333E 02 | 0.68067838E 02 | -0.54106369E 02 | 0.11274991E 03 |
| 0.11180555E 02 | 0.70249500E 02 | -0.54950400E 02 | 0.11192211E 03 |
| 0.11527778E 02 | 0.72431161E 02 | -0.55766835E 02 | 0.11114777E 03 |
| 0.11875000E 02 | 0.74612823E 02 | -0.56557392E 02 | 0.11041987E 03 |
| 0.12222222E 02 | 0.76794485E 02 | -0.57323647E 02 | 0.10973219E 03 |
| 0.12569444E 02 | 0.78976146E 02 | -0.58067060E 02 | 0.10907916E 03 |

TABLE II

Data For Nyquist In F(z)-Plane

| FREQ(HERTZ) | FREQ(RADIANS) | MAGNITUDE IN DB | ANGLE IN DEG |
|---|---|---|---|
| 0.34722222E 00 | 0.87266460E-01 | -0.14533446E 02 | -0.16112409E 03 |

RTCT1R = 4157.7798
RTCT1C = -0.39062500E-04
RTCT2R = -12500.338
RTCT2C = 286304.85
RTCT3R = 8483.0793
RTCT3C = -286524.08
RTCT4R = -117.18671
RTCT4C = 227.21452
RTCT5R = -0.50012680E-02
RTCT5C = 0.20592762E-03
HCLCR = -0.76106031E-02
HCLCC = -0.79427573E-10

| | | | |
|---|---|---|---|
| 0.62500000E 01 | 0.15707963E 01 | -0.48830329E 02 | -0.16539395E 03 |

RTCT1R = 15.821607
RTCT1C = 0.10222422E-06
RTCT2R = -12500.339
RTCT2C = 12500.340
RTCT3R = 12497.045
RTCT3C = -12512.371
RTCT4R = -12.525165
RTCT4C = 12.030177
RTCT5R = -0.18404927E-03
RTCT5C = 0.20179548E-02
HCLCR = -1.9999999
HCLCC = 0.12922103E-07

TABLE II (continued)

| | | | |
|---|---|---|---|
| 0.12500000E 02 | 0.31415926E 01 | -0.48154400E 02 | 0.18000000E 03 |

```
RTOT1R =          7.9108031
RTOT1C =   0.00000000E-38
RTOT2R =        -12500.339
RTOT2C =   0.38490861E-03
RTOT3R =         12504.713
RTOT3C =  -0.38527923E-03
RTOT4R =        -12.282660
RTOT4C =   0.37058194E-06
RTOT5R =  -0.29828380E-03
RTOT5C =   0.43981973E-10
HOLOR  =        -4.0000000
HOLOC  =   0.35527137E-14
```

Data For Nyquist In F(w)-Plane

| FREQ(HERTZ) | FREQ(RADIANS) | MAGNITUDE IN DB | ANGLE IN DEG |
|---|---|---|---|
| 0.34722222E 00 | 0.43660941E-01 | -0.14537638E 02 | -0.16109542E 03 |

```
RTOT1R =          4157.7797
RTOT1C =   0.00000000E-38
RTOT2R =        -12500.339
RTOT2C =         286304.85
RTOT3R =         8483.0653
RTOT3C =        -286524.08
RTOT4R =        -117.18670
RTOT4C =         227.21452
RTOT5R =  -0.50012680E-02
RTOT5C =   0.20592764E-03
HOLOR  =  -0.76106033E-02
HOLOC  =  -0.00000000E-38
```

TABLE II (continued)

0.62500000E 01 0.99999996E 00 -0.49226293E 02 -0.16045855E 03

```
RTOT1R =          15.821607
RTOT1C =    0.00000000E-38
RTOT2R =       -12500.339
RTOT2C =        12500.340
RTOT3R =        12497.045
RTOT3C =       -12512.371
RTOT4R =       -12.525165
RTOT4C =        12.030176
RTOT5R =   -0.18404931E-03
RTOT5C =    0.20179548E-02
HOLDR  =         -1.9999999
HOLDC  =   -0.00000000E-38
```

0.12500000E 02 0.32476123E 08 -0.47130621E 02 -0.18000000E 03

```
RTOT1R =          7.9108031
RTOT1C =    0.00000000E-38
RTOT2R =       -12500.339
RTOT2C =    0.38490861E-03
RTOT3R =        12504.713
RTOT3C =   -0.38527923E-03
RTOT4R =       -12.282659
RTOT4C =    0.37058193E-06
RTOT5R =   -0.29828380E-03
RTOT5C =    0.43981974E-10
HOLDR  =         -4.0000000
HOLDC  =   -0.00000000E-38
```